Optimal Operation and Maximal Hosting Capacity of High-Renewable Islanded Microgrids

Author:
Liu, Daichen

Publication Date:
2022

DOI:
https://doi.org/10.26190/unsworks/24492

OPTIMAL OPERATION AND MAXIMAL HOSTING CAPACITY OF HIGH-RENEWABLE ISLANDED MICROGRIDS

Daichen Liu

A thesis submitted in partial fulfilment

of the requirements for the degree of

Doctor of Philosophy

School of Electrical Engineering and Telecommunications

Faculty of Engineering

June 2022

DECLATRATIONS

ORIGINALITY STATEMENT

☑ I hereby declare that this submission is my own work and to the best of my knowledge it contains no materials previously published or written by another person, or substantial proportions of material which have been accepted for the award of any other degree or diploma at UNSW or any other educational institution, except where due acknowledgement is made in the thesis. Any contribution made to the research by others, with whom I have worked at UNSW or elsewhere, is explicitly acknowledged in the thesis. I also declare that the intellectual content of this thesis is the product of my own work, except to the extent that assistance from others in the project's design and conception or in style, presentation and linguistic expression is acknowledged.

COPYRIGHT STATEMENT

☑ I hereby grant the University of New South Wales or its agents a non-exclusive licence to archive and to make available (including to members of the public) my thesis or dissertation in whole or part in the University libraries in all forms of media, now or here after known. I acknowledge that I retain all intellectual property rights which subsist in my thesis or dissertation, such as copyright and patent rights, subject to applicable law. I also retain the right to use all or part of my thesis or dissertation in future works (such as articles or books).

For any substantial portions of copyright material used in this thesis, written permission for use has been obtained, or the copyright material is removed from the final public version of the thesis.

AUTHENTICITY STATEMENT

☑ I certify that the Library deposit digital copy is a direct equivalent of the final officially approved version of my thesis.

PUBLICATIONS STATEMENT

UNSW is supportive of candidates publishing their research results during their candidature as detailed in the UNSW Thesis Examination Procedure.

Publications can be used in the candidate's thesis in lieu of a Chapter provided:

- The candidate contributed greater than 50% of the content in the publication and are the "primary author", i.e. they were responsible primarily for the planning, execution and preparation of the work for publication.
- The candidate has obtained approval to include the publication in their thesis in lieu of a Chapter from their Supervisor and Postgraduate Coordinator.
- The publication is not subject to any obligations or contractual agreements with a third party that would constrain its inclusion in the thesis.

☑ The candidate has declared that **their thesis has publications - either published or submitted for publication - incorporated into it in lieu of a Chapter/s. Details of these publications are provided below.**

Publication Details #1

Full Title:	Stochastic Security-Constrained Optimal Power Flow for A Microgrid Considering Tie-Line Switching
Authors:	Daichen Liu, Cuo Zhang, Guo Chen, Yan Xu, Zhao Yang Dong
Journal or Book Name:	International Journal of Electrical Power & Energy Systems
Volume/Page Numbers:	Volume 134
Date Accepted/Published:	January 2022
Status:	published
The Candidate's Contribution to the Work:	I completed the work of mathematical modeling, programming, simulation and writing.
Location of the work in the thesis and/or how the work is incorporated in the thesis:	This work is Chapter 4 of my thesis.

Publication Details #2

Full Title:	Sensitivity Region Based Optimization for Maximizing Renewable Generation Hosting Capacity of An Islanded Microgrid
Authors:	Daichen Liu, Cuo Zhang, Yan Xu, Zhao Yang Dong, Chi Yuan
Journal or Book Name:	IEEE Transactions on Smart Grid
Volume/Page Numbers:	
Date Accepted/Published:	
Status:	submitted
The Candidate's Contribution to the Work:	I completed the work of mathematical modeling, programming, simulation and writing.
Location of the work in the thesis and/or how the work is incorporated in the thesis:	This work is Chapter 5 of my thesis.

Publication Details #3

Full Title:	Stochastic Optimal Power Flow for Islanded Microgrids Considering Droop Control
Authors:	Daichen Liu, Cuo Zhang and Zhao Yang Dong
Journal or Book Name:	2019 IEEE Innovative Smart Grid Technologies - Asia
Volume/Page Numbers:	pp. 3156-3161
Date Accepted/Published:	October 2019
Status:	published
The Candidate's Contribution to the Work:	I completed the work of mathematical modeling, programming, simulation and writing.
Location of the work in the thesis and/or how the work is incorporated in the thesis:	This work is Chapter 2 of my thesis.

Publication Details #4

Full Title:	A New Stochastic Optimal Power Flow Method for Isolated Microgrids under Uncertainties
Authors:	Daichen Liu, Cuo Zhang and Zhao Yang Dong
Journal or Book Name:	2021 IEEE Sustainable Power and Energy Conference
Volume/Page Numbers:	pp. 163-168
Date Accepted/Published:	March 2022
Status:	published
The Candidate's Contribution to the Work:	I completed the work of mathematical modeling, programming, simulation and writing.
Location of the work in the thesis and/or how the work is incorporated in the thesis:	This work is Chapter 3 of my thesis.

Candidate's Declaration

I confirm that where I have used a publication in lieu of a chapter, the listed publication(s) above meet(s) the requirements to be included in the thesis. I also declare that I have complied with the Thesis Examination Procedure.

ABSTRACT

With the advancement of technology, renewable power generators such as solar photovoltaics and wind turbines have become cost-effective and competitive compared to traditional generators. On the other hand, carbon emission issues have been globally focused, promoting development of renewable energy. Meanwhile, microgrids have been widely constructed with increasing installation of distributed generators including microturbines and renewable power generators. Challenges from intermittent and uncertain renewable sources, low operating efficiency as well as system stability in the islanded mode still exist for microgrid operation and renewable hosting capacity assessment. To address these unsolved issues, it is worth developing advanced optimal operation and hosting capacity maximization approaches for high-renewable microgrids, which are presented in this thesis.

For microgrid operation, economic efficiency, solution robustness and system stability are major concerns to be addressed. In order to achieve cost-effective operation, firstly a new stochastic optimal power flow (OPF) is proposed for islanded microgrids. A linear network operating model which can be used in the OPF problem is specifically developed, while uncertainties of photovoltaic power and loads are addressed by Monte Carlo simulation. Secondly, an improved OPF method with a new iterative solution algorithm is proposed to enhance the accuracy of network operating model and the computing speed. Besides, an advanced probabilistic modelling method is adapted to present real-time uncertainties in the OPF method. Thirdly, a novel stochastic OPF method with consideration of tie-line switching from the grid-connected to the islanded mode while the main grid in contingency is proposed. Security constraints to guarantee the system stability in the islanded mode are formulated. Moreover, a Benders decomposition based solution algorithm is developed, to efficiently solve the OPF problem with a master problem and a sub-problem which formulate the grid-connected and the islanded modes, respectively. Fourthly, a renewable hosting capacity maximization approach for an islanded microgrid, considering system frequency deviation, is proposed. An advanced

sensitivity region based optimization method is proposed to address the uncertainties of wind power and loads, thus obtaining a robust solution.

The proposed methods have been successfully demonstrated and compared with existing works. Simulation results have verified their feasibility and effectiveness.

To My Family

ACKNOWLEDGEMENTS

Firstly, I would like to take this opportunity to express my true gratitude to my supervisor Prof. Zhao Yang Dong for his warm encouragement, continuous support and patient guidance. Without him, I would not have this precious chance to study in a brilliant group. His leadership, scientific attitude and helpfulness navigate my research life and future development. I would also like to sincerely thank my co-supervisor Dr. Cuo Zhang. His advice, guidance and support on my research are indispensable to me. I learned how to be a qualified researcher from the discussion of research with them.

Secondly, I would like to convey my heartfelt thanks to my colleagues, Dr. Ke Meng, Dr. Ziyuan Tong, Dr. Wang Zhang, Dr. Guo Chen from The University of New South Wales, A/Prof. Yan Xu from Nanyang Technological University, and Dr. Yuan Chi from Chongqing University, for their assistance and support to my completion of thesis and research life. I am honored to work with these excellent, friendly people.

Thirdly, I would like to thank my friends, Mr. Ruipeng Xu, Mr. Dong Liang, Mr. Jinlong Yang, Mr. Ziyuan Wang, Dr. Kang Huang and Mr. Muxin Xu for the joy and comfort they bring to me during this arduous journey.

Most importantly, I sincerely feel grateful to my parents, Mr. Qun Liu and Mrs. Shilian Sun. Their selfless love crutches me to reach the end of this journey and my gratefulness is beyond any word.

LIST OF PUBLICATIONS

The following publications and submitted manuscript as the major research results of this candidate are included as part of this thesis.

Publications

- **Daichen Liu**, Cuo Zhang, Guo Chen, Yan Xu, Zhao Yang Dong, "Stochastic Security-Constrained Optimal Power Flow for A Microgrid Considering Tie-Line Switching," *International Journal of Electrical Power & Energy Systems*, Volume 134, 2022.
- **Daichen Liu**, Cuo Zhang and Zhao Yang Dong, "Stochastic Optimal Power Flow for Islanded Microgrids Considering Droop Control," *2019 IEEE Innovative Smart Grid Technologies - Asia (ISGT Asia)*, 2019.
- **Daichen Liu**, Cuo Zhang and Zhao Yang Dong, "A New Stochastic Optimal Power Flow Method for Isolated Microgrids under Uncertainties," *2021 IEEE Sustainable Power and Energy Conference (istochastic programmingEC)*, 2021.

Submitted Manuscript

- **Daichen Liu**, Cuo Zhang, Yan Xu, Zhao Yang Dong, Chi Yuan “Sensitivity Region Based Optimization for Maximizing Renewable Generation Hosting Capacity of An Islanded Microgrid,” submitted to *IEEE Transactions on Smart Grid* (Under Review).

CONTENTS

LIST OF ABBREVIATIONS

DG	Distributed Generation
DER	Distributed Energy Resource
PV	Photovoltaic
WT	Wind Turbine
CHP	Cogeneration Heat and Power
RES	Renewable Energy Source
ESS	Energy Storage System
BESS	Battery Energy Storage System
NSGA II	Non-dominated Sorting Genetic Algorithm II
PCC	Point of Common Coupling
EMS	Energy Management System
SOC	State of Charge
OPF	Optimal Power Flow
PDF	Probability Density Function
BIBC	Bus-injection to Branch-current
BCBV	Branch-current to Bus-voltage
ED	Economic Dispatch
BFS	Backward Forward Sweep
MAPE	Mean Absolute Percentage Error
RSP	Relaxed Sup-problem
SR	Sensitivity Region
FSR	Feasibility Sensitivity Region
WCSR	Worst-case Sensitivity Region
WCFSR	Worst-case Feasibility Sensitivity Region

GA	Genetic Algorithm

LIST OF FIGURES

LIST OF TABLES

Chapter 1 INTRODUCTION

1.1 Distributed Generation

Distributed generation (DG) is a category of distributed energy resource (DER), and it is defined by Institute of Electrical and Electronics Engineers (IEEE) [1] as "*generation of electricity by facilities that are sufficiently smaller than central generating plants so as to allow interconnection at nearly any point in the power system*." Summarized by [2], there are various definitions of DG, given by International Council on Large Electric Systems (CIGRE), International Conference on Electricity Distribution (CIRED) and International Energy Agency (IEA). It can be seen that two major differences exist in voltage level and capacity scale of DG, while the established consensus on DG is the small scale and the location near consumers.

The authors of [3] categorize DG based on whether it is renewable. Typical non-renewable DG devices include reciprocating engine, microturbine, combustion gas turbine, while typical renewable DG devices (DERs) include solar photovoltaic (PV), wind turbine (WT), fuel cell, micro-hydro, geothermal and biomass. In the following two sections, microturbine is briefly introduced as a representative of non-renewable DG devices, while PV and WT are compactly introduced as predominant renewable DG.

1.1.1 Microturbine

As Fig. 1.1 shows, the mechanism of a microturbine is converting the thermal energy generated by burning fuel to the mechanical energy that drives the turbine with a gas flow. Then, the turbine motion makes the small-size generator generate controllable electric power. Since the exhaust gas temperature is high, microturbine can be used to establish a cogeneration or combined heat and power (CHP) system. The thermal efficiency of microturbine is generally about 30%, while the capacity range is from 20 kW to 500 kW [4].

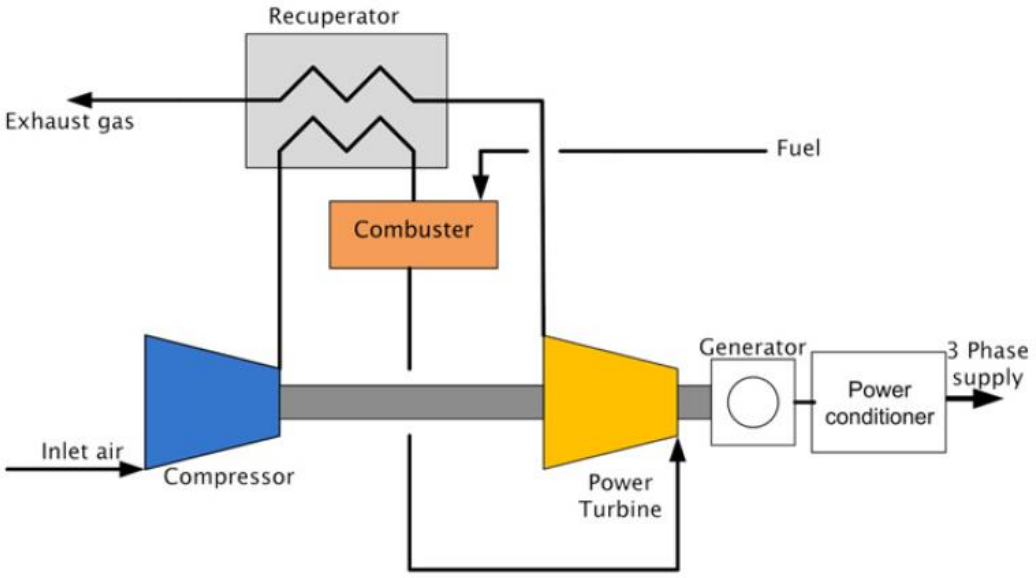

Figure 1.1. Schematic Diagram of a Single-shaft Microturbine [5].

The number of microturbine shafts determine its classification [5]. The microturbine is presented in Fig. 1.1 is a single-shaft one which means its power turbine and air compressor share the same shaft. This design ensures that it is simple to generate power, which is the most prominent advantage. The disadvantage of microturbine is that its AC power frequency is very high, ranging from 1500-4000 Hz. This is because its electric generator is directly coupled with the power turbine whose rotating speed is between 50000-120000 rpm. Therefore, a power conditioner is essential for synchronizing the power frequency to 50 or 60 Hz.

A two-shaft microturbine is shown in Fig. 1.2. In this microturbine, the processes of compressing air and power generation are separated. An additional power turbine is utilized for this purpose, while the turbine connected with a combuster is only coupled with the air compressor. A gear box is installed for adjusting the rotation speed to a lower level than the compressor shaft, ranging from 3000-3600 rpm. This design promises that the AC power generated is with a lower frequency than that of a single-shaft microturbine, eventually to 50 or 60 Hz. Compared with a single-shaft one, a two-shaft microturbine is more expensive, caused by the more complex manufacturing and the more maintenance demand. However, a two-shaft microturbine is easier to be integrated into a power system for no requirement of power electronics interface.

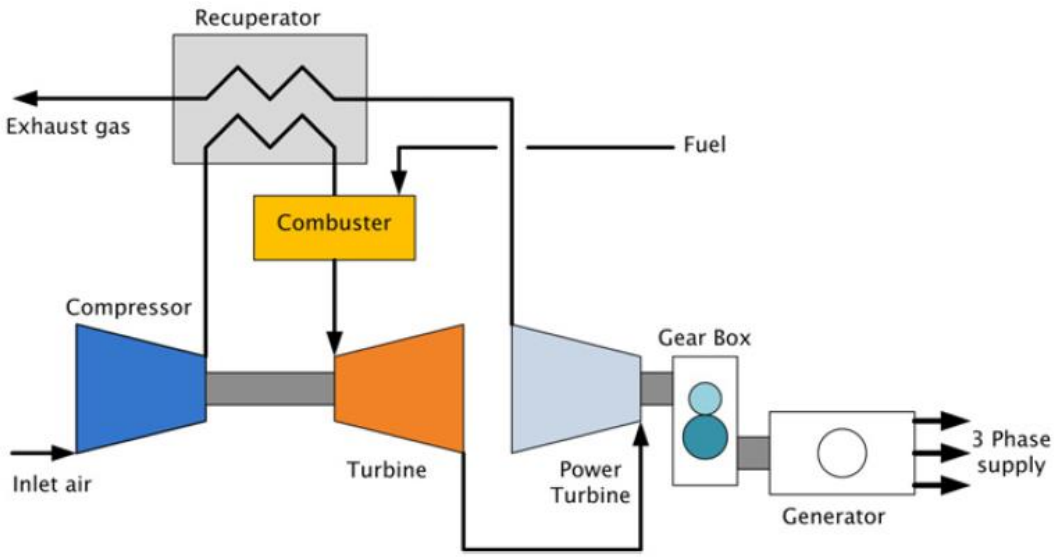

Figure 1.2. Schematic Diagram of a Two-shaft Microturbine [5].

1.1.2 Solar and Wind Energy

Solar energy is in a form of DC power generated by PV cells. Discrete PV cells are arranged in series and then in parallel, forming a module, to increase their output voltage and current. For connecting to an electrical power system, an inverter is essential to convert the DC power into AC power for practical use. The factors influencing the PV output power include solar irradiance, temperature, humidity, PV module cooling, humidity, and surface condition [6]. The solar irradiance is the most decisive factor among those, as Fig 1.3 from [7] shows the PV output voltage and current are affected by solar irradiance (G_T).

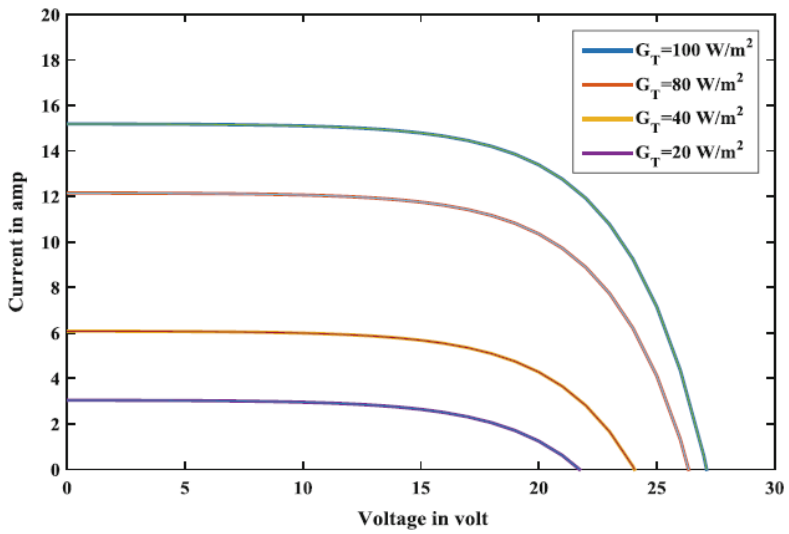

Figure 1.3. Variation in I–V Curve When Solar Irradiance Value Changes [7].

The major advantage of PV is environmentally friendly since there is no pollution and greenhouse gas emission during the power generation process. Besides, with the advanced development of PV technologies, the efficiency of power generation has been continuously increasing, while the manufacturing costs are continuously decreasing, given by [8], [9]. This fact enhances economic competitiveness of PV installation and utilization. However, unpredictability and intermittency of the power generation majorly caused by the irradiance bring challenges and risks to power system operation.

The mechanism of a WT is firstly converting kinetic energy of wind into mechanical energy of its rotor, then converting the mechanical energy into electricity with a proper generator. The relationship between the wind speed and the output power is shown in Fig. 1.4 from [10]. Three critical wind speeds are cut-in wind speed, rated wind speed, and cut-off wind speed, which are used to determine the output power.

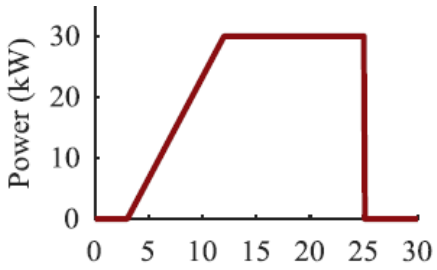

Figure 1.4. Wind Power Generation Function [10].

Cut-in wind speed is the minimum wind speed at which a WT can generated electrical power.

Rated wind speed is the minimum wind speed at which a WT can generate the rated power.

Cut-off wind speed is the maximum wind speed which a WT can withstand.

The advantages of wind energy are similar to those of solar energy, including the environmentally friendly, renewable and sustainable features. Compared with PV, the capacity of a single WT can be much larger. For example, the capacity of Sierra onshore WT manufactured by GE is 3 MW [11]. As the main drawback, the wind energy is also stochastic, uncertain, and intermittent.

1.2 Microgrid

Microgrid, as a technical concept, is firstly introduced in [12] and [13] as a reliable operation platform for DERs. The benefits of microgrid, such as economical savings, a proper solution for renewable integration and enhancing grid resilience, have been recognized. the scale of microgrid is changing from <1 MW to 2–10 MW, and even 60–100 MW in the recent years [14].

In [15], microgrid is defined by CIGRE working group C6.11 as below.

Microgrids are electricity distribution systems containing loads and distributed energy resources, (such as distributed generators, storage devices, or controllable loads) that can be operated in a controlled, coordinated way either while connected to the main power network or while islanded.

On the other hand, the definition given by IEEE in [16] provides the main features of a microgrid. A microgrid is composed by a set of interconnected loads, a certain number of DERs and managed with hierarchical control schemes. Besides, microgrids have a clear electric boundary which can be considered as a local electric power system [17]. Most of microgrids are connected to upstream area electric power systems of distribution level by the point of common coupling (PCC). For the main utility grid, these grid-connected microgrids are regarded as individual autonomous entities, which are capable of operating in grid-connected and island modes as well as seamless transition between two modes. Some microgrids are always isolated from the main grid, and only operate in the islanded mode, which can be named stand-alone or islanded microgrids. Comparing the two definitions, [16] further involves the operation modes.

The microgrids can significantly assist development of smart grid. For the smart grid construction, typical challenges include renewable energy integration, bidirectional communication systems, ineffective utilization of DG, as well as insufficient grid infrastructure and storage [18]. At the same time, the essential requirements for microgrids, helping the smart grid development, are summarized by [19] as follows.

1. Supply main local load and exchange energy with main utility grid.
2. Capable of handling intermittent renewable energy sources (RESs).

3. Capable of measuring critical parameters of the grid (voltage, current, active and reactive power, load demand) with smart meters and sensors.

4. Secure and reliable communication among system components.

Since a microgrid can be defined as an autonomous entity with a series of requirements to be qualified. There are noteworthy aspects of microgrid planning and operation. In the microgrid planning and operation, economic efficiency, system stability and reliability as well as environmental concern can be optimization objectives [16]. To achieve an efficient design, load and renewable output power forecasting, DER configuration, power balancing, operating constraints, system self-protection capability for system faults are all essential in consideration. In the following two sub-chapters, literature review on the existing works of grid-connected and island microgrids is presented.

1.2.1 Grid-Connected Microgrid

In [20], an optimal power flow (OPF) method for a grid-connected microgrid with PV units and batteries is proposed to obtain an economically optimal solution, with forecast of PV output power and load. In [21], the authors present an economic dispatch (ED) algorithm for microgrids. Dispatchable and non-dispatchable DG units are considered, the output power of dispatchable DG is optimized to realize an economical operation. In [22], the authors focus on control strategy for energy storage systems (ESSs) in a grid-connected microgrid. The non-dispatchable DG output power and user load demand are predicted by an advanced prediction algorithm which integrates weather and electricity market information. With predicted data, a mixed integer linear programming problem is formulated and solved over a rolling horizon window. In [23], an energy management problem with two targets, which are providing reliable power supply for local loads and participating in utility grid frequency regulation, is proposed. The microgrid modelled in [23] is composed of non-dispatchable DG units, ESSs, deferrable loads and uncontrollable loads. The uncertainties of renewable output power and loads are considered in energy management system (EMS) optimization and solved by a chance constrained programming method. In [24], a two-layer EMS for a microgrid which consists of batteries and supercapacitors is proposed. The degradation of the hybrid energy storage devices is premeditated. The system operating cost is

minimized on the first layer while the power fluctuations caused by forecasting errors is minimized on second layer. In [25] and [26], a dynamic economic dispatch algorithm based on quadratic programming is proposed for minimizing operating cost of a microgrid with PVs, batteries, and loads, by optimizing the state of charge (SOC) of batteries. In [27], a group of interconnected grid-connected microgrids are operated together, while the power exchange among the microgrids is incentivized over the power exchange with the main utility grid. A multi-objective problem, minimizing the costs for buying electricity from local microgrids and utility grid, minimizing the peak shaving cost, maximizing profits by selling electricity to local microgrids and utility grid, is solved using a compromise programming approach. In [28], a dispatch optimization problem for a microgrid is modelled with considering economic performance, gas emission, peak shaving, and load curve smoothing, and it is solved in a decentralized framework. The output power of renewable DG and loads are also considered and addressed. In [29], a robust control method for a grid-connected microgrid is proposed to minimize the overall economic cost under the worst case of load and PV power output. In [30], the authors introduce an energy management and system control method for a grid-connected microgrid, considering two energy storage operation modes dependent on whether the sum of available PV output power can cover the load demand. Besides, a strategy of power sharing according to the SOC of batteries is adopted for reducing charge/discharge rates during long-term operation.

From the above literature review, it can be clearly found that since the power mismatch caused by the non-dispatchable DG devices (such as PV and WT) and the load demand can be addressed by the power exchanged with the main utility grid, dispatchable DG devices may not be implemented in a grid-connected microgrid in most instances. The major target of grid-connected operation research is economic enhancement with a reasonable operation and control strategy on the microgrids.

1.2.2 Islanded Microgrid

In [31], a two-layer energy management approach of an islanded microgrid is proposed while dispatchable DG units, RES, ESS, interruptible loads and rigid loads are considered. The objective for the islanded operation mode is to maximize contentment rate of load supply with the minimum

cost. In [32], an EMS designed for a microgrid located in a remote area, operating only in the islanded mode, is proposed to minimize the fuel cost of dispatchable diesel generator. The control variables include diesel generator set points, on-off states and SOC of batteries, while the forecast of renewable output power and load demand is the input data for this EMS. In [33], a centralized EMS for a multi-party microgrid is introduced, while power balance is used as a constraint in optimization for maintaining microgrid stability. In [34], the authors focus on microgrid islanded operation caused by the main grid fault during natural disasters. The objective is to maximize the critical loads to be picked up after unexpected islanded operation, while the automatic switches determine the line open/closed state and the load connected/disconnected state to form a new topology of microgrid. Similarly, the authors of [35] focus on load restoration during unscheduled islanded operation. Compared to [34], the uncertainties of islanded operation duration and output power of RES are considered and formulated via a stochastic optimization problem. In [36], a stochastic optimal planning method for a stand-alone microgrid is proposed. The variables to be optimized include the number and type of WTs and diesel generators, the capacity of PVs, the type and placement of batteries as well as the capacity of converters for batteries. There are multiple objectives such as minimizing the net present cost and the pollutant emission, and the multi-objective optimization problem is solved by Non-dominated Sorting Genetic Algorithm II (NSGA II). The authors of [37] study networked microgrids planning considering contingent islanded operation. Compared with [36], second-order conic programming constraints of power flow are applied to obtain bus voltages and line currents which are restricted in practice. Besides, due to involving integer variables, a Benders decomposition technique is adopted to solve this mixed integer second-order conic programming problem. The authors of [38] consider switching between grid-connected mode and islanded mode, aiming at preventing load shedding. An adaptive robust optimization method with a column-and-constraint generation algorithm is utilized to deal with uncertainties caused by renewable output power and grid connection condition. Similar to [38], islanding is also considered as an uncertainty in [39] and [40]. From an uncertainty-consideration point of view, the authors of [39] develop multistage stochastic optimization to deal with the islanding uncertainty, while improving microgrid multi-period islanding criterion is introduced in [41] for reducing computing burdens. In [40], a model for determining islanding occurrence probability is proposed. The concept of the model is similar to

Bernoulli experiment, while islanding is treated as "success" of the experiment. Stage and step are time units of the model, and each stage consists of a certain number of steps. Once islanding occurs at any step, it lasts till the end of current stage. In [42], an EMS for islanded microgrid including various DG units, ESSs, critical and flexible loads is proposed. A chance-constrained model is used to formulate the power balance conditions for allowing specified small-probability power unbalance to occur, which can benefit maximizing economic costs.

From the above literature review, the topics for islanded microgrid research can be classified as planning and operation of islanded microgrid, and the unexpected switch between grid-connected and islanded modes. It can find the different objectives in terms of economic, technical and environment benefits. In addition, the features the above literatures have in common are considering the uncertainties caused by renewable power outputs, loads and operation mode states. It is worth noting that these uncertainties adversely affect islanded operation efficiency and even stability and security. Various optimization approaches such as stochastic optimization and robust optimization, are normally utilized to deal with the uncertainties.

1.3 Power Flow Models

A power flow model plays an important role in a power system planning of operation problem, normally used as equality constraints in the optimization problem for estimating the network operating conditions. The results including bus voltages, branch currents and power flows gained by the power flow model are expected to be kept within limits. In this sub-chapter, two widely used power flow models are introduced and discussed in terms of accuracy and computing complexity.

1.3.1 Dist-Flow

Distribution load flow, as known as Dist-Flow, is firstly proposed in [43]. Its core idea is to calculate the power values in a recursive manner. The structure of a radial network can be illustrated as Fig. 1.1.

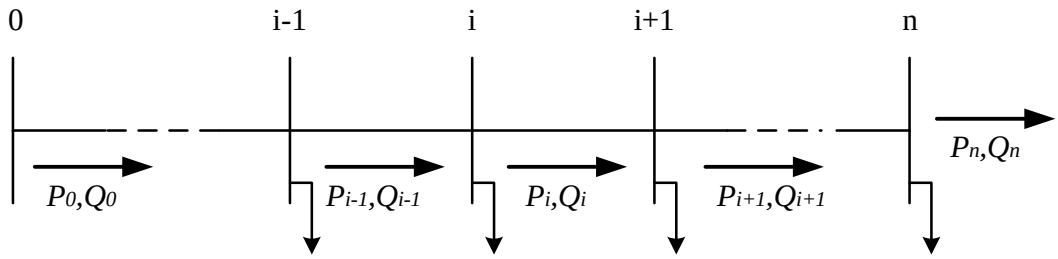

Figure 1.5. One-line Diagram of Radial Distribution Network (Used for Dist-Flow).

The power flow equations from sending end i to receiving end $i+1$ are written as follows.

$$P_{i+1} = P_i - r_i \frac{P_i^2 + Q_i^2}{V_i^2} - P_{Li+1} \tag{1.1}$$

$$Q_{i+1} = Q_i - x_i \frac{P_i^2 + Q_i^2}{V_i^2} - Q_{Li+1} \tag{1.2}$$

$$V_{i+1}^2 = V_i^2 - 2(r_i P_i + x_i Q_i) + (r_i^2 + x_i^2) \frac{P_i^2 + Q_i^2}{V_i^2} \tag{1.3}$$

Herein, r_i and x_i are resistance and reactance of the line from bus i, P_i and Q_i are active and reactive power of the line from bus i, and V_i is the bus voltage at the sending end i. Besides, P_{Li+1} and Q_{Li+1} are active and reactive power of the loads. By assuming that the loads of all buses are constant, once P_i, Q_i, V_i are obtained, $P_{i+1}, Q_{i+1}, V_{i+1}$ can be further calculated via (1.1) - (1.3). It is noted that P_0, Q_0, V_0 are the key data to be known (or estimated) at the beginning of the calculation, so that other values can be obtained by applying (1.1) - (1.3) successively. Since the calculation begins with first node and ends with last node, this model can be named as a forward update model.

There is also a backward update model denoted by (1.4) - (1.7).

$$P_{i-1} = P_i + r_i \frac{P_i'^2 + Q_i'^2}{V_i^2} + P_{Li} \tag{1.4}$$

$$Q_{i-1} = Q_i + x_i \frac{P_i'^2 + Q_i'^2}{V_i^2} + Q_{Li} \tag{1.5}$$

$$V_{i-1}^2 = V_i^2 + 2(r_i P_i + x_i Q_i) + (r_i^2 + x_i^2) \frac{P_i^2 + Q_i^2}{V_i^2} \tag{1.6}$$

$$P_i' = P_i + P_{Li}, Q_i' = Q_i + Q_{Li} \tag{1.7}$$

This backward update model requires calculating the sending end results with the receiving end known inputs. Hence, the data of the last node needs to be known (or estimated).

However, when utilizing the above equations as constraints in an optimization problem, the quadratic parts as non-convex terms are obstacles for solution efficiency, leaving an issue of computing complexity.

As the quadratic terms are the power losses through the branch lines, they are much smaller than their corresponding power flows. The approximated equations for (1.1) - (1.3) are further developed by ignoring the branch power losses as below.

$$P_{i+1} = P_i - P_{Li+1} \tag{1.8}$$

$$Q_{i+1} = Q_i - Q_{Li+1} \tag{1.9}$$

$$V_{i+1}^2 = V_i^2 - 2(r_i P_i + x_i Q_i) \tag{1.10}$$

Furthermore, simplification for (1.10) is essential to linearize the quadratic terms. This work is done by the authors of [44]. By assuming $(V_i^2 - V_0^2) \approx 0$, it is reasonable to get $V_i^2 \approx V_0^2 + 2V_0(V_i - V_0)$. With this assumption, (1.10) is linearized as follows.

$$V_{i+1} = V_i - \frac{(r_i P_i + x_i Q_i)}{V_0} \tag{1.11}$$

Thus, a linearized Dist-Flow model is formed by (1.8), (1.9) and (1.11).

The Dist-Flow models are widely used in power system optimization problems. In [45], the authors relax the original Dist-flow equations to inequalities and transform them into a second-order cone form for a distribution system OPF problem. In [46], (1.8)-(1.10) are applied to an operation problem whose objective is to minimize the active power required by a distribution system over discrete time steps by controlling PV inverters and energy storage devices. In [10], [47] and [48], the linearized model proposed by [44] is adopted as power flow constraints in optimization problems. The authors of [10] focus on a long-term DG planning problem, developing a probability-weighted robust optimization with a new solution algorithm. In [47], a planning problem for enhancing distribution network resilience is formulated with the linearized

Dist-Flow constraints. In [48], the linearized Dist-Flow model is used in a voltage/var control problem.

The main reason that they choose the linearized model is to reduce the computing burdens, thus making the problems solvable to commercial solvers, which is regarded as an advantage of the Dist-Flow model. However, such approximations to the original model may lead to large errors, causing low accuracy issues.

It is worth noting that the Dist-Flow model requires a slack bus and it is suitable for planning and operation optimization problems of grid-connected microgrid. However, it does not work for problems of islanded microgrid.

1.3.2 Direct Load Flow

The direct load flow model is firstly proposed by [49] with two effective matrices based on the network topology and branch impedances, i.e., bus-injection to branch-current (BIBC) matrix and branch-current to bus-voltage (BCBV) matrix.

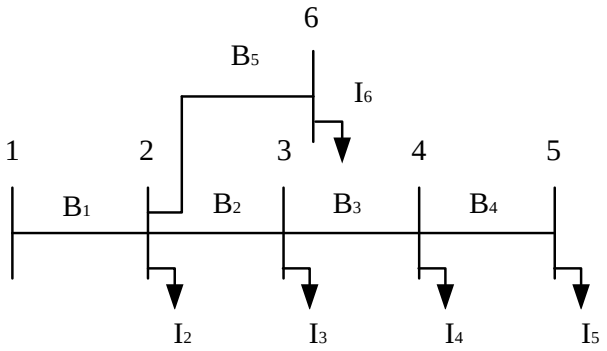

Figure 1.6. One-line Diagram of Radial Distribution Network (Used for Direct Load Flow).

The basic concepts of this direct load flow model are demonstrated in Fig. 1.6. Herein, B and I represent branch currents and bus injection currents, respectively. The complex power of the load at bus i is denoted by $S_i = P_i + jQ_i$. Then, the bus injection current is denoted by (1.12). With Kirchhoff's Current Law, the branch currents can be calculated by (1.13) and the parameter matrix is defined as the BIBC matrix.

$$I_i = \left(\frac{P_i + jQ_i}{V_i}\right)^* \tag{1.12}$$

$$\begin{bmatrix} B_1 \\ B_2 \\ B_3 \\ B_4 \\ B_5 \end{bmatrix} = \begin{bmatrix} 1 & 1 & 1 & 1 & 1 \\ 0 & 1 & 1 & 1 & 1 \\ 0 & 0 & 1 & 1 & 0 \\ 0 & 0 & 0 & 1 & 0 \\ 0 & 0 & 0 & 0 & 1 \end{bmatrix} \begin{bmatrix} I_2 \\ I_3 \\ I_4 \\ I_5 \\ I_6 \end{bmatrix} \tag{1.13}$$

$$[B] = [BIBC][I]$$

For a radial network, its BIBC matrix is determined by its topology. The procedure to derive the BIBC matrix is introduced as the following two steps.

Step 1: For a radial n-bus distribution network, there are $n-1$ branches in total. Since there is no bus injection current at the first bus, the BIBC matrix is a $(n-1) \times (n-1)$ matrix. For convenience, set all elements of the BIBC matrix equal to 0 at the beginning.

Step 2: Sequences of BIBC rows and columns represent the sequences of branches and buses, respectively. The matrix is formed column by column. For the i^{th} column (for the $(i+1)^{th}$ bus), if the current flows into the first bus from the $(i+1)^{th}$ bus through the j^{th} branch, the element at the i^{th} column and the j^{th} row of the BIBC matrix is set to 1. Otherwise, it is still equal to 0.

After calculating the branch currents with the BIBC matrix, the branch voltage variation over branch j is calculated by (1.14). With the voltage of bus 1 as a reference, the other bus voltages can be calculated by applying (1.14) successively. For all the buses, a BCBV matrix can be formulated based on this progress and shown in (1.15).

$$\Delta V_j = B_j Z_j \tag{1.14}$$

$$\begin{bmatrix} V_1 - V_2 \\ V_1 - V_3 \\ V_1 - V_4 \\ V_1 - V_5 \\ V_1 - V_6 \end{bmatrix} = \begin{bmatrix} Z_{12} & 0 & 0 & 0 & 0 \\ Z_{12} & Z_{23} & 0 & 0 & 0 \\ Z_{12} & Z_{23} & Z_{34} & 0 & 0 \\ Z_{12} & Z_{23} & Z_{34} & Z_{45} & 0 \\ Z_{12} & Z_{23} & 0 & 0 & Z_{36} \end{bmatrix} \begin{bmatrix} I_2 \\ I_3 \\ I_4 \\ I_5 \\ I_6 \end{bmatrix} \tag{1.15}$$

$$[\Delta V] = [BCBV][B]$$

The BCBV matrix is formulated by transposing the BIBC matrix and then replacing 1 with the corresponding branch impedances.

With these two matrices, branch currents and bus voltages are efficiently obtained with system parameters. However, V_i in (1.12) is not known at the beginning of calculation process. To address this obstacle, V_i^0 is assumed to be a certain value at the beginning. Then, the bus voltages are calculated by (1.12)-(1.15) and used to update V_i for the next round of calculation with (1.12)-(1.15). This is an iterative process which terminates until V_i^k, the result of the *k*th iteration, is approximately equal to V_i^{k-1}.

The direct load flow model is adopted in [50]-[54]. In [50], a multi-objective optimization model with distribution network reconfiguration is proposed and solved by a heuristic method. The direct load flow model is an internal program for obtaining bus voltages and branch currents of the system. The authors of [51] propose a loss allocation method for a multi-participant distribution network, while the direct load flow model is used to calculate the total power loss across the network. In [52], the direct load flow model is utilized for obtaining bus voltages in a voltage regulation model for a distribution network. In [53], the authors propose a linear power flow algorithm with proper approximation based on the direct load flow model, and then apply it to control flexible energy resources for guaranteeing customer service quality. The authors of [54] propose a new power flow method with the direct load flow model, and then apply it to a planning problem which optimizes placement and sizing of ESSs.

Compared to the Dist-Flow model, the direct load flow model has the higher accuracy as one advantage. However, such the iterative process required can result in computing complexity and burdens in the optimization problems. Besides, the direct load flow model is also not suitable for the islanded microgrid operation either.

1.4 Optimization Methodologies

From the literature review in Chapter 1.2, uncertainties caused by intermittent renewable power generation and load power consumption need to be carefully addressed. In this sub-chapter, two optimization methodologies to address uncertainties are briefly introduced and discussed.

1.4.1 Stochastic Optimization

A conventional deterministic optimization model can be expressed as follows. There is no consideration of uncertainties.

$$min\, f(x) \tag{1.16}$$

s.t. $$h(x) = 0$$

$$g(x) \leq 0$$

To consider uncertainties, a vector ξ is defined to present possible realization of the uncertainties and then a stochastic optimization model is formulated as follows.

$$\min f(x, \xi) \tag{1.17}$$

s.t. $$h(x, \xi) = 0$$

$$g(x, \xi) \leq 0$$

Since the realization ξ is unknown, the minimization function and constraints cannot be clearly defined. Thus, a large number of scenarios is generated to present the realization of the uncertainties, thus forming a scenario-based stochastic optimization model. The occurrence probability of each scenario can be calculated according to probability density function. A general scenario-based stochastic optimization is formulated as below.

$$min \sum_{s \epsilon S} \rho_s f(x, \xi_s) \tag{1.18}$$

s.t. $$h(x, \xi_s) = 0, \forall s \epsilon S$$

$$g(x, \xi_s) \leq 0, \forall s \epsilon S$$

Herein, ξ_s is a certain scenario of uncertainty realization, while ρ_s is the corresponding occurrence probability. Hence, the objective of (1.18) becomes an expectation corresponding to the probability density function (PDF) of uncertainties, while the consolidation of all the scenarios is considered in the constraints. This guarantees the solution of stochastic optimization is robust against all the scenarios.

In [55], a stochastic optimization method is applied for a security-constrained unit commitment problem to address uncertainties caused by load forecasting errors, transmission line faults and generation unit faults. The authors of [56] propose a two-stage stochastic program for unit commitment. The first stage aims to obtain commitment decisions, while the second stage is a stochastic optimization based dispatch for dealing with uncertainties of loads and available generation capacities. In [57], a stochastic optimization method is utilized to address wind energy uncertainty in an expansion planning model of a stand-alone microgrid. A stochastic optimization method is used to solve a distribution system energy management problem in [58] and a microgrid optimal operation problem in [59]. The authors of [60] develops a two-stage stochastic optimization method an EMS of microgrid with plug-in electric vehicles, aiming at minimizing power loss, while location of electric vehicle, vehicle battery capacity and electricity consumption per km are considered as uncertainties.

It is worth noting that stochastic optimization methods have some drawbacks. The first one is inaccurate PDF or non-existent PDF. An inaccurate PDF leads to a non-optimal solution without solution robustness. Another drawback lies in that a large number of scenarios cause heavy computing burdens. If a scenario reduction method is adopted for mitigating the computing burdens, a much less robust solution may be obtained.

1.4.2 Sensitivity Region Method

In [61], the authors introduce a sensitivity region (SR) method for assessing the robustness of design solution. Its mechanism can be described as that a candidate solution $\boldsymbol{x}_0$ is gained by a deterministic optimization with a certain realization of uncertainty $\boldsymbol{p}_0$, the robustness of $\boldsymbol{x}_0$ is evaluated and an indicator is sent to the deterministic optimization to obtain a better solution with the higher robustness. This progress is a bi-level solution approach and shown in Fig. 1.7.

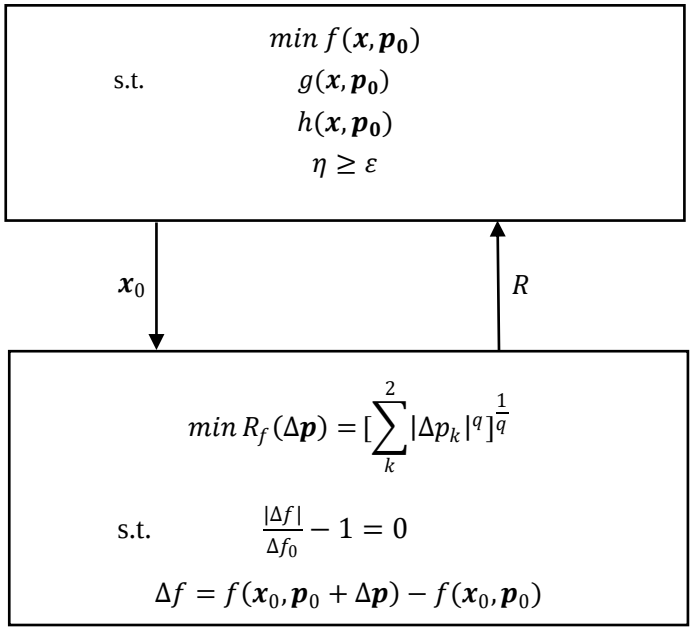

Figure 1.7. Bi-level Solution Approach to Robust Optimization.

In the lower level problem, the variation of objective result is caused by the changed realization of uncertainty ($\Delta \boldsymbol{p}$) while Δf_0 is the maximal acceptable variation of objective result. A set of $\Delta \boldsymbol{p}$ which meets the condition $\frac{|\Delta f|}{\Delta f_0} - 1 = 0$ forms a region in a normalized $\Delta \boldsymbol{p}$ space, named as a SR. The area is defined as the robustness (or sensitivity) of the design solution $\boldsymbol{x}_0$. Since it is hard to find the mathematical formulation of the SR, the Euclidean distances from all the points located at the bound of SR to the origin, denoted as $R_f(\Delta \boldsymbol{p})$, are calculated. The point with the shortest distance R is regarded as the worst case of the design solution, which is used to further enhance the robustness of $\boldsymbol{x}_0$. For example, if the $\Delta \boldsymbol{p}$ space is a two-dimension space, all possible values of $\Delta \boldsymbol{p}$ form a rectangle which is further normalized to a square, and its circumcircle radius is R_E. A robustness index is determined as $\eta = \frac{R}{R_E}$ which is expected to be enlarged enough. This bi-level optimization model can be solved by a heuristic algorithm such as a genetic algorithm (GA). The robustness indices of individuals directly influence offspring generation in the GA.

In [62], a SR method is applied for a microgrid planning problem where STATCOMs are installed for enhancing voltage stability, while load and wind power are regarded as uncertainties.

Despite the SR method has the advantages of wide applicability and adjustable robustness degree, its disadvantage is also obvious in terms of computing complexity. However, this method can be used for planning problems and assessment of long-term system performance.

1.5 Hosting Capacity

DG penetration growth is driven by a variety of factors, such as environmental concern, economic effectiveness and policy [63]. From an environmental perspective, renewable DG devices play an important role in reducing greenhouse gas emissions. Stated by [64], European countries agree on increasing investment in renewable energy. From an economic perspective, DG units are economically advantageous over constructing long transmission lines and large power plants. Besides, Singapore invests significantly in renewable energy for saving lands. Moreover, renewable DG devices contribute to the construction of energy security for those countries whose energy severely depends on imports.

However, the growth of DG penetration also adversely influences the system performance. Overvoltage, decline in power quality, thermal overloading in transmission lines and transformers, and protection equipment faults are typical issues. Hence, it is necessary to carefully determine new DG integration. On the other hand, it is imperative to evaluate the system maximum bearable DG integration, which bring in the concept of hosting capacity of a network. The definition of HC is given in [65] as *"the amount of distributed generation, integrated into the power system, above which the system performance becomes unacceptable."*

In [66], the authors apply ESSs, reactive power compensation sources and network reinforcement strategies to realize increased performance in integrating large-scale renewable DG units. A multi-stage stochastic optimization method is developed to optimize the support measures and renewable DG integration jointly. In [67], a probabilistic assessment method of hosting capacity, considering uncertainties caused by PV, WT and load, with a sparse grid technique is proposed. This method demonstrates its benefit of a fast-computing speed, compared to a conventional Monte Carlo simulation based method. The authors of [68] improve DG hosing capacity with network reconfiguration. Voltage control by on-load tap-changing transformers,

DG power factor control and power curtailment as well as dynamic reconfiguration with remotely controlled switches are utilized. A mixed integer non-linear OPF model is formulated, then several relaxions are applied for reducing the computing burden. In [69], the authors introduce a concept, i.e., interval overvoltage probability, to evaluate the overvoltage risk which is caused by uncertainties of load and PV in a three-phase distribution network. The uncertainties are addressed with affine arithmetic and interval arithmetic while their results are validated with compared to that of a conventional stochastic method. In [70], the authors propose a stochastic optimization method of hosting capacity to deal with the uncertainties including load, the PV power output corresponding to solar irradiation, and PV location. In [71], a multi-objective optimization for maximizing PV hosting capacity and minimizing voltage deviation is proposed. Smart inverter control, PV and battery energy storage system (BESS) optimal placement, sizing and dispatch are utilized in the optimization model.

It is essential to assess and enhance renewable power hosting capacity of a power system, but there is not any report demonstrating model or method for high-renewable islanded microgrid, leaving a research gap.

1.6 Research Problem Statement

From Chapters 1.2-1.5, some imperative research problems can be found, in terms of microgrid operation, system stability and optimization method, as well as hosting capacity assessment and maximization. The research problems which would be solved by this thesis are summarized as follows.

Firstly, the two introduced power flow models are not suitable for islanded microgrid OPF and other power flow calculation methods have to relax or approximate the models when used for optimization constraints. Thus, there is a significant research point for developing an efficient islanded microgrid OPF method with a suitable power flow model. Besides, uncertainties of load and renewable DG should also be addressed by this OPF method, and an effective uncertainty scenario sampling method is expected.

Secondly, a contingency of the main grid, resulting in a sudden disconnection to a microgrid can impair the microgrid internal operation, i.e., the islanded microgrid operation, leading to system instability and operating constraint violations. Hence, a security-constrained model for the situation of tie-line switching from the grid-connected to the islanded operation mode is of research significance. Besides, due to the model complexity, a new solution algorithm is expected to be developed.

Thirdly, the islanded microgrid hosting capacity maximization is limited by the operating constraint violations caused by the uncertainties. On the other hand, since the stochastic optimization method cannot guarantee solution robustness on both objective and constraints, a new method for dealing with the uncertainties is worth being developed. Besides, the system frequency deviation is a vital indicator for islanded microgrid operation. Therefore, it should be a significant optimization objective as well when assessing the islanded microgrid hosting capacity.

1.7 Research Contributions

The emphasis of this thesis is the optimal operation of an islanded microgrid with controllable and non-controllable DG units for minimizing the system operating cost and maximizing the hosting capacity while preventing violations of the operating constraints with full consideration of the uncertainties. Firstly, a stochastic OPF method for an islanded microgrid has been developed and improved with high computing efficiency. This OPF method has been further extended for fully considering the tie-line switching between the grid-connected and islanded operation modes, while a new solution algorithm has been developed to handle the coupling constraints of the two modes. This OPF method is also the basis for a hosting capacity maximization problem. A SR based optimization method which can guarantee solution robustness on both objective and constraints as well as adjust robustness level quantitatively has been established. In the comprehensive case study, numerical simulation results have validated the efficiency and advantages of the proposed models and methods, in comparison with the existing ones.

The contributions of this thesis can also be categorized as follows.

Contributions to OPF method

1. A stochastic OPF method for an islanded microgrid based on a backward forward sweep (BFS) power flow calculation method.
2. A stochastic OPF method addressing tie-line switching from the grid-connected to islanded mode of a microgrid and guaranteeing system stability and operating security.

Contributions to Optimization Model

1. An optimization model for renewable generation hosting capacity of an islanded microgrid, with the system frequency deviation considered as an objective.
2. A SR based optimization model to quantify the solution robustness on both objective and constraints.

Contributions to Solution Algorithm

1. An enhanced solution algorithm for the proposed stochastic OPF method.
2. A Benders decomposition based solution algorithm to address the coupling constraints of grid-connected and islanded modes.
3. An effective solution algorithm solving the SR based optimization model while involving the islanded microgrid power flow calculation.

1.8 Thesis Outline

In Chapter 1, the background of DG and microgrid is briefly introduced, showing the related existing issues given by the literature. Then, two widely used power flow models and two optimization approaches to deal with uncertainties are introduced, while the literature review shows their application conditions. Furthermore, the concept of hosting capacity is introduced and the research gaps are discussed. At the end of Chapter 1, the research motivations and contributions, as well as the thesis outline are given.

In Chapter 2, a stochastic OPF method for islanded microgrid considering droop control of microturbines is proposed and presented. A linear power flow model is utilized to formulate network operating constraints of OPF. Besides, non-linear operating constraints are linearized to reduce computing burdens. Then a stochastic optimization method is applied for handling uncertainties caused by load and PV power generation. Last, the results obtained by the proposed OPF method is verified by a real-time test.

In Chapter 3, based on the OPF method proposed in Chapter 2, an enhanced method for islanded microgrids is developed with a new solution algorithm. Besides, a probabilistic modelling method is developed for representative scenario sampling to deal with uncertainties in the stochastic optimization method. Compared to that of Chapter 2, the stochastic OPF method of Chapter 3 can achieve a faster computing speed, better for practical use.

In Chapter 4, tie-line switching from the grid-connected to the islanded mode is identified as the main problem to address. Grid-connected OPF and islanded OPF models are formulated and then coupled in the development of a new security-constrained OPF method. To solve the developed complex optimization problem, a Benders decomposition based solution algorithm is proposed with applying a stochastic optimization method to deal with the uncertainties. In case study, the effective convergence of the proposed OPF method, the robustness and security checks, in comparison with conventional methods, are demonstrated.

In Chapter 5, maximizing the hosting capacity of an islanded microgrid is modelled as an optimization problem with minimizing the system frequency deviation as well. A SR based optimization method is developed for dealing with uncertainties of renewable generation and load. Herein, two robustness indices are defined to quantify solution robustness on both objective and constraints. In case study, the convergence of the solution process and the solution robustness are tested, and the sensitivity analysis is carried out, verifying the high efficiency of the proposed hosting capacity maximization method.

In Chapter 6, conclusions of this thesis and future works are given.

The relationship among Chapters 2-5 is described in Figure 1.8. As it shows, the work of Chapter 3 is developed from the work of Chapter 2, while Chapters 4-5 are based on Chapters 2-3.

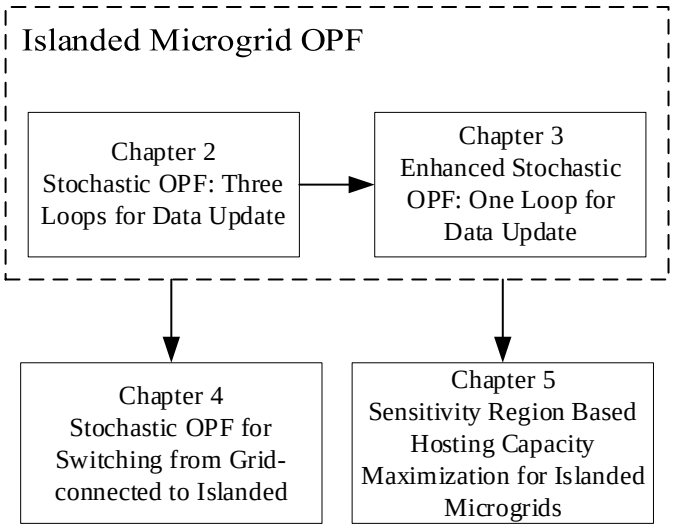

Figure 1.8. Relationship Among Chapters 2-5.

Chapter 2 STOCHASTIC OPTIMAL POWER FLOW FOR ISLANDED MICROGRIDS CONSIDERING DROOP CONTROL

Renewable power generators such as photovoltaic (PV) panels penetrate fast in islanded microgrids where microturbines can provide droop control to keep the system reliable and stable. However, renewable power generation is highly intermittent and uncertain, impairing microgrid operation. To address the uncertainty issue, this chapter proposes a stochastic optimal power flow (OPF) approach for islanded microgrids considering droop control of the microturbines. In this OPF, microturbine generation set points are optimized to minimize the total operating cost while keeping operating constraints. Moreover, frequency and voltage droop control functions of the microturbines are modelled in the OPF. Monte Carlo sampling and a backward reduction method are applied to generation scenarios which model uncertainty realization in stochastic optimization formulation. Accordingly, a solution algorithm based on the backward forward sweep (BFS) algorithm is developed to solve the proposed stochastic OPF problem. The proposed stochastic OPF is tested on an islanded microgrid system with real-time uncertainty realization simulation and the results show high operation reliability under the uncertainties.

2.0 Nomenclature

A. Sets and Indices

K, k	The set and the index of scenarios
i, j	The index for microgrid buses
t	The index for iterations

B. Parameters

a	The cost parameters of generation ($/kW)

b	The penalty cost of load shedding ($/kW)
V_{min}, V_{max}	Operating voltage lower/upper limit (p.u.)
Δf_{max}	Maximal frequency deviation limit (p.u.)
$\Delta U_{r,max}$	Maximal reference bus voltage deviation limit (p.u.)
m_p, m_q	Coefficients of frequency droop and voltage droop
V_0	Reference voltage (p.u.)
P_{Li}, Q_{Li}	Active/reactive load demand at Bus *I* (kW/kVar)
$S_{Gi,max}$	Generator thermal capacity (kVA)
γ	The node incidence matrix of microgrids
Z_{branch}	The branch impedance matrix (p.u.)
ε	Termination threshold
ρ_k	The probability of scenario k

C. Variables

C_g	Generation cost ($)
C_{ls}	Load shedding cost ($)
P_{Gi}, Q_{Gi}	Real-time generator active/reactive power output at Bus *I* (kW/kVar)
P_{G0i}, Q_{G0i}	Set point of generator active/reactive power output at Bus *I* (kW/kVar)
P_i, Q_i	Active/reactive power injection at Bus *I* (kW/kVar)
P_{pvi}	PV power generation at Bus *I* (kW)
I_{node}	Bus injection current (A)
I_{branch}	Branch current (A)
V_r	Reference bus voltage (p.u.)
V	Bus voltage (p.u.)
$\Delta P_{Gi}, \Delta Q_{Gi}$	Real-time generator active/reactive power output variation at Bus *I* (kW/kVar)
ΔU	Branch voltage drop (p.u.)
Δf	Frequency deviation (p.u.)
ΔU_r	Reference bus voltage deviation (p.u.)
LS	Load shedding percentage (%)
P_{lsi}	Shed power load demand at Bus *I* (kW)

2.1 Introduction

With the development of renewable energy sources (RESs) such as PV generation systems, microgrids become increasingly attractive as they support an efficient platform to integrate RESs. Microgrids have economic and technical advantages such as cost-efficient energy management, reliable and flexible operation and self-healing ability. Microgrids can exchange power with the main grid in the grid-connected mode or support the local loads independently in the islanded mode. Normally, the islanded mode aims to minimize the total operating cost while keeping the system reliable and stable and the grid-connected mode aims to maximize the profits for the operators due to transactions with the main grid [72].

Considering these two aims, OPF methods for microgrids have been developed as a research focus. The works of [73], [74] propose a two-stage decision process where the first stage is unit commitment and the second stage is an OPF model. The OPF in [73], [74] is nonlinear programming which may lead to low efficiency of the optimization and even failure to solve. In [75], [76], the OPF model with frequency considered aims to minimize the unsupplied load demand and the distributed generator operating cost. The authors of [75], [76] use a set of linearization formulation to convert the nonlinear OPF into a linear programing problem with complicated linearization process. In the above works, the high non-linearity of the OPF models bring a challenge for microgrid operation.

To conquer this challenge, a direct load flow method is developed in [49]. This method can linearly compute microgrid power flow with network topology and parameters which can be expressed as two matrices, i.e., bus-injection to branch-current matrix (BIBC) and branch-current to bus-voltage matrix (BCBV). These two matrices can be formed offline, which can efficiently simplify the OPF model and reduce the computing time. However, this original direct load flow is not suitable for islanded microgrids since the droop-based generator and system frequency cannot be modeled. The work of [77] reforms the direct load flow with integrating generator droop control into the power flow problem. More importantly, this work develops a BFS algorithm to solve the droop-based islanded microgrid power flow problem. A significant advantage of BFS is that the frequency is computable which enables to consider the droop-based OPF. In addition, adding frequency constraint can be implemented in a droop-based OPF. The BFS algorithm uses

frequency calculation to update the droop control results and it updates bus voltage until converging to a threshold. Furthermore, ref. [78] modifies the BFS based power flow with AC load deviations caused by frequency. It is also verified in [78], the BFS base power flow method can be also further developed into an OPF model. Thus, the non-linearity issue can be solved by the BFS based OPF model.

Besides, as the RESs penetrate fast in power systems, uncertainty degree increasingly impairs the islanded microgrid operation, leading to issues such as over/under voltage and large frequency deviations. Ref. [41], [79] consider the islanding uncertainty issues including islanding time and duration standpoints in the OPF model, but without considering system operating constraints such as bus voltage limits. On the other hand, the uncertain renewable power generation also negatively impacts the operating costs in microgrids [80]. To address the uncertainties, stochastic optimization methods which model the uncertainties as scenarios provide an efficient way. The stochastic optimization is applied by [55] to solve security-constrained unit commitment problems with load uncertainty scenario modelling. In [81], a stochastic model is used to model the intermittent RESs such as wind power. Furthermore, [82] applies this method for microgrid energy management problems with modelling the intermittent RESs in scenarios. In [83], the method proposed in [78] is developed to a stochastic power flow. It can be proved by these works that applying the stochastic optimization method to deal with microgrid system uncertainties is efficient.

However, the BFS based PF for islanded in microgrid [77] has not been developed with the stochastic optimization model to address the uncertainties, leaving a research gap.

Based on the above literature review, the uncertainty issues have not been efficiently solved in the islanded microgrid operation. Thus, this chapter proposes a stochastic OPF method utilizing droop-based BFS power flow. The uncertainties of load demand and PV power are considered in this OPF through a small number of scenarios. The proposed stochastic OPF is verified by a test on an islanded microgrid system with real-time uncertainty realization simulation.

2.2 Droop Control Based Optimal Power Flow

2.2.1 Objective Function and Constraints

2.2.1.1 Objective Function

The objective of this OPF problem is to minimize the total operating cost consisting of the generation and the load shedding penalty cost. The generation and load shedding costs are presented by (2.1) and (2.2) respectively. The overall objective function is further formed by (2.1) and (2.2) as (2.3).

$$C_g = \sum a \times P_{Gi} \tag{2.1}$$

$$C_{ls} = \sum b \times P_{lsi} \tag{2.2}$$

$$\min C_g + C_{ls} \tag{2.3}$$

2.2.1.2 Power Flow Constraints

The power flow constraints are a set of equations representing the relationship between variables and system parameters. These constraints are used for power flow calculation procedure and they are modelled as the follows.

$$P_{Gi} = P_{Gi0} + \Delta P_{Gi}, \Delta P_{Gi} = \frac{\Delta f}{m_{pi}}, \forall i \tag{2.4}$$

$$Q_{Gi} = Q_{Gi0} + \Delta Q_{Gi}, \Delta Q_{Gi} = \frac{\Delta U_r}{m_{qi}}, \forall i \tag{2.5}$$

$$P_i + Q_i = (P_{Gi} + jQ_{Gi}) - (1 - LS)(P_{Li} + jQ_{Li}) + P_{pvi}, \forall i \tag{2.6}$$

$$I_{nodei} = \frac{P_i - jQ_i}{V_i^*}, \forall i \tag{2.7}$$

$$I_{branch} = [BIBC] I_{node} \tag{2.8}$$

$$\Delta U = [BCBV] I_{branch} \tag{2.9}$$

$$V = V_r - \Delta U \tag{2.10}$$

$$\Delta f = -m_{peq}\left[P_{Li} - P_{Gi0} + Re\left(\sum U_i I_{ij}^*\right)\right], \forall i \tag{2.11}$$

$$\Delta U_r = -m_{qeq}\left[Q_{Li} - Q_{Gi0} + Im\left(\sum U_i I_{ij}^*\right)\right], \forall i \tag{2.12}$$

$$V_r = V_0 - \Delta U_r \tag{2.13}$$

Equations (2.4) and (2.5) describe frequency droop control by active power generation and the voltage droop control by the reactive power generation of microturbines. The real-time power generation output consists of the base output which is determined by the set point and the real-time output variation which is determined by the droop control functions.

Eq. (2.6) calculates the power injection at each bus which consist of microturbine power generation, PV power generation and load demand with shedding implemented. Then based on the power injection, the injection current at each bus is calculated by (2.7).

The branch current is calculated by (2.8) based on the bus injection current with the help of the BIBC matrix. Then, the branch current is further used to compute branch voltage drop with the help of the BCBV matrix in (2.9). BIBC matrix and BCBV matrix are derived by the node incidence matrix of the microgrid γ which describes the relationship between buses and branches. The node incidence matrix is a $N_b \times N$ matrix. N_b is the number of branches and N is the number of buses. The elements of the node incidence matrix are defined as:

1) $n_{bi} = 1$, when the current of branch *b* leaves bus *i*;

2) $n_{bi} = -1$, when the current of branch *b* flow toward bus *i*;

3) $n_{bi} = 0$, when no connection exists between branch *b* and bus *i*.

For a pure radial system, $N_b = N - 1$. To make the node incidence matrix reversible, the column of reference node which provides the reference voltage for the system in the backward process is eliminated. The reason is that the reference node is not used in BFS power flow backward process. With the node incidence matrix, BIBC and BCBV are derived as the follows respectively.

$$\mathrm{BIBC} = (\gamma^{-1})^T \tag{2.14}$$

$$\mathrm{BCBV} = \gamma^{-1} diag(Z_{branch}) \tag{2.15}$$

Eq. (2.10) computes the bus voltage with reference bus voltage and the branch voltage drop.

The system frequency deviation and the reference bus voltage deviation are calculated by (2.11) and (2.12). Herein, $Re\left(\sum U_i I_{ij}^*\right)$ presents the outflow active power of bus *i*, while $Im\left(\sum U_i I_{ij}^*\right)$ expresses the outflow reactive power of bus *i*. Since the frequency deviation and the reference bus voltage deviation are both global variables, it requires a global droop coefficient to compute them when there are multiple generators existing in the system. The function of global frequency droop coefficient is denoted as the follows.

$$m_{eq} = \frac{1}{\sum_{i=1}^{d} \frac{1}{m_i}} \tag{2.16}$$

Hence, the frequency deviation and the reference bus voltage deviation are both computable by assuming all the generators located are at the reference bus.

Last, the reference bus voltage is obtained by (2.13) considering the deviation.

2.2.1.3 Operation Constraints

The OPF model also considers operation constraints. Including voltage constraints, frequency deviation limits, generator thermal capacity and load shedding limits.

$$V_{min} \leq \sqrt{V_{real}^2 + V_{imag}^2} \leq V_{max} \tag{2.17}$$

$$-\Delta f_{max} \leq \Delta f \leq \Delta f_{max} \tag{2.18}$$

$$-\Delta U_{r,max} \leq \Delta U_r \leq \Delta U_{r,max} \tag{2.19}$$

$$\sqrt{P_{Gi}^2 + Q_{Gi}^2} \leq S_{Gi,max} \tag{2.20}$$

$$LS_{min} \leq \text{LS} \leq LS_{max} \tag{2.21}$$

Constraints (2.17), (2.18) and (2.20) set the limits for each bus voltage, the frequency deviation and the reference bus voltage deviation, respectively. Constraint (2.21) indicates that the generator power outputs must be limited within the thermal capacity. It is limited by (2.22) that the load shedding percentage should be within the allowed range.

Remarks

Since both constraints (2.17) which can be re-modeled in a complex number form with quadratic calculation and (2.20) are quadratic inequality which increase computing burden of optimization. As (2.20) can be considered as the area of a circle whose radius is S_{Gmax} and (2.17) is equivalent to the area between a small circle whose radius is V_{min} and a large circle whose radius is V_{max} . Hence, in order to linearize (2.17) and (2.20), an inner approximation method is applied where the circles are approximated as inscribed regular polygons of circles. Accordingly, some linear constraints which present the edges of the polygons replace the circle constraints, which is demonstrated in Fig. 2.1. Therefore, (2.17) is linearized as a set of inequalities as shown in (2.22) and (2.23). V_x and V_y are the real and imaginary parts of V. Set A is for the lower-bound polygon while set B is for the upper-bound polygon.

$$V_y \geq a_i V_x + d, \qquad i \in A \tag{2.22}$$

$$V_y \leq b_i V_x + e_i, \qquad i \in B \tag{2.23}$$

Since there is only the upper bound in (2.20), the linearized constraints for (2.20) is denoted as (2.24).

$$Q_G \leq c_i P_G + f_i, \qquad i \in C \tag{2.24}$$

Hence in constraints (2.22), (2.23) and (2.24) substitute (2.17) and (2.20) in the OPF model.

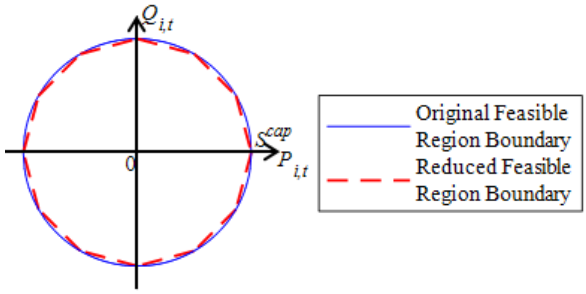

Figure 2.1. Inner Approximation Demonstration for Thermal Capacity.

2.2.2 Proposed Optimal Power Flow

In the modified BFS power flow process, the power flow variables including the bus voltages, the frequency deviation and the reference bus voltage deviation are continually calculated and updated. The OPF procedure is presented in Fig. 2.2.

As the bus voltage is firstly used for obtaining bus injection current in (2.7), then from (2.8) to (2.10), the bus voltage is deduced from the bus injection current. The frequency deviation and the reference bus voltage deviation have similar condition and they can be calculated by (2.11) and (2.12). The updated frequency deviation and reference bus voltage deviation are used to update the power flow and bust voltage through (2.4)-(2.6). This indicated the basic update procedure.

At the beginning, it is essential to assign initial values to ΔU, Δf and ΔU_r to start the OPF algorithm. The initial values of ΔU, Δf and ΔU_r are all set as 0. After the first iteration, the results of current OPF will be used for next iteration. To distinguish the values obtained from last iteration and the variables of current iteration, this chapter introduces index t representing tth iteration. Hence, in the OPF process, the variables obtained in the tth iteration can be updated as the initial values in the $(t+1)$th iteration.

After the calculation and optimization of each iteration, ΔU_t, Δf_t and ΔU_r are compared with the with their values in the last iteration for determining whether to update the values or not. The three above variables are updated until they are converged within preset termination thresholds.

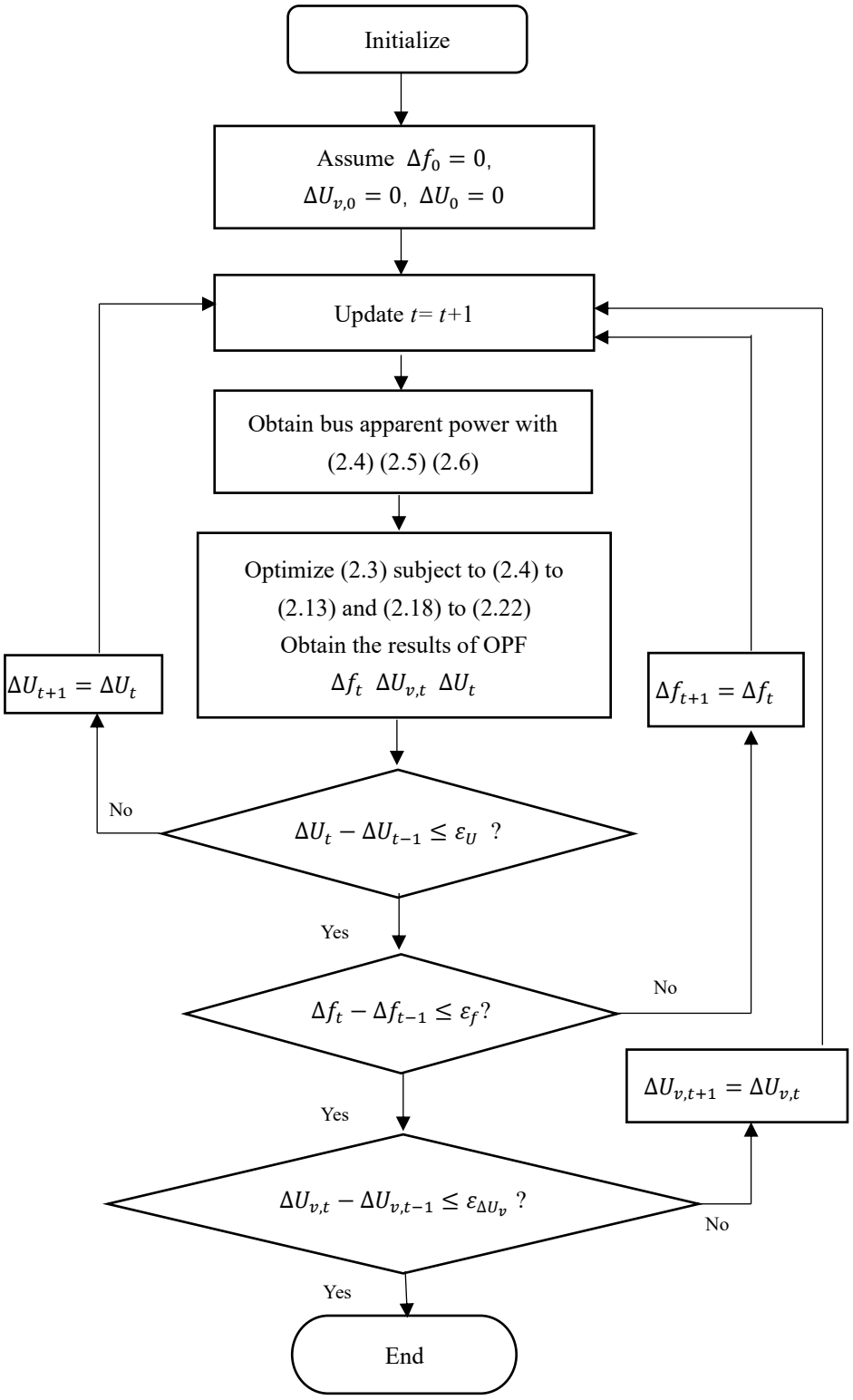

Figure 2.2. OPF Flow Chart.

In order to guarantee the convergence and enhance the converging speed, the variable updating process is divided into three loops. The innermost loop is for branch voltage drop while the middle loop and outer loop are for the frequency deviation and the reference bus voltage

deviation, respectively. In branch voltage drop loop, firstly the OPF is implemented and only the branch voltage drop is updated. In this loop, ΔU_t is compared with ΔU_{t-1} while the frequency deviation and the reference bus voltage deviations are not considered. If the error is more than the threshold, ΔU_t is used as ΔU_{t-1} for the OPF of next iteration. If the error is less than the threshold, then the process enters the middle and the outer loops where only the frequency deviation and the reference bus voltage deviation are to be updated. By doing so, the updating process can converge at a faster speed.

This OPF is linear programming which can be efficiently solved by linear solvers.

2.3 Stochastic Optimization

2.3.1 Stochastic Model

This chapter applies the stochastic optimization model to fully consider the uncertainty in the proposed droop control based OPF. In this model, this chapter considers the uncertainties caused by the load demand and PV output power. This chapter assumes the uncertainties have a finite number of realizations (scenarios) ξ_K. The objective function in stochastic model is denoted as

$$min \sum_{k=1}^{K} \rho_k f(P_{G0}, LS, \xi_k) \tag{2.25}$$

s.t. $$g(x, u, \xi_k) = 0, \forall k \epsilon K \tag{2.26}$$

$$h(x, u, \xi_k) \leq 0, \forall k \epsilon K \tag{2.27}$$

$f(P_{G0}, ls, \xi_k)$ is an OPF sub-model described in Chapter 2.2 based on scenario k with probability ρ_k. (2.26) and (2.27) denote the equality and inequality constraints under all the realization scenarios. The purpose of this objective function is to consider all the uncertainty scenarios in the OPF model. For each scenario of the uncertain load demand and PV power, the operation constraints are modelled for the specified variables in this scenario. Hence, the decision variables are optimized to guarantee feasible operation for all the scenarios, i.e., the operation is

reliable for all the uncertainty realization. The total cost is the weighted sum of the cost of each scenario.

2.3.2 Scenario Construction and Reduction

In order to efficiently simulate the uncertainty of load demand and PV power, an assumption is proposed that the load demand and PV power are subject to two normal distributions $N_1(\mu_1, \sigma_1^2)$, $N_2(\mu_2, \sigma_2^2)$ [82]. This chapter utilizes Monte Carlo sampling to generate a large number of scenarios for load demand and PV power. To reduce the computing burden, scenario reduction scheme is utilized to reduce the scenario number. In this chapter, a backward reduction method [84][85] is applied. The principle of the reduction technique is to eliminate redundant scenarios and aggregate similar scenarios. A brief description of the backward reduction is presented below.

Step 1: S is the initial set of scenarios. The distance between two scenarios is defined as,

$$D_{mn} = \sqrt{(V_s^m - V_s^n)^2}, m \neq n. \tag{2.26}$$

Compute the distances of all scenario pairs

Step 2: For each scenario ξ_m, find the nearest scenario ξ_d. Hence $D_{md} = \min(D_{mn})$.

Step 2: For all the pairs of scenarios obtained from step 2, multiply the probability of ξ_m to $\min(D_{mn})$ to obtain,

$$PD_{md} = \rho_{\xi m} \times min\,(D_{mn}). \tag{2.27}$$

Step 3: Find the pair of scenarios which has the minimum $PD_{md'}$.

Step 4: Delete the scenario d' to construct a new set of scenarios and add its probability to the nearest scenario.

Step 5 Repeat step 2 to 4 until the number of deleted scenarios meets the reduction requirement.

2.4 Case Study

2.4.1 Test System

The proposed stochastic OPF method is tested on an IEEE 33-bus system [43]. The one-line diagram is shown in Fig. 2.3. As this is a test for microgrids islanded mode, the connection between Bus 1 and the substation is cut off. A microturbine with capacity of 3.5 MVA is located at Bus 6. The PV systems which are aggregated PV panels are located at Buses 9, 11, 13, 21, 22, 27, 25, 27 and 29 while their predicted mean active power outputs are 150 kW. The total load demand is predicted as 3.715 MW and 2.3 MVar. The reference voltage V_0 is 1 p.u. and V_{min} and V_{max} are set as 0.9 p.u. and 1.1 p.u. The limits of the frequency deviation and reference bus deviation are set as [-0.1, 0.1] p.u. and [-0.02, 0.02] p.u., respectively. The dispatch interval is set as 15 minutes, i.e., OPF decisions are updated every 15 minutes.

This simulation is conducted on a 64-bit PC with 3.40-GHz CPU and 16 GB RAM using Yalmip [86] toolbox in the MATLAB platform. The proposed stochastic OPF is solved by GUROBI solver [87].

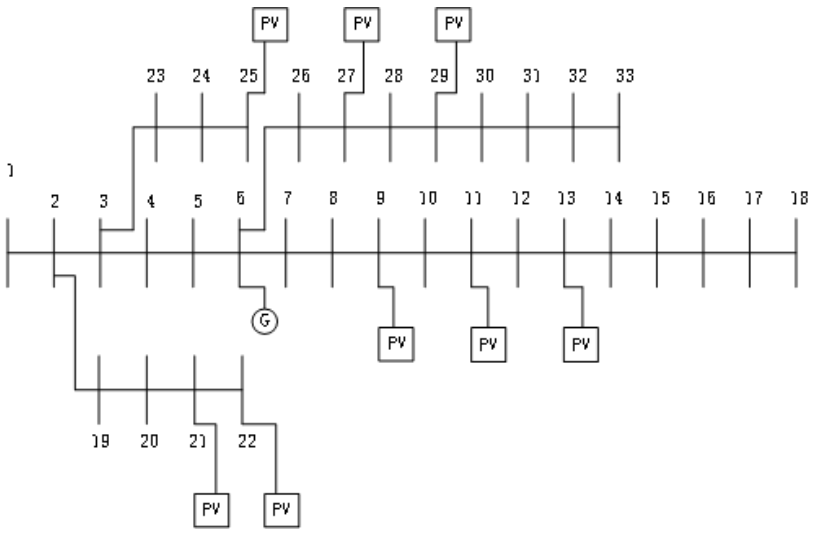

Figure 2.3. One-line Diagram of IEEE 33-bus Microgrid.

2.4.2 Stochastic OPF Results

Firstly, this chapter generates a set of scenarios by Monte Carlo sampling. In this sampling, normal probability distribution is used and the predicted values are set as the mean values. Besides, the standard deviation is set as 10% of the predicted value for the PV power generation and 3%

for the load demand. The sampling generates 800 scenarios which are regarded as the initial set. Then, the backward reduction method which is introduced in Chapter 2.3.2 is applied to reduce the initial set to a small set of 100 representative scenarios. The scenario distribution statistics of the initial and the reduced sets is demonstrated in Fig. 2.4. Although the scenarios are significantly reduced, the probability distributions are quite similar. In addition, a real-time performance simulation will be applied to verify whether the reduced scenarios can efficiently present the uncertainty realization in Chapter 2.4.3.

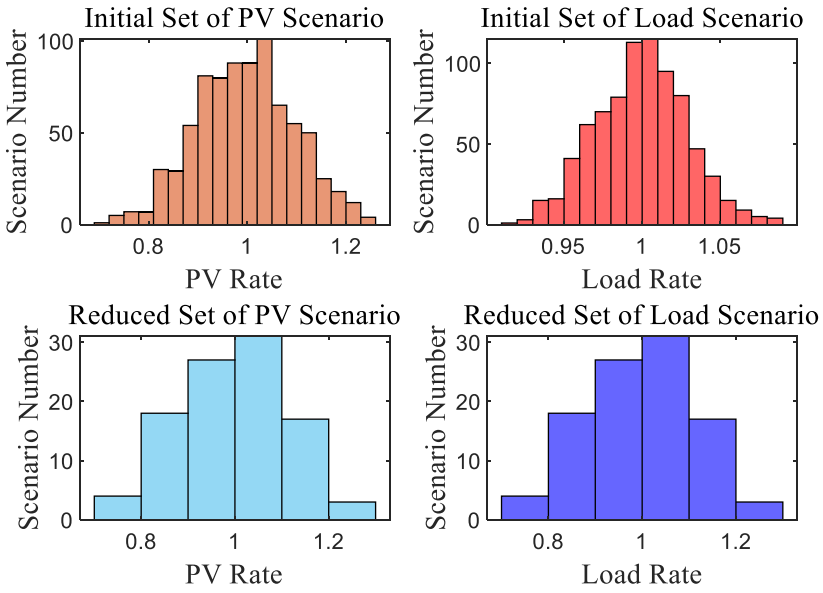

Figure 2.4. Scenarios Distribution Statistics.

Then, with the 100 representative scenarios, the proposed stochastic OPF is carried out to obtain the optimal set points of the microturbine generation and the load shedding decision. After all the deviations are reduced within the termination thresholds, the optimization process is terminated. The optimized set points of the microturbine generation P_{G0} is 1.51 MW and Q_{G0} is 2.07 MVar and the load shedding percentage LS is optimized as 10.42%.

The microturbine generates active and reactive power which consist of the set point base power and the real-time variation. For some scenarios, with the real-time variations, the total generation of the microturbine can be up to 2.51 MW and 2.27 MVar, which still operates within the thermal capacity. Besides, the load shedding percentage is also within its limits. Thus, for

these representative scenarios, there are always solutions, indicating operation reliability under uncertainties.

In terms of the computing efficiency, the solver time is 43.676 seconds which is fully compatible for on-line use.

2.4.3 Real Time Performance

To verify the efficiency of the stochastic OPF, a real-time simulation is implemented. Firstly, a 15-min real-time case where PV power generation and load demand are randomly realized is generated. The real-time PV power output is shown in Fig. 2.5. Then, with the OPF results obtained in Chapter 2.4.2, the BFS power flow [77] is implemented to obtain the system operation results under this real-time case. The results of the frequency deviation, the reference bus deviation and the voltages at Buses 18 and 33 are illustrated in Fig. 2.6-2.9.

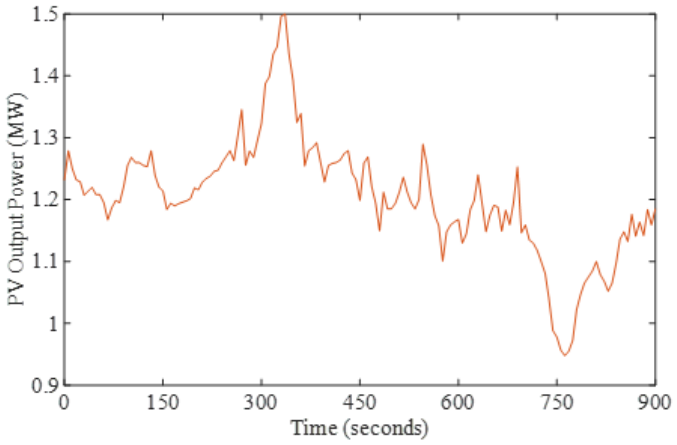

Figure 2.5. Real-time PV Power Output.

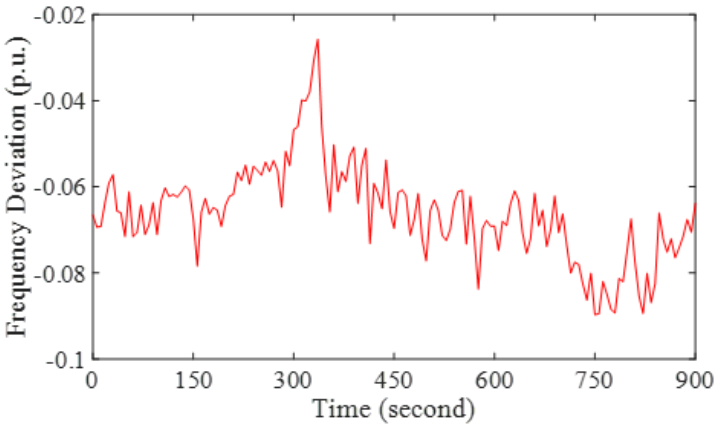

Figure 2.6. Frequency Deviation.

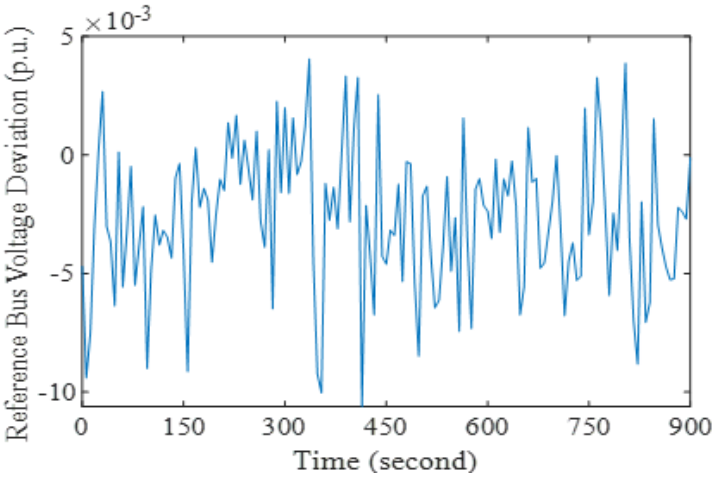

Figure 2.7. Reference Bus Voltage Deviation.

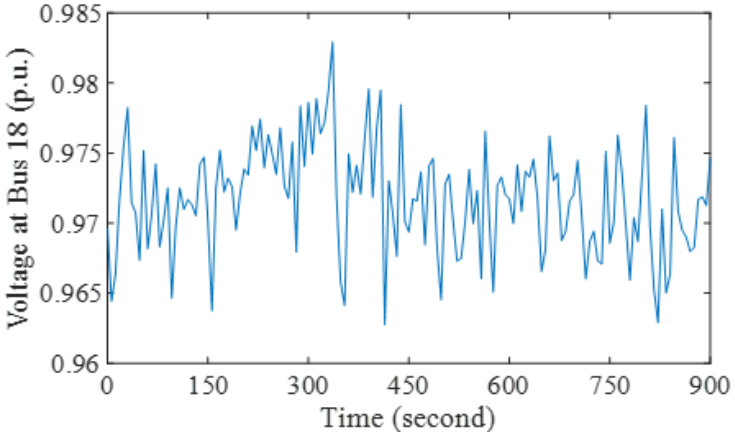

Figure 2.8. Voltage at Bus 18.

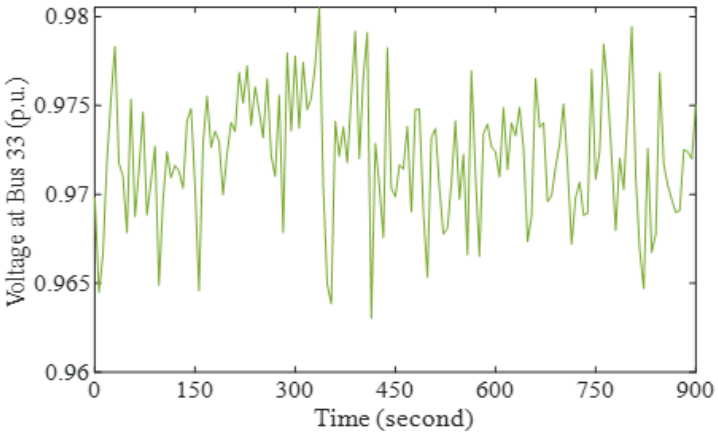

Figure 2.9. Voltage at Bus 33.

It can be seen from Fig. 2.6-2.9 that all the operating results are kept within the allowed limits. As the PV power generation and the load demand vary in real time, the microturbine can generate varying power with the droop control functions in which the set points are optimized in the

proposed OPF, to keep the operating constraint satisfied. Thus, this simulation verifies that the proposed stochastic OPF method can efficiently consider the uncertainty real-time realization through the 100 representative scenarios, such that the results lead to operation reliability under the uncertainties.

2.5 Conclusion

In this chapter, a stochastic OPF method for islanded microgrid considering droop control of the microturbines is proposed. The OPF model is developed based on the BFS droop-based OPF with linearization to improve the computing efficiency. To deal with the uncertainties, a stochastic model with a backward scenario reduction technique is applied to achieve a stochastic OPF model. The proposed method is tested on an islanded microgrid system which is based on the IEEE 33-bus system. The test results verify that the proposed stochastic OPF method can achieve reliable microgrid islanding operation under uncertainties without any operating constraint violation.

Chapter 3 ENHANCED STOCHASTIC OPTIMAL POWER FLOW METHOD FOR ISLANDED MICROGRIDS UNDER UNCERTAINTIES

With development of renewable energy sources (RESs), microgrids have been applied more widely since they are more suitable platforms for distributed generation (DG). Considering emergencies encountered by the main grid can force microgrids to be switched from grid-tied mode to islanded one, a fast and effective optimal power flow (OPF) method for islanded microgrids is imperative to minimize operational cost and keep network operational constraints. Thus, this chapter proposes a new OPF approach which is based on a linear power flow method with high computing efficiency. In this OPF approach, microturbine setpoints and load shedding rates are optimized to minimize the total system operational cost. Besides, uncertainties of renewable power generation and loads are formulated by a probabilistic state generation method and solved by a stochastic optimization. Thus, this chapter finally proposes a new stochastic OPF approach for islanded microgrids under uncertainties, and its high computing efficiency and accuracy is validated by simulations.

3.0 Nomenclature

A. Sets and Indices

k, n_b	Index and set of buses
i, n_g	Index and set of microturbines
M, N	Predefined number of uncertainty states.
R	Sets of OPF results

B. Parameters

a	Generation cost parameters($/kW)
b	Load-shedding cost parameters ($/kW)

m_p, m_q	Droop control coefficients used in P-f and Q-V functions
m_{peq}, m_{qeq}	Equivalent droop control coefficients for the islanded microgrid
P_{Lk}, Q_{Lk}	Load active/reactive power consumption at bus *k* (kW/kVar)
V_0	Nominal voltage (per unit)
ρ_s	Probability of scenario *s*
$\boldsymbol{BCBV}$	Branch current to branch voltage drop matrix
$\boldsymbol{BIBC}$	Bus current to branch current matrix
ε	Termination threshold

C. Variables

C_g	Cost of microturbine power generation ($)
C_{ls}	Penalty cost of load shedding ($)
P_{Gi}, Q_{Gi}	Real-time microturbine active/reactive power output (kW/kVar)
P_{Gi}^0, Q_{Gi}^0	Microturbine active/reactive power output setpoint (kW/kVar)
ΔP_{Gi}, ΔQ_{Gi}	Deviation of real-time microturbine active/reactive power output (kW/kVar)
P_k, Q_k	Active/reactive power injection at bus *k* (kW/kVar)
ΔU	Deviation of bus voltage (per unit)
Δf	Deviation of system frequency (per unit)
ΔU_r	Deviation of reference bus voltage (per unit)
$/s$	Load shedding rate (%)
I_{node}	Injection current at a bus (A)
I_{branch}	Current through a branch (A)
V_r	Reference bus voltage (per unit)
V	Bus voltage (per unit)
$(.)^*$	Conjugate of complex number.

3.1 Introduction

Growing penetration of RESs provides a high potential of constructing microgrids which can supply local loads by themselves. By reducing relying on large-scale coal-fired generation, such

highly RES-penetrated microgrids can efficiently contribute to reducing greenhouse gas emission and achieving carbon neutrality [88].

However, serious natural disasters such as storms, typhoons and blizzards have significantly adverse impacts on the resilience of the power systems. For example, the South Australia blackout in September 2016 caused by two almost simultaneous tornadoes resulted in loss of electricity supply for 850,000 customers [89]. In February 2021, the Texas blackout caused by the severe storms demonstrated another example of heavy economic loss and significant inconvenience for customers. Meanwhile, sufficient RESs can recover power generation once weather events end, enhancing the microgrid ability to work independently in an islanded operation mode [13]. Moreover, as the work [90] concluded that microgrids working as independent entities during faults of the main grid are also able to strengthen the resilience of the power system.

Recently, researchers have paid attention to the prospect of applying microgrids for enhancing the power system resilience. In [91], an algorithm based on risk assessment and defensive islanding control is developed to mitigate cascading effects caused by extreme weather conditions. The concept of defensive islanding control is to determine which branches are actively disconnected during contingency to keep the system secure. Similarly, enhancing the main grid resilience by an islanding approach is investigated in [92]. On the other hand, since grid-tied microgrids can be considered as distribution loads for the upstream network, there is naturally a high probability of disconnecting microgrids while the main grid is undergoing emergency [93]. The recent work [94] considers probable tie-line switching after system contingency and proposes a security-constrained OPF for microgrids. Thus, in response to deal with the islanded operational conditions of the microgrids, a fast and effective OPF approach for islanded microgrids is imperative.

In [95], the authors propose a multi-stage energy management method for an islanded microgrid. An energy management optimization problem is formulated and decomposed into a unit commitment problem and an OPF problem which are the first stage and the second stage respectively. However, this nonlinear programming OPF problem cannot be directly or efficiently solved by commercial solvers. In [96], an OPF model for microgrids is developed, which is still a non-convex programming problem. To efficiently solve non-convex optimization problems,

semidefinite programming methods with proper relaxation techniques can be used [97]. In addition, in [98], the authors adopt generalized Benders decomposition to solve an OPF model where the non-linear terms are treated as complex number variables. Then, replacing the mixed integer non-linear problem, two quadratically constrained quadratic problems are modelled and solved iteratively. Because of inevitable non-convex or non-linear terms in these power flow models, the above works relax or linearize the power flow constraints, which may lose accuracy of network models.

From the above literature review, most of the OPF methods for microgrids, such as branch flow based and conventional AC power flow based methods, have to be relaxed or linearized to promise the convexity by approaches like semi-finite programming.

On the other hand, in [49], a backward forward sweep (BFS) algorithm with a linear branch flow model is developed for power flow problems in distribution networks. In addition, this algorithm is applied to solve power flow problems for islanded microgrids by the authors of [77]. It is indicated that this algorithm can efficiently calculate power flow for islanded microgrids with high accuracy. Furthermore, the work [77] modifies the BFS algorithm with three iterative loops to achieve a fast convergence speed. However, this kind of iterative algorithm cannot be directly used as constraints in OPF problems.

Considering the high accuracy and fast convergence speed, a new OPF method based on this modified BFS algorithm is proposed, which can avoid the non-convex and non-linear issues in the conventional OPF methods. It is worth noting that a new solution algorithm for the OPF problem is developed to achieve high computing speed and accuracy. Moreover, considering the uncertainties from loads and renewable power generation, an efficient stochastic optimization method with probabilistic state generation is adopted. Thus, this chapter eventually proposes a new stochastic OPF method for islanded microgrids, which can efficiently minimize operational cost with accurate network models while keeping network operational constraints satisfied under the uncertainties.

The contributions of Chapter 2 are described in Question 3. In Chapter 3, the stochastic OPF proposed in Chapter 2 is further developed.

On one hand, the iteration method of BFS OPF is improved, including data update mechanism and convergence criterion. In Chapter 2, three loops are occupied by three sets of data, reference bus voltage deviation, frequency deviation and bus voltage drop. In Chapter 3, they are updated together by computing PF with the results gained in the optimization of each iteration. Besides, the convergence criterion of OPF proposed in Chapter 2 is substituted by the optimization results, which means once the optimization results of two iterations is nearly equal the iteration will terminate.

On the other hand, the probabilistic model is also improved according to [100] to reduce the number of scenarios. With these two improvements, the OPF proposed in Chapter 3 is with higher accuracy and lower computing time, verified in Chapter 3.4.

3.2 OPF For Islanded Microgrid

With the BFS algorithm given in [77], this chapter proposes a new OPF method for islanded OPF to minimize operational cost and keep network operational constraints by optimizing microturbine power generation setpoints and load shedding rates. Load shedding is used to keep system stability, and it is considered to develop a general OPF model.

3.2.1 OPF Formulation

The OPF for islanded microgrids is formulated in the following compact model.

$$\min f(x,u) = C_g + C_{ls} \tag{3.A}$$

s.t. $$g(x,u) = 0 \tag{3.B}$$

$$h(x,u) \leq 0 \tag{3.C}$$

The objective function (3.A) of this OPF model is to minimize the total operational cost composed of generation cost of microturbines and penalty cost of load shedding. The generation cost is modelled as (3.1) and the load shedding cost, which is determined by load shedding rate decision ls, is modelled as (3.2) below.

$$C_g = \sum a \times P_{Gi} \tag{3.1}$$

$$C_{ls} = b \times (1 - ls) \times \sum P_{Lk} \tag{3.2}$$

In addition, (3.B) presents a set of linear power flow equations and (3.C) is a set of inequalities as microgrid operational constraints. x, u are decision variables and state variables, respectively. The constraints (3.B) and (3.C) will be elaborated in next two sections.

3.2.2 Islanded Microgrid Power Flow Algorithm

The BFS power flow algorithm is linear programming with iterations, which can significantly reduce the computational burden. The power flow model for islanded microgrids is expressed as follows. This chapter considers photovoltaics (PVs) as renewable power generation and others can also be used without affecting the high efficiency of the BFS algorithm.

$$P_{Gi} = P_{Gi}^0 + \Delta P_{Gi}, \Delta P_{Gi} = \frac{\Delta f_0}{m_{pi}}, \forall\, i \in n_g \tag{3.3}$$

$$Q_{Gi} = Q_{Gi}^0 + \Delta Q_{Gi}, \Delta Q_{Gi} = \frac{\Delta U_{r0}}{m_{qi}}, \forall\, i \in n_g \tag{3.4}$$

$$P_k + jQ_k = (P_{Gi} + jQ_{Gi}) - (1 - ls)(P_{Lk} + jQ_{Lk}) + P_{pvk}, \forall i \in n_g, \forall k \in n_b \tag{3.5}$$

$$I_{nodek} = \frac{P_k - jQ_k}{V_k^*}, \forall k \in n_b \tag{3.6}$$

$$\boldsymbol{I_{branch}} = [\boldsymbol{BIBC}]\, \boldsymbol{I_{node}} \tag{3.7}$$

$$\Delta \boldsymbol{U} = [\boldsymbol{BCBV}]\, \boldsymbol{I_{branch}} \tag{3.8}$$

$$\boldsymbol{V} = \boldsymbol{V_r} - \Delta \boldsymbol{U} \tag{3.9}$$

$$\Delta f = \left(-m_{peq}\right)\left[P_{Lk} - P_{G1}^0 + Re\left(\sum U_1 I_{1k}^*\right)\right], \quad \forall i \in n_g, \forall k \in n_b \tag{3.10}$$

$$\Delta U_r = \left(-m_{qeq}\right)\left[Q_{Lk} - Q_{G1}^0 + Im\left(\sum U_1 I_{1k}^*\right)\right], \tag{3.11}$$

$$\forall i \in n_g, \forall\, k \in n_b$$

$$V_r = V_0 - \Delta U_r \tag{3.12}$$

$$m_{(.)eq} = \frac{1}{\sum_{i=1}^{d} \frac{1}{m_{(.)i}}}, \quad \forall i \in n_g \tag{3.13}$$

Equations (3.3) and (3.4) are expressions of output power of microturbines, consisting of setpoints (P_{gi}^0, Q_{gi}^0) and variations responding to droop control (ΔP_{gi}^0, ΔQ_{gi}^0) which are calculated with the droop coefficients. In the chapter, both P-f and Q-V droop control functions are considered. In (3.5), the bus injection power is determined by predicted values of loads and PV output power as well as the load shedding rate ls.

In addition, equations (3.6) to (3.9) compute bus injection current, branch current, bus voltage with deviation. BIBC and BCBV are the network parameter matrices consisting of system information such as topology and branch impedances [49]. It is noted that the V_k^* in (3.6) is the value from the last iteration, and it is used as a parameter in the current iteration of the BFS algorithm. In (3.7)-(3.9), the symbols in the bold type mean the vectors of the corresponding variables of currents and voltages.

Moreover, the microgrid frequency deviation is calculated with system equivalent droop coefficient m_{peq} in (3.10). The reference bus voltage V_r which is the benchmark for computing the other buses' voltages is computed by (3.11) and (3.12). Because of an islanded microgrid operation mode, there is no slack bus. However, this chapter selects a bus with the main microturbine as the reference bus for power flow calculation. Hence, it is essential to obtain the difference between the reference bus voltage and the nominal one, i.e., ΔU_r in (3.11).

Last, (3.13) expresses computing the equivalent droop coefficient for the whole system with all the droop coefficients of the microturbines installed in the microgrid. More detailed information for this power flow model can be found in [77].

With these equations (3.3) to (3.13), a BFS Algorithm for islanded microgrids is developed as below.

Step 1 Calculate bus injection power by (3.3) (3.4) (3.5) with $\Delta f_0, \Delta U_{r0}$

Step 2 Calculate bus voltage deviation by (3.6) (3.7) (3.8) with V_k^*, and bus voltage V by (3.9)

Step 3 Calculate frequency deviation Δf and reference bus voltage deviation ΔU_r by (3.10) and (3.11)

Step 4 Check if $\left|\frac{V_k - V_k^*}{V_k^*}\right| \leq \varepsilon$?

Yes: Go to Step 5. No: Return to Step 1 with replacing V^* by V

Step 5 Check if $\left|\frac{\Delta f - \Delta f_0}{\Delta f_0}\right| \leq \varepsilon$?

Yes: Go to Step 6. No: Return to Step 1 with replacing Δf_0 by Δf

Step 6 Check if $\left|\frac{V_r - V_{r0}}{V_{r0}}\right| \leq \varepsilon$?

Yes: Go to Step 7. No: Return to Step 1 with replacing ΔU_{r0} by ΔU_r

Step 7 End

3.2.3 Operational Constraints

In the OPF model, this chapter considers the following microgrid operational constraints.

$$V_{min} \leq V \leq V_{max} \tag{3.14}$$

$$P_{Gi}^2 + Q_{Gi}^2 \leq S_{Gi.max}^2 \tag{3.15}$$

$$-\Delta f_{max} \leq \Delta f \leq \Delta f_{max} \tag{3.16}$$

$$-\Delta U_{r,max} \leq \Delta U_r \leq \Delta U_{r,max} \tag{3.17}$$

$$ls_{min} \leq ls \leq ls_{max} \tag{3.18}$$

The microgrid operational constraints include the bus voltage limit in (3.14), the microturbine power capacity limit in (3.15), the frequency deviation limit in (3.16), the reference bus voltage deviation limit in (3.17) as well as load shedding limit in (3.18). These constraints can ensure the islanded microgrids are operated securely and reliably.

3.2.4 Proposed OPF Method

To solve an OPF problem more efficiently for islanded microgrids, this chapter proposes a new method based on the modified BFS power flow algorithm, which is introduced below.

As the initial values V_k^*, Δf_0 and ΔU_{r0} used in (3.3) (3.4) and (3.6) are not accurate with errors, leading to that the OPF result is not actually optimal. Hence, it is essential to develop a new and efficient iterative algorithm to reduce the errors to an acceptable magnitude. In [77], each set of V_k^*, Δf_0 and ΔU_{r0} requires one loop to reach its own convergence. However, the overall number of iterations is the product of three loops, which results in long program computing time. As a result, the OPF method based on these three loops is computationally expensive. To overcome the computing challenge, this chapter aims to improve the convergence progress by updating all three sets of V_k^*, Δf_0 and ΔU_{r0} simultaneously in a new OPF loop and checking the overall convergence on the OPF result instead. The flowchart of the proposed OPF method is demonstrated in Fig. 3.1.

As Fig. 3.1 shows, in this OPF loop, the first step is to run the OPF model (3.A)-(3.C) with initial values V_k^*, Δf_0 and ΔU_{r0} and obtain the results, i.e. microturbine output active and reactive power and load shedding rate as a vector R^t. t means the tth iteration. Then, the relative gap of R^t is calculated by comparing the current result with that in the last iteration. In the first iteration, this chapter sets R^0 as a vector of zero. If any gap of two corresponding values of R^{t-1} and R^t is greater than a preset termination threshold, BFS Algorithm is applied to calculate and update V_k^*, Δf_0 and ΔU_{r0} simultaneously. Last, the updated V_k^*, Δf_0 and ΔU_{r0} are used for the OPF model in the next iteration. The above OPF loop is repeated until the gap of R^t converges to the threshold. Thus, with the help of R^t, three sets of the initial values can be updated simultaneously, to enhance the computing speed.

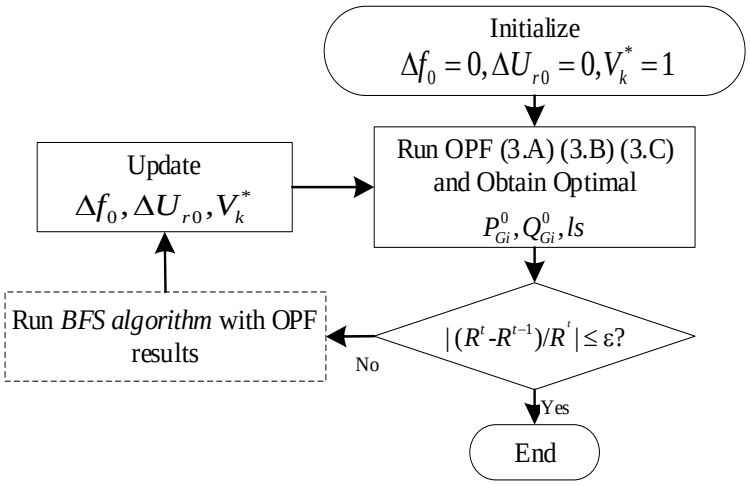

Figure 3.1. Proposed OPF Method for Islanded Microgrids.

3.3 Stochastic OPF With Probabilistic Models

Based on the proposed OPF method, a stochastic optimization method [99] is applied to address uncertainties of renewable power generation and loads. With their probability density functions (PDFs), the uncertainties are modelled as presentative scenarios by a probabilistic state generation method [100] to generate scenarios. Thus, a stochastic OPF method is developed for islanded microgrids.

3.3.1 Stochastic OPF Formulation

Firstly, the uncertainties concerned in the OPF problem are PV output power and loads. By reforming (3.A) into a general stochastic programming model, a stochastic objective function is modelled as (3.19).

$$minE_{\xi}[f(x,\xi)] \tag{3.19}$$

Herein, x is the set of decision variables, and ξ indicates uncertainty realizations. $f(x,\xi)$ is the subproblem of (3.19) under the certain uncertainty realization ξ, while E_{ξ} is the expectation of $f(x,\xi)$. The above general stochastic programming model can be transformed into an equivalent deterministic model (3.20) with finite realization scenarios, $\xi_1, \xi_2, \xi_3, \ldots, \xi_s$ and their probabilities of occurrence $\rho_1, \rho_2, \rho_3, \ldots, \rho_s$. Here, s is the serial number of a scenario and S means a set of these scenario numbers.

$$min \sum_{s \epsilon S} \rho_s f(x, \xi) \tag{3.20}$$

3.3.2 Probabilistic State Generation

Conventionally, Monte Carlo sampling methods are applied to generate random scenarios and then reduce them with forward or backward scenario reduction methods, thus enhancing the computing efficiency by using representative scenarios in stochastic programming problems [101]. However, the scenario reduction methods are also computationally expensive if a large number of scenarios to be merged into the remaining. Considering the scenario reduction time, even with the limited representative scenarios, the OPF efficiency can be significantly impaired. To address this issue, this chapter adopts a probabilistic state generation method developed in the recent work [100]. This method for the renewable power uncertainty consideration in Chapters 3 and 4 are verified to be effective in [100]. Besides, the probabilistic modelling of Chapters 3 and 4 can also be effective when the probabilistic density function is changed.

Both PDFs for the PV power and loads are assumed as Gaussian distribution in this chapter. P^u which represents the value of uncertainty is divided into M states according to the PDF of the uncertainty with the limits $\bar{P}_m^u$ and $\underline{P}_m^u$ for the state *m*. Equation (3.21) calculates the mean value of this uncertainty state as the representative value of the interval $[\bar{P}_m^u, \underline{P}_m^u]$.

$$P_m^u = \frac{\int_{\underline{P}_m^u}^{\bar{P}_m^u} P^u PDF \, dP^u}{\int_{\underline{P}_m^u}^{\bar{P}_m^u} PDF \, dP^u}, m = 1,2,3, \dots, M \tag{3.21}$$

The PDF of the uncertainty is also used to calculate the occurrence probability of the state *m*, which is shown as (3.22).

$$\rho_m^u = \int_{\underline{P}_m^u}^{\bar{P}_m^u} PDF \, dP^u, m = 1,2,3, \dots, M \tag{3.22}$$

Using this method, a set of M PV power states, expressed by $S^{PV} = \{P_m^{PV}, \rho_m^{PV}\}$, and a set of N load states, presented by $S^D = \{P_n^D, \rho_n^D\}$ can be generated. Then, the above separate sets S^{PV} and S^D used to form a combined set by (3.23), (3.24) and (3.25).

$$S = \{(P_m^{PV}, P_n^D), \rho_s\} \tag{3.23}$$

$$\psi^{PV} = \{P_m^{PV}\}, \psi^D = \{P_n^D\}, \quad \{(P_m^{PV}, P_n^D)\} = \psi^{PV} \times \psi^D \tag{3.24}$$

$$\rho_s = \rho_m^{PV} \times \rho_n^D, \forall (P_m^{PV}, P_n^D) \tag{3.25}$$

$\{(P_m^{PV}, P_n^D)\}$ means a combined state and ρ_s is its corresponding joint occurrence probability. The detailed introduction of this probabilistic state generation method can be referred to [16]. By using this method, a total number ($M \times N$) of the combined states are applied as the representative scenarios for the proposed stochastic OPF model (3.20) while modifying (3.B) and (3.C) under all the representative scenarios.

3.4 Case Study

3.4.1 Test System

A 33-bus distribution network originally from [43] is used as a qualified islanded microgrid for operation/control tests [78]. The network topology with microturbines (labelled "G" with circles) and PVs (labelled "PV" with squares) is shown in Fig. 3.2. The loads are increased to the total active and reactive power consumption of 7.43MW and 4.60MVar.

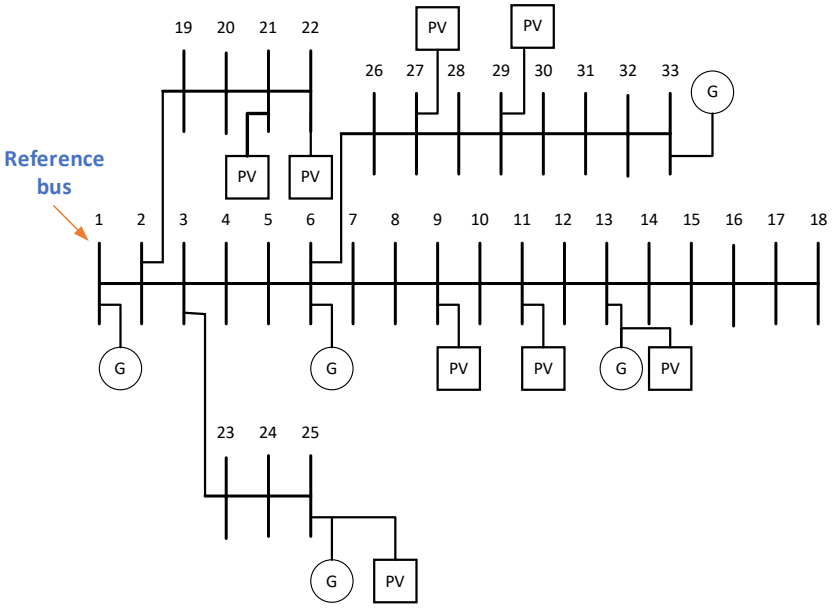

Figure 3.2. Microgrid System for Case Study.

Five microturbines are utilized in this islanded microgrid, and their parameters are presented in Table 3.1. In addition, 8 PV power generation units are located in the islanded microgrid as shown in Fig. 3.2, and their predicted active power outputs are all set as 100 kW.

Table 3.1 Microturbine Parameters

Microturbine No.	Bus No.	Capacity (MVA)	P-f Coefficient (per unit)	Q-V Coefficient (per unit)
1	1	2	-0.04	-0.04
2	6	1	-1	-1
3	13	1.5	-0.2	-0.1
4	25	1.2	-0.5	-0.3
5	33	1.4	-0.2	-0.2

According to [78], bus 1 is selected as the reference bus for the OPF method while the nominal voltage is set as 1 per unit Moreover, V_{min} and V_{max} are 0.95 per unit and 1.05 per unit, respectively. The allowed ranges of reference bus voltage deviation and system frequency deviation are set as [-0.04, 0.04] per unit and [-0.02, 0.02] per unit. In addition, the allowed load shedding range is [0, 20%]. This OPF method is applied for a short dispatch interval, depending on the grid code, e.g., 15 minutes.

Note that any parameters of network, DG and operational limits can also be used without affecting the simulation effectiveness.

The termination threshold ε is set as 0.001.

This simulation is carried out on a 64-bit operating system with AMD Ryzen 3700x CPU and 16 GB RAM. The toolbox YALMIP [86] is used for simulation coding in MATLAB. In this chapter, the GUROBI solver [87] is used to solve the OPF problem.

3.4.2 Uncertainty Probabilistic States

In this chapter, PV output power and loads are both assumed to fit to Gaussian probability distribution. The means of their PDFs are set to 1 (100% of predicted values), while the standard deviation of loads is 0.04 and that of PV power is 0.05. With the method introduced in Chapter 3.3.2, the loads and PV output power are modelled into 4 and 8 probabilistic states, respectively. The PDFs of loads and PV power (red and blue curves) as well as the proposed state intervals (black lines) are presented in Fig. 3.3. Then, using (4.22), occurrence probabilities of these states

are calculated and demonstrated in Fig. 3.4. These states finally construct 32 combined states with joint probabilities, which are used as representative scenarios of uncertainty realization in the proposed stochastic OPF model.

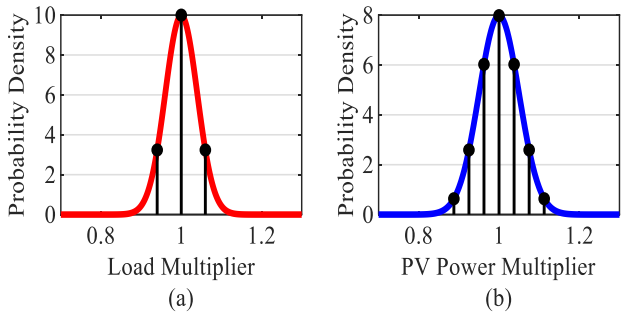

Figure 3.3. Probability Density: (a) Load; (b) PV Output.

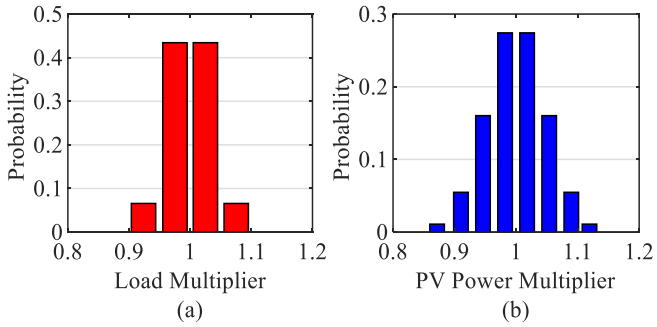

Figure 3.4. State Occurrence Probability: (a) Load; (b) PV Output.

3.4.3 Performance of Proposed OPF Method

With the above uncertainty representative scenarios, the proposed stochastic OPF method is implemented to optimize decision variables and minimize the total operational cost. To indicate the high efficiency of the proposed method, an existing OPF method [102] which is based on the three loops of the efficient power flow algorithm [77] is also implemented for comparison. The optimized power setpoints of microturbines are illustrated in Fig. 3.5. The OPF results of these two methods are shown in Table 3.2.

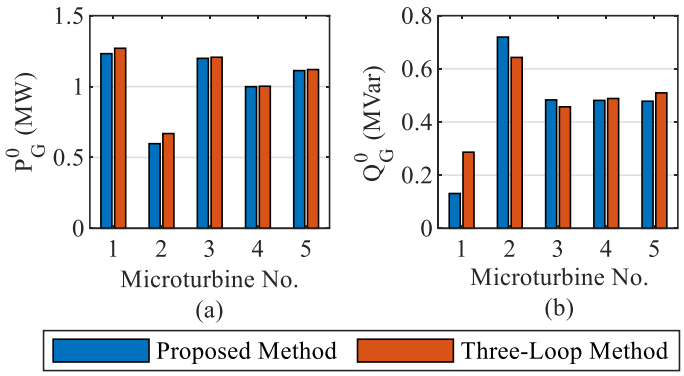

Figure 3.5. Microturbine Setpoints by Two Methods: (a) Active Power; (b) Reactive Power.

Table 3.2 OPF Results

Method	***Proposed***	***Three-Loop Based***
Number of Iterations	9	36
Solver Time (s)	1.046	4.438
Shed Loads (MW)	1.033	1.085
Objective ($)	23.770	24.023

From Fig. 3.5, it is seen that the optimized power setpoints are somewhat different and the active power outputs of the proposed method are slightly less, leading to the less generation cost.

Moreover, as can be seen from Table 3.2, the GUROBI solver time of the proposed OPF method is significantly less than that of three-loop based method, which indicates that computing efficiency of the proposed method is extremely high.

For the shed loads, the proposed method achieves less values to reduce the penalty cost. Thus, the objective obtained by the proposed OPF method is less than that of the three-loop based method.

In order to further check the accuracy of the OPF methods on the system operational conditions, the efficient BFS algorithm [77] is implemented to get power flow results as benchmark. Then, compared to the benchmark, the mean absolute percentage error (MAPE) of the frequency deviations, all the bus voltages and the reference bus voltages obtained by these two methods are calculated by (3.26)-(3.27) and shown in Table 4.3.

$$APE_s = \left| \frac{Res_{OPF,s} - Res_{PF,s}}{Res_{PF,s}} \right|, \forall s \tag{3.26}$$

$$MAPE = \frac{1}{S}\sum_{s=1}^{S} APE_s \tag{3.27}$$

Table 3.3 Absolute Percentage Errors

Method	***Proposed***	***Three-Loop Based***
MAPE of Δf (%)	0.0012	0.90
MAPE of V (%)	0.000005	0.51
MAPE of V_r (%)	0.000003	0.53

Since the MAPE and Max-APE of the proposed OPF method is significantly small, it is concluded that the proposed method is almost consistent with the power flow results accurately considering the operational conditions with the optimized decision variables.

In conclusion, the proposed OPF method can efficiently minimize the total operational cost for the islanded microgrid at a fast speed.

3.4.4 Monte Carlo Simulation Results

In this section, the OPF results obtained by the proposed OPF method are tested with 1800 random scenarios generated by Monte Carlo sampling which are used as uncertainty realizations. These scenarios follow the same Gaussian probability distribution given in Chapter 3.4.2. The BFS algorithm is used to complete power flow for these scenarios and the operational conditions are checked.

For these scenarios, all of the bus voltages are within the constraints, and only 0.28% scenarios incur violations for the system frequency deviation. Thus, it is indicated with the stochastic optimization with the probabilistic state generation, a highly robust solution against uncertainty realizations can be obtained.

3.5 Conclusion

This chapter proposes a new stochastic OPF method for islanded microgrids with a new solution algorithm.

Via the numerical simulations, it is validated that the proposed method can obtain an optimal decision of microturbine generation setpoints at a fast computing speed. In addition, the obtained solution is highly robust against uncertainty realizations of renewable power generation and loads. The proposed method can outperform the existing method in terms of optimum and computing efficiency.

Chapter 4 STOCHASTIC SECURITY-CONSTRAINED OPTIMAL POWER FLOW FOR A MICROGRID CONSIDERING TIE-LINE SWITCHING

With the rapid development of microgrid, its tie-line switching from grid-connected to islanded mode is a topic worth discussing for considering both main grid resilience and microgrid security. In this chapter, a stochastic security-constrained optimal power flow (OPF) method is proposed to deal with these conditions under high uncertainties. Firstly, a linear load flow model and a backward forward sweep (BFS) algorithm are applied to present microgrid power flow with reduced computing burdens. Secondly, with consideration of tie-line switching from grid-connected to islanded operation mode, a security-constrained OPF problem for a microgrid is proposed to minimize operating cost and by optimizing microturbine setpoints and load shedding coefficient. To promise stable islanded operation after disconnection from the main grid, a Benders decomposition method is developed to decouple the OPF problem into a grid-connected master problem and an islanded sub-problem and then solve them iteratively with Benders cuts to guarantee microgrid security after tie-line switching. Last, a stochastic optimization method with probabilistic modelling is adopted to address the uncertainty issue caused by renewable energy sources (RESs) and loads. The proposed stochastic security-constrained OPF method has been verified with high computing efficiency and robust security via comprehensive numerical simulations.

4.0 Nomenclature

A. Sets and Indices

b, B	Index and set of microgrid branches
k, n_b	Index and set of microgrid buses
i, n_g	Index and set of microturbines

B. Parameters

a_i, b_i	Cost parameters of power generation ($/kW)
c	Price of power exchange with main grid ($/kW)
d_k	Penalty cost of load shedding ($/kW)
$I_{branch,b}^{max}$	Maximum current limit of branch b (A)
m_p, m_q	Coefficients of frequency droop and voltage droop
m_{peq}, m_{qeq}	Equivalent coefficients of frequency droop and voltage droop for the whole system
P_{Lk}, Q_{Lk}	Active/reactive load at bus k (kW/kVar)
S_{Gi}^{cap}	Power capacity of microturbine i (kVA)
V_0	Substation voltage in grid-connected mode, and nominal voltage in islanded mode (p.u.)
ρ_s	Probability of scenario s
$()_{min/max}$	Minimum/Maximum limit for variables
$\boldsymbol{BCBV}$	Branch current to branch voltage drop matrix
$\boldsymbol{BIBC}$	Bus current to branch current matrix

C. Variables

P_{Gi}, Q_{Gi}	Real-time microturbine active/reactive power output (kW/kVar)
P_{Gi}^0, Q_{Gi}^0	Setpoint of microturbine active/reactive power output (kW/kVar)
P_{grid}	Active power from main grid to microgrid (kW)
P_{PVk}	Photovoltaic active power generation at bus k (kW)
ΔP_{Gi}, ΔQ_{Gi}	Real-time microturbine active/reactive power output variation (kW/kVar)
P_k, Q_k	Active/reactive power injection at bus k (kW/kVar)
$\Delta \boldsymbol{U}$	Vector of bus voltage deviations (p.u.)
Δf	System frequency deviation (p.u.)
ΔV_r	Reference bus voltage deviation (p.u.)
LS	Load shedding rate (%)
$\boldsymbol{I_{node}}$	Vector of bus injection currents (A)
$\boldsymbol{I_{branch}}$	Vector of branch currents (A)
$I_{branch,b}$	Current of branch b (A)

V_r	Reference bus voltage (p.u.)
$\boldsymbol{V_r}$	Vector of V_r (p.u.)
V_k	Bus voltage at bus k (p.u.)
$\boldsymbol{V}$	Vector of bus voltages (p.u.)
x_0, x_1	All the state variables of grid-connected OPF and islanded OP, respectively
u_0, u_1	All the controllable variables of grid-connected OPF and islanded OPF, respectively
y_0, y_1	All the variables (both state and controllable) of grid-connected OPF and islanded OPF, respectively

4.1 Introduction

RESs, such as solar and wind power, enhancing the microgrid ability to work independently, provide a broad prospect of developing microgrids as a suitable platform for these RESs [13]. However, the RESs are significantly affected by severe weather events, such as typhoons and storms, which is challenging resilience of the power system. Some extreme circumstances can lead to blackouts including the South Australia blackout in 2016 [89], causing tremendous economic loss.

To cope with contingent disturbances and uncertainties of renewable power generation, it is essential to provide effective operation frameworks and methods for microgrids to minimize the economic loss during contingency and guarantee operational security under uncertainties. The authors of [21][103][41] propose economic dispatch (ED) models to minimize operating cost. These ED models consider power balancing within microgrids and operation constraints of system components such as distributed generators and energy storage systems (ESSs). The authors of [21] take a grid-connected mode and a steady islanded mode of microgrids into account. An ED model for an AC/DC hybrid microgrid considering controllable loads including electric vehicles is developed by [103]. In [41], grid-connected and islanded operation modes are integrated into one optimization problem with a Benders decomposition method, where the grid-connected operation is formulated as a master problem and the islanded operation is a sub-problem. The Benders cuts generated by the islanded operation problem can guarantee that the microgrid can securely react to unknown disturbances from the main grid. To this end, the Benders decomposition method shows advantages in guaranteeing system security. However, the

above works do not consider microgrid network models and corresponding network operation constraints.

On the other hand, OPF methods have been widely applied for microgrid operation. In the following literature review, several microgrid OPF methods reported in recent years are briefly described and discussed. In [104], a grid-connected microgrid OPF method is presented with focus of optimizing energy storage devices, considering renewable power generation and loads as fixed power injection. The authors of [74] develop a two-stage optimization method for energy management of islanded microgrids, where the first stage is a unit commitment problem while the second stage is an unbalanced three-phase OPF problem. The unit commitment problem which is mixed integer programming and the nonlinear OPF problem are separately solved. The work of [95] is based on [74]. The first-stage unit commitment problem is extended to a robust optimization problem which is solved by primal cutting plane decomposition for addressing uncertainties of RESs. A distributed OPF method for microgrids is introduced in [96]. The original OPF model in this paper is a non-convex problem and it is further reformed by relaxing power flow constraints. Moreover, the authors of [96] make great efforts to transform a centralized optimization problem to a distributed one with predictor corrector proximal multipliers. It is worth noting that the above models are non-linear programming problems which are intractable.

For a purpose of solving non-linear microgrid OPF problems, semi-definite programming and second order cone programming methods have been recently applied. The OPF problem for unbalanced three-phase systems proposed in [97] is formulated from an originally non-linear problem by a semidefinite programming method. In addition, in [76], a generalized optimal operation method for both grid-connected and islanded modes is proposed, where the nonlinear terms are reformed into second order conic constraints. In [75], mathematical models of objective function, power flow, distributed generators, and battery systems are linearized or approximated, thus making the optimization problem easily solvable. In [98], a generalized Benders decomposition method is utilized to solve a non-linear OPF problem. In this method, non-linear components in the OPF model are extracted as complex number variables, while the original mixed integer non-linear problem is decomposed into quadratically constrained quadratic

subproblems. By using the Benders decomposition method, the intractable optimization problems can be solved, such that this method is expected for microgrid OPF problems.

However, from the above literature review, there is a research gap, i.e., optimization models considering tie-line switching from the grid-connected to the islanded operation mode are not well developed. Thus, when the main grid suffers from contingency, the microgrid operation cannot be optimized after sudden disconnection from the main grid for a secure islanded operation purpose.

Considering the main grid in contingency, efficient models of islanded microgrid power flow are imperative. Due to no slack bus and system frequency fluctuations, the conventional power flow model cannot be used for islanded microgrids. To this point, power flow algorithms specific for islanded microgrids have become a research focus. In [105] and [106], the distribution generation (DG) with highest rating is selected as slack bus then conventional power flow is applied. In [107], the authors take Newton trust regions to solve the nonlinear power flow problem. In [108], a modified Newton Raphson algorithm is proposed for the islanded microgrid power flow. These power flow algorithms all include non-linear terms which aggravate the computing burden when they are involved in OPF problems. Recently, in [77] and [78], two linear power flow models for radial or weakly meshed islanded microgrids considering droop control are proposed. Considering their high computing efficiency, these power flow methods are expected to be adapted in islanded microgrid OPF problems.

Besides, to address uncertainties caused by RESs and loads, stochastic programming methods can be used for microgrid OPF problems [99]. In order to enhance the computing speed of stochastic programming, a probabilistic modelling method is introduced by [100] to generate representative scenarios of uncertainty realizations. Thus, a stochastic OPF method with probabilistic modelling is expected.

In summary, the research gaps are found in the literature, e.g., low efficiency of conventional OPF methods, no consideration of tie-line switching from the grid-connected to the islanded mode, and heavy uncertainties of renewable power generation. To fill these research gaps, this chapter proposes a new stochastic security-constrained OPF method for microgrids. The major contributions of this chapter include the following.

1. A new OPF problem for microgrids is formulated with consideration of tie-line switching from the grid-connected to the islanded mode while the main grid in contingency.

2. A new Benders decomposition based solution algorithm is developed to solve the proposed OPF problem, thus guaranteeing the system security.

3. A stochastic programming method with probabilistic modelling is applied for the proposed security-constrained OPF method to deal with uncertainties.

The remainder of this paper is organized as follows. Chapter 4.2 introduces mathematical formulations of microgrid OPF in both grid-connected and islanded modes. Chapter 4.3 presents integration of two OPF problems with security constraints and a new Benders decomposition based solution algorithm. Chapter 4.4 extends the deterministic OPF model to a stochastic one with probabilistic modelling to deal with uncertainties. Chapter 4.5 carries out numerical simulations of the proposed OPF model with different tests and demonstrates results. At last, Chapter 4.6 concludes the whole paper.

4.2 Optimal Power Flow for Microgrid

In this section, firstly, two microgrid OPF models for the grid-connected and the islanded operation modes are developed, respectively. Then, a BFS algorithm is introduced in this section, for solving the proposed microgrid OPF models.

4.2.1 Grid-Connected OPF Model

4.2.1.1 Objective Function

The objective of grid-connected OPF aims to minimize the total operating cost. The objective function is formulated as below.

$$f^{gc} = min \sum_{i \in n_g} (a_i P_{Gi}^0 + b_i) + cP_{grid} \tag{4.1}$$

This objective function consists of the power generation cost of each microturbine $(a_i P_{Gi}^0 + b_i)$ and the power exchange cost with the main grid cP_{grid}.

4.2.1.2 Power Flow Constraints

To fully consider the system operating conditions, this chapter applies the direct load flow model introduced in [49] as follows.

$$P_k + jQ_k = \left(P_{Gi}^0 + jQ_{Gi}^0\right) - (P_{Lk} + jQ_{Lk}) + P_{pvk}, i \in n_g, k \in n_b \tag{4.2}$$

$$\boldsymbol{I_{nodek}} = \frac{P_k - jQ_k}{V_k} \ , k \in n_b \tag{4.3}$$

$$\boldsymbol{I_{branch}} = [\boldsymbol{BIBC}]\boldsymbol{I_{node}} \tag{4.4}$$

$$\Delta \boldsymbol{U} = [\boldsymbol{BCBV}]\ \boldsymbol{I_{branch}} \tag{4.5}$$

$$\boldsymbol{V} = \boldsymbol{V_r} - \Delta \boldsymbol{U} \tag{4.6}$$

$$P_{grid} = Re(V_0\ I_{branch\,1}{}^*) - P_{G1} \tag{4.7}$$

Eq. (4.2) indicates active and reactive power injections at bus k, which are composed by microturbine output power, loads and photovoltaic (PV) output power. (4.3) calculates the current injection at bus k. Branch current and branch voltage drop are calculated by (4.4) and (4.5), respectively. BIBC and BCBV are two matrices derived based on the network topology, and the details of how to derive these two matrices can be found in [49]. (4.6) is used to calculate the bus voltage by the reference voltage V_r minus the branch voltage drop. In this chapter, for grid-connected operation mode, V_r is equal to V_0, since the root bus, i.e., bus 1 is connected to the main grid via the substation.

Particularly, with Fig. 4.1 for illustration, (4.7) calculates the active power exchanged between the microgrid and the main grid, i.e., P_{Grid}. It is noted that a positive value of P_{Grid} indicates the main grid supplies power to the microgrid, while a negative value means the main grid generates power to the main grid. Herein, V_0 is the substation voltage of the microgrid in the grid-connected mode. With the neglectable voltage drop, it is assumed that the voltage of bus 1 is equal to V_0. Besides, $I_{branch1}$ is the current through the branch starting from bus 1, which connects bus 1 and bus 2 in the illustration figure. Moreover, $Re(V_0 I_{branch\,1}{}^*)$ means the active power through the branch starting from bus 1. The microturbine installed at bus 1 is defined as

MT1, and P_{G1} indicates the real-time active power generated at bus 1. Since droop control is not applied in the grid-connected mode, P_{G1} is a constant power output setpoint in the OPF. Based on the Kirchhoff law, the active power from bus 1 to bus 2, i.e., $Re(V_0 {I_{branch\,1}}^*)$ is the sum of P_{G1} and P_{Grid}, so that eq (4.7) holds.

Eq. (4.2)-(4.7) can be used as power flow constraints in an OPF problem for the grid-connected operation mode. Detailed explanation of the direct load flow model can be found in [49].

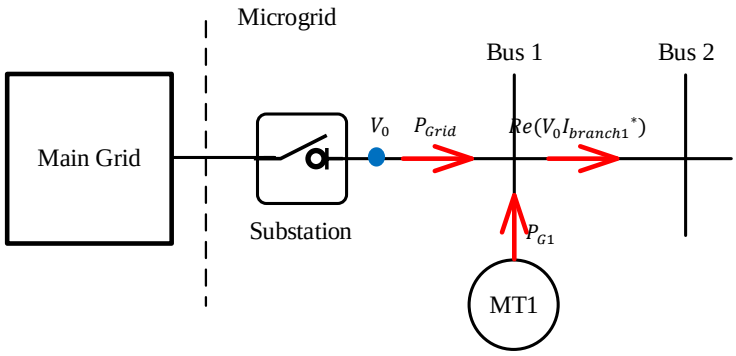

Figure 4.1. Illustration for Active Power Exchange in Grid-Connected Mode.

4.2.1.3 Operation Constraints

This OPF model involves the follow operation constraints.

$$V_{min} \le V_k \le V_{max} \ , k \in n_b \tag{4.8}$$

$$-I_{branch,b}^{max} \le I_{branch,b} \le I_{branch,b}^{max}, b \in B \tag{4.9}$$

$${P_{Gi}^0}^2 + {Q_{Gi}^0}^2 \le {S_{Gi}^{cap}}^2, i \in n_g \tag{4.10}$$

The operation constraints (4.8) and (4.9) represent the bus voltage requirement and the transmission line capacity limit. (4.10) is the microturbine power capacity limit.

In this grid-connected OPF model, microturbine power output setpoints P_{Gi}^0 and Q_{Gi}^0 are the control variables.

4.2.2 Islanded OPF Model

4.2.2.1 Objective Function

The objective of islanded OPF also aims to minimize the total operating cost as follows.

$$f^i = min \sum_{i \in n_g} (a_i P_{Gi} + b_i) + \sum_{k \in n_b} d_k LS \cdot P_{Lk} \tag{4.11}$$

Herein, LS is the load shedding rate (%), as one control variable in the microgrid islanded operation mode. Thus, $LS \cdot P_{Lk}$ is the load shed at bus k, and $d_k LS \cdot P_{Lk}$ calculates the corresponding load shedding penalty cost.

In addition to the microturbine power generation cost $(a_i P_{Gi} + b_i)$, the objective function of the islanded OPF also takes the load shedding penalty cost $d_k LS \cdot P_{Lk}$ into account.

4.2.2.2 Droop Control Functions

To control the system frequency and the bus voltages, droop control functions are enabled in the microturbines. The droop control functions are formulated as below.

$$P_{Gi} = P_{Gi}^0 + \frac{\Delta f}{m_{pi}} \ , i \in n_g \tag{4.12}$$

$$Q_{Gi} = Q_{Gi}^0 + \frac{V_k - V_0}{m_{qi}} \ , i \in n_g \tag{4.13}$$

The microturbine real-time power outputs (P_{Gi} and Q_{Gi}) are sum of the constant setpoints (P_{Gi}^0 and Q_{Gi}^0) and the real-time variations responding to the frequency and voltage deviations. In (4.12) and (4.13), m_{pi} and m_{qi} are active power and reactive power droop gains of microturbine i, respectively. When the system frequency and the local bus voltages vary, the microturbine power outputs respond to the corresponding deviations of the system frequency and the bus voltages.

4.2.2.3 Power Flow Constraints

Considering varying system frequency and reference bus voltage, a power flow model from [77] is used as constraints in the optimization problem and shown below.

$$P_k + jQ_k = (P_{Gi} + jQ_{Gi}) - (1 - LS)(P_{Lk} + jQ_{Lk}) + P_{pvk}\,, i \in n_g\,, k \in n_b \tag{4.14}$$

$$\boldsymbol{I_{nodek}} = \frac{P_k - jQ_k}{V_k}\ \,, k \in n_b \tag{4.15}$$

$$\boldsymbol{I_{branch}} = [\boldsymbol{BIBC}]\ \boldsymbol{I_{node}} \tag{4.16}$$

$$\Delta \boldsymbol{U} = [\boldsymbol{BCBV}]\ \boldsymbol{I_{branch}} \tag{4.17}$$

$$\boldsymbol{V} = \boldsymbol{V_r} - \Delta \boldsymbol{U} \tag{4.18}$$

$$\Delta f = \left(-m_{peq}\right)[P_{L1} - P_{G1}^0 + Re\left(\sum U_1 I_{1j}^*\right)] \tag{4.19}$$

$$\Delta V_r = \left(-m_{qeq}\right)[Q_{L1} - Q_{G1}^0 + Im\left(\sum U_1 I_{1j}^*\right)] \tag{4.20}$$

$$V_r = V_0 - \Delta V_r \tag{4.21}$$

$$m_{(.)eq} = (\sum m_{(.)i}^{-1})^{-1} \tag{4.22}$$

Models (4.14)-(4.18) share the same meanings with (4.2)-(4.6). It is worth noting that emergency load shedding is considered in islanded microgrid operation and the loads are determined by the shedding rate LS. The system frequency deviation is determined in (4.19) by multiplying the system equivalent active power droop gain m_{peq} and the summed active power variation at reference bus (bus 1). Similar with (4.19), the reference bus voltage drop ΔU_r is calculated in (4.20) by multiplying the system equivalent reactive power droop gain m_{qeq} and the summed reactive power variation at reference bus. Herein, the microturbine installed at bus 1 is defined as MT1, and P_{G1}^0 and Q_{G1}^0 are the active power and reactive power output setpoints. Besides, due to an islanded microgrid, the reference bus voltage V_r is not equal to the default value V_0, but it is required to be updated by (4.21). Last, (4.22) shows the calculation of the equivalent system droop gains.

Eq. (4.14)-(4.22) can be used as power flow constraints in an OPF problem for the islanded operation mode.

4.2.2.4 Operation Constraints

This OPF model involves the follow operation constraints.

$$V_{min} \leq V_k \leq V_{max} \;\; k \in n_b \tag{4.23}$$

$$-I_{branch,b}^{max} \leq I_{branch,b} \leq I_{branch,b}^{max}, b \in B \tag{4.24}$$

$$P_{Gi}^2 + Q_{Gi}^2 \;\leq S_{Gi}^{cap\,2} \;\; , i \in n_g \tag{4.25}$$

$$-\Delta f_{max} \leq \Delta f \leq \Delta f_{max} \tag{4.26}$$

$$-\Delta V_{r,max} \leq \Delta V_r \leq \Delta V_{r,max} \tag{4.27}$$

In addition to the constraints in the grid connected OPF, (4.23) to (4.25), there are three new operation constraints. Moreover, (4.26) and (4.27) limit the system frequency and the reference bus voltage.

In this islanded OPF model, the real-time microturbine power outputs P_{Gi} and Q_{Gi} as well as the load shedding rate LS are the control variables. In addition, it is noted that the islanded OPF model is not for an independent problem, but it is treated as response of the microgrid to disconnection from the main grid during a contingency. Thus, when the power system encounters a contingency, the microgrid automatically switches from the grid-connected to the islanded mode with the islanded OPF decision. Hence, the control variables in the grid-connected OPF model, i.e. P_{Gi}^0 and Q_{Gi}^0 must be considered as constants in the islanded OPF model.

4.2.3 Backward Forward Sweep Algorithm

The above two OPF models require update of system operating condition state variables, i.e., the bus voltages for the grid-connected OPF, as well as the bus voltages, the system frequency and the reference bus voltage for the islanded OPF. By applying a BFS algorithm, these values are calculated iteratively until they converge. This algorithm can be presented as follows.

Step 1 Calculate all of system operating condition state variables with the determined control variables.

Step 2 Check the convergence of the bus voltages. If the errors are beyond the convergence threshold, then update the bus voltages and return to Step 1. If the errors are under the convergence threshold, the bus voltages are kept.

Step 3 Check the convergence of the system frequency. If not converging, then, update the system frequency and return to Step 1; otherwise keep the current system frequency.

Step 4 Check the convergence of the reference bus voltage. If not converging, then, update the reference bus voltage and return to Step 1; otherwise keep the current reference bus voltage and terminate the algorithm.

Depending on the numbers of the system operating condition state variables, the grid-connected OPF only requires one loop for the bus voltages, while the islanded OPF requires three loops. The details of this algorithm can be found in [102].

4.3 Security-Constrained OPF for A Microgrid

Based on the OPF models for the grid-connected and the islanded operation modes, a security-constrained OPF model is firstly formulated. The OPF model aims to minimize generation cost in a microgrid working in the grid-connected mode with full consideration of tie-line switching into the islanded mode with load shedding, which forms an optimization problem. Additionally, a coupling constraint is developed and used for the microgrid automatic disconnection.

Then, to solve this security-constrained OPF problem, this chapter proposes a Benders decomposition based solution algorithm which involves the BFS algorithm for microgrid power flow calculation. This algorithm can guarantee a feasible solution of the secure operation by Benders cuts while ensuring optimality by minimizing the total operating cost covering generation and emergency load shedding.

4.3.1 Security-Constrained OPF Model

When system contingency occurs, microgrids can automatically disconnect from the main grid to keep supplying power to local loads. However, during this process, the islanded microgrids

may become unstable, due to possible large power imbalances. To guarantee system security for the microgrids after disconnection, tie-line switching from the grid-connected to the islanded mode is expected to be considered and modelled in the microgrid OPF. Thus, this chapter proposes a security-constrained OPF model considering tie-line switching, which is formulated as an optimization problem.

The objective is to minimize the total operating cost for both grid-connected and islanded operation modes. Hence, the grid-connected cost $f_0(x_0, u_0)$ corresponding to (4.1) and the islanded cost $f_1(x_1, u_1)$ corresponding to (4.11) are premeditated and combined together. Both grid-connected and islanded OPF models are used to formulate the following security-constrained OPF model with full consideration of tie-line switching process.

$$min f^{gc}(x_0, u_0) + f^{i}(x_1, u_1) \tag{4.28}$$

s.t.
$$g_0(x_0, u_0) = 0 \tag{4.29}$$

$$h_0(x_0, u_0) \leq h_0^{max} \tag{4.30}$$

$$g_1(x_1, u_1) = 0 \tag{4.31}$$

$$h_1(x_1, u_1) \leq \mu \cdot h_0^{max} \tag{4.32}$$

$$|u_1 - u_0| \leq \varepsilon^{max} \tag{4.33}$$

Herein, x and u represent state variables and controllable variables, respectively, and subscripts 0 and 1 means the grid-connected and islanded modes, respectively. Equality constraint set (4.29) presents the power flow constraints (4.2)-(4.7) and inequality constraint set (4.30) denotes the operation constraints (4.8)-(4.10) in the grid-connected mode. Similarly, (4.31) and (4.32) express the equality constraints (4.12)-(4.22) and inequality ones (4.23)-(4.27), respectively, for the islanded mode. It is noted that μ in (4.32) is a coefficient which determines how much the operation constraints in the islanded mode are allowed to be relaxed.

In addition, due to tie-line switching from the grid-connected mode to the islanded one, the microturbines adjust power generation heavily to reduce the deviations of system frequency and

bus voltages by droop control functions. To this end, constraint (4.33) is called coupling constraints which aims to prevent unrealistic tie-line switching movements from the grid-connected mode to the islanded one. The following constraint (4.34) is developed and used as (4.33) to limit the active power ramping limit of the microturbines.

$$\left|P_{Gi} - P_{Gi}^{0}\right| \leq \Delta P_{Gmax} \quad i \in n_g \tag{4.34}$$

4.3.2 Benders Decomposition Solution Method

In the proposed problem (4.28)-(4.33), the OPF models of the grid-connected and the islanded operation are combined with the coupling constraints to consider the tie-line switching movement, thus guaranteeing security by solving this problem.

As the proposed problem involves variables of two OPF models, these models can be considered as 'complicating constraints' [109]. Once 'complicating constraints' occur in an optimization problem, it means the outcome of one problem affects the solution to another problem. Generally, it is hard to minimize (4.28) with complicating constraints, and Benders decomposition methods are introduced to solve the proposed problem. In Benders decomposition, the original problem is decomposed into a master problem and a sub-problem, while the master problem does not include the complicating constraints [110]. Firstly, the master problem is solved and the solution indicating the optimized variables is given to the sub-problem. If the sub-problem is infeasible, a feasibility cut is generated and added to the master problem. Otherwise, the upper and lower bounds are checked for whether convergence is reached. When these two bounds do not converge, an optimality cut is generated and added to the master problem. The master problem and the sub-problem are solved iteratively until convergence.

Therefore, a modified Benders decomposition method is developed, and it is specific for the proposed security-constrained OPF problem considering tie-line switching. In this method, the OPF problem (4.28)-(4.33) is divided into a master problem for the grid-connected OPF and a sub-problem for the islanded OPF. In addition, this method generates feasibility cuts to consider conditions of possible tie-line switching in the grid-connected master problem. Key steps of this method are introduced as follows.

Step 1 - Optimize the grid-connected OPF master problem.

$$min\ f^{gc}(x_0, u_0) \tag{4.35}$$

s.t. $$g_0(x_0, u_0) = 0 \tag{4.36}$$

$$h_0(x_0, u_0) \leq h_0^{max} \tag{4.37}$$

By solving this master problem (4.35) to (4.37), a set of u_0 which consists of all the setpoints of microturbines is obtained without considering islanded operating conditions. The u_0 is regarded as constant u_0^r in the later sub-problem.

Step 2 - Check feasibility of the islanded OPF sub-problem with the results u_0^r as parameters, by solving the dual problem.

The islanded OPF sub-problem is formulated below.

$$minf^i(x_1, u_1) \tag{4.38}$$

s.t. $$g_1(x_1, u_1) = 0 \tag{4.39}$$

$$h_1(x_1, u_1) \leq \mu \cdot h_0^{max} \tag{4.40}$$

$$|u_1 - u_0^r| \leq \varepsilon^{max} \tag{4.41}$$

The aim of this step is checking the feasibility of islanded OPR problem when disconnecting from the main grid. If the sub-problem is feasible then the current u_0^r is the solution of the whole security-constrained OPF problem and the algorithm is terminated. Otherwise, the operation constraint (4.40) or the coupling constraint (4.41) cannot be fulfilled, a feasibility cut is required to be generated.

To check the feasibility of the sub-problem (4.38)-(4.41), its dual problem is formulated and solved. First, the islanded OPF sub-problem is reformed into the following matrix form.

$$\min h^t y_1 \tag{4.42}$$

s.t. $$\boldsymbol{L}y_0^* + \boldsymbol{N}y_1 = w \tag{4.43}$$

$$\boldsymbol{J}y_0^* + \boldsymbol{K}y_1 \leq v \tag{4.44}$$

Here, y_0^* is the result set of all the variables gained in Step 1, i.e., x_0 and u_0, while y_1 represents all the variables of islanded OPF sub-problem, i.e., x_1 and u_1.

A dual problem is then formulated as follows.

$$\max[(\boldsymbol{J}y_0^* - v)^T\varphi + (w - \boldsymbol{L}y_0^*)^T\omega] \tag{4.45}$$

s.t. $$\boldsymbol{K}^T\varphi - \boldsymbol{N}^T\omega + h = 0, \varphi \geq 0 \tag{4.46}$$

Here, ω and are φ dual variables for constraints (4.43) and (4.44), respectively. If the dual problem is feasible, then the primal problem (4.42)-(4.44) is feasible and this Benders decomposition progress will end If the dual problem is unbounded, this means the primal problem is infeasible and a feasibility cut is required.

Step 3 - Generate a feasibility cut for master problem.

A Benders feasibility cut is generated when the dual problem is unbounded. For generating this feasibility cut, the primal problem is relaxed to ensure that a relaxed sub-problem (RSP) is always feasible. The RSP programming is expressed as follows.

$$\min \mathbf{1}^T Rel \tag{4.47}$$

s.t. $$\boldsymbol{L}y_0^* + \boldsymbol{N}y_1 = w \tag{4.48}$$

$$\boldsymbol{J}y_0^* + \boldsymbol{K}y_1 \leq v + \boldsymbol{E} \cdot Rel \tag{4.49}$$

Herein, $\mathbf{1}$ is a vector of 1 and $\boldsymbol{E}$ is an identity matrix. Rel means the matrix of the relaxed variables added to the right side of (4.49) for constraint relaxation. It is obvious that there is always a set of Rel allowing feasibility of the Rstochastic programming. Thus, the dual variables of (4.49) are defined as φ_1 and the objective of Rstochastic programming can be obtained as $\mathbf{1}^T Rel^r$.

With the dual variables, a feasibility cut is generated below.

$$1^T Rel^r + (y_0 - y_0^*)^T \boldsymbol{J}^T \varphi_1^r \leq 0 \quad (4.50)$$

Therefore, Step 3 generates feasibility cuts for the master problem (4.35)-(4.37) until the sub-problem (4.38)-(4.41) is feasible.

Step 4 – Reformulate the grid-connected OPF master problem with the generated feasibility cut.

The feasibility cut (4.50) is added and the grid-connected OPF master problem is reformulated as follows.

$$min f^{gc}(x_0, u_0) \quad (4.35)$$

s.t. $$g_0(x_0, u_0) = 0 \quad (4.36)$$

$$h_0(x_0, u_0) \leq h_0^{max} \quad (4.37)$$

Feasibility cut: (4.50)

$$\mathbf{1}^T Rel^r + (y_0 - y_0^*)^T \boldsymbol{J}^T \varphi_1^r \leq 0$$

In this problem, the new feasibility cut is used as a constraint.

Compared to step 1, it is found that only the feasibility cut is adopted. This is because this security-constrained OPF problem aims to optimize the cost of grid-connected mode while guaranteeing islanded constraints without violation. In fact, when the sub-problem (4.38)-(4.41) is feasible and solved, the solution is naturally optimal without optimality cuts required.

The whole process of the developed Benders decomposition method is shown in Fig. 4.2 and its convergence will be analysed in Chapter 4.5- Case Study.

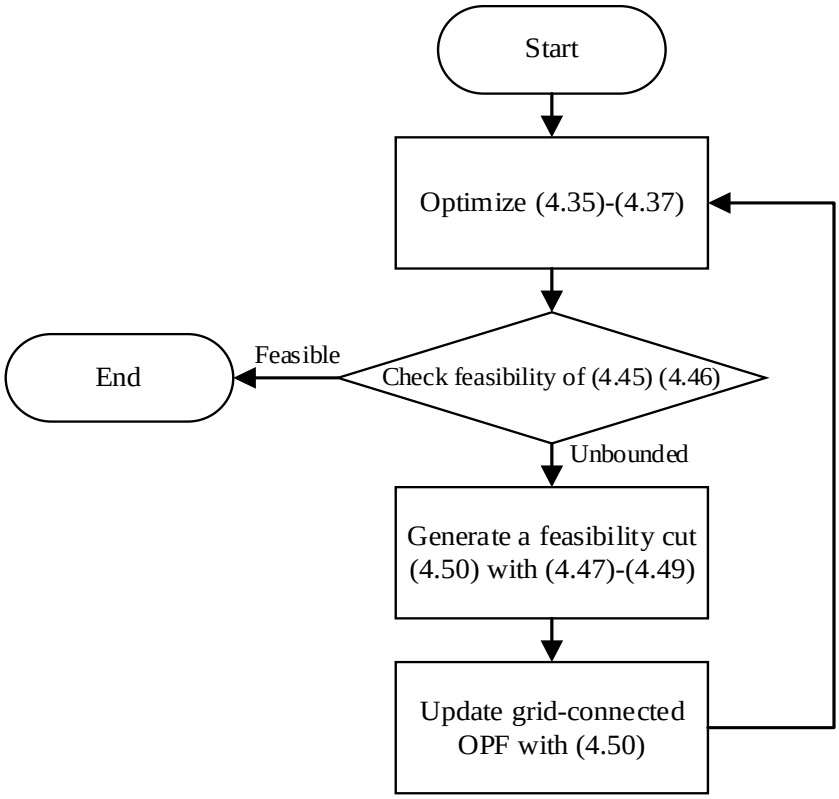

Figure 4.2. Flowchart of Benders Decomposition Method.

4.3.3 Solution Algorithm for Security-Constrained OPF

With the modified Benders decomposition method, a new solution algorithm is developed for the proposed security-constrained OPF problem considering tie-line switching from grid-connected to islanded mode. This algorithm utilizes and combines the modified Benders decomposition method and the BFS algorithm.

The modified Benders decomposition method is applied as an inner loop to solve the grid-connected and the islanded OPF problems, as well as generate feasibility cuts. However, this loop cannot guarantee OPF results, since the microgrid operating conditions are changing. Thus, an outer loop that applies the BFS algorithm to update the microgrid operating conditions is adopted.

In this outer loop, four sets of variables, i.e., islanded bus voltages, islanded system frequency, islanded reference bus voltage and grid-connected bus voltages, are updated and checked for convergence. It is noted the bus voltages in both islanded and grid-connected modes may not completely converge, due to mutual impacts among such a large number of bus voltages in networks. However, despite the bus voltage variations, the objectives can be fully converged,

which implies an unchanged solution in terms of the optimization objective. Therefore, this chapter also checks the objectives in both islanded and grid-connected modes as alternative convergence criteria when the bus voltages cannot fully converge.

The whole Benders decomposition based solution algorithm is illustrated as a flowchart in Fig. 4.3.

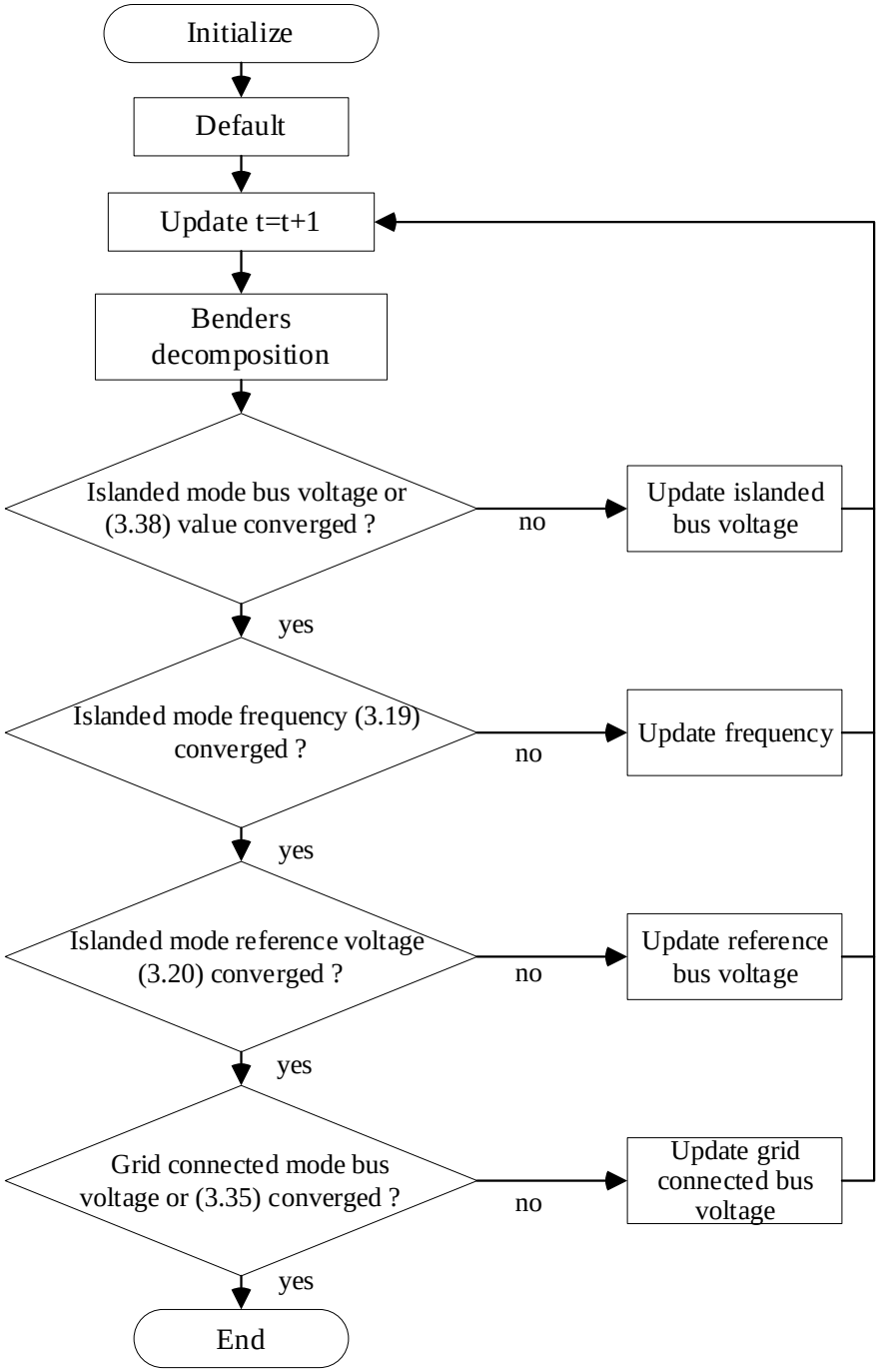

Figure 4.3. Solution Algorithm for Security-Constrained OPF.

4.4 Stochastic Security-Constrained OPF

For addressing uncertainties of renewable power generation and load demand, a stochastic programming method is adopted for the proposed security-constrained OPF problem. The uncertainties are considered as determinate scenarios which are generated with their probability distributions through a probabilistic modelling approach [100]. Thus, a stochastic security-constrained OPF problem is finally developed in this chapter.

4.4.1 Stochastic Programming Model

To deal with uncertainties of PV power generation and loads, scenario-based stochastic programming methods can be used. The basic model of scenario-based stochastic programming is introduced in this sub-section.

Firstly, the general stochastic programming has the following objective function.

$$minE_{\xi}[f(x,u,\xi)] \tag{4.51}$$

Herein, u is the set of control variables, x is the set of state variables and ξ indicates certain realization of uncertainties. Under the certain realization of ξ, $f(x,u,\xi)$ is treated as the objective of a deterministic problem with ξ as parameters. E_{ξ} is the expectation of $f(x,u,\xi)$.

Then, the above objective function can be transformed with realization scenarios, and a scenario-based stochastic programming model can be formulated as follows.

$$min\sum_{s\epsilon S}\rho_s f(x,u,\xi_s) \tag{4.52}$$

s.t. $$g(x,u,\xi_s)=0,\forall s\epsilon S \tag{4.53}$$

$$h(x,u,\xi_s)\leq 0,\forall s\epsilon S \tag{4.54}$$

In this model, a set of realization scenarios, $\xi_1,\xi_2,\xi_3,\ldots,\xi_s$ are generated, while their probabilities of occurrence are $\rho_1,\rho_2,\ \rho_3,\ \ldots,\rho_s$. S represents a set of scenario numbers composed by s which is the serial number of each scenario.

Minimization of the probability weighted objective function is presented by (4.52), while (4.53) and (4.54) denote the equality and inequality constraints under all the realization scenarios.

4.4.2 Probabilistic Modelling of Uncertainties

Conventionally, scenarios are generated by Monte Carlo sampling techniques and reduced to an acceptable number by scenario reduction methods [101]. However, since each realization scenario corresponds to a unique group of constraints, the conventional Monte Carlo sampling techniques will cause heavy computing burdens. Besides, the reduction methods will reduce the accuracy of the scenarios for representing the uncertainty probability distribution. To improve the efficiency of the proposed stochastic OPF method, a direct scenario-generating approach introduced in [100] is applied.

With the probability density function (PDF) of the uncertainty, the value of the uncertainty P^u is divided into a number of M states with limits $\bar{P}_m^u$ and $\underline{P}_m^u$ for the state m. The mean of this state is computed as (4.55), which is treated as the value of the interval of $[\bar{P}_m^u, \underline{P}_m^u]$.

$$P_m^u = \frac{\int_{\underline{P}_m^u}^{\bar{P}_m^u} P^u PDF\, dP^u}{\int_{\underline{P}_m^u}^{\bar{P}_m^u} PDF\, dP^u}, m = 1,2,3,\dots,M \tag{4.55}$$

Then, the occurrence probability of state *m* defined as ρ_m^u is also derived from the PDF of the uncertainty as below.

$$\rho_m^u = \int_{\underline{P}_m^u}^{\bar{P}_m^u} PDF\, dP^u, m = 1,2,3,\dots,M \tag{4.56}$$

Through this approach, a set of PV power generation states with the total number *M*, $S^{PV} = \{P_m^{PV}, \rho_m^{PV}\}$, and a set of load states with the total number *N*, $S^D = \{P_n^D, \rho_n^D\}$ can be generated. Based on these two sets, a combined set of all PV power generation and load states is formed as follows.

$$S = \{(P_m^{PV}, P_n^D), \rho_s\} \tag{4.57}$$

$$\{(P_m^{PV}, P_n^D)\} = \psi^{PV} \times \psi^D, \tag{4.58}$$

$$where\ \psi^{PV} = \{P_m^{PV}\}, \psi^D = \{P_n^D\}$$

$$\rho_s = \rho_m^{PV} \times \rho_n^D, \forall (P_m^{PV}, P_n^D) \tag{4.59}$$

$\{(P_m^{PV}, P_n^D)\}$ represents a set of combined states calculated by the Cartesian product of the sets ψ^{PV} and ψ^D. Its corresponding joint occurrence probability is ρ_s. By using this approach, a number (M× N) of combined states as uncertainty realization scenarios are used in the stochastic OPF model (4.52)-(4.54). Besides, M and N are expected to be selected as small as possible to avoid heavy computing burdens for the stochastic OPF method. Details of this probabilistic modelling approach can be found in [100].

4.4.3 Formulation of Stochastic Security-Constrained OPF

Lastly, with the scenario-based stochastic programming model (4.52)-(4.54) and the uncertainty realization scenarios generated as (4.57)-(4.59), the final stochastic security-constrained OPF is formulated into the following model.

$$min \sum_{s \epsilon S} \rho_s [f^{gc}(x_0, u_0, \xi_s) + f^i(x_1, u_1, \xi_s)] \tag{4.60}$$

s.t.
$$g_0(x_0, u_0, \xi_s) = 0, \forall s \epsilon S \tag{4.61}$$

$$h_0(x_0, u_0, \xi_s) \leq h_0^{max}, \forall s \epsilon S \tag{4.62}$$

$$g_1(x_1, u_1, \xi_s) = 0, \forall s \epsilon S \tag{4.63}$$

$$h_1(x_1, u_1, \xi_s) \leq \mu \cdot h_0^{max}, \forall s \epsilon S \tag{4.64}$$

$$|u_1 - u_0| \leq \varepsilon^{max}, \forall s \epsilon S \tag{4.65}$$

Compared to the deterministic model (4.28)-(4.33) given by Chapter 4.3.1, this stochastic security-constrained OPF model makes the objective function as well as all the constraints hold under all the uncertainty realization scenarios.

In this model, all the scenarios s are contained in the set S as (4.57), ξ_s presents each combined state (P_m^{PV}, P_n^D) from (4.58) and the occurrence probability ρ_s is calculated by (4.59). The combined states ξ_s are involved in the objective function (60) and all the constraints except the coupling constraint, i.e. (4.61)-(4.64). Since (4.33) only contains the control variables, the corresponding constraint in the stochastic programming, i.e. (4.65), does not contain the combined states ξ_s. However, (4.65) also holds under all the scenarios.

The Benders decomposition based solution algorithm developed in Chapter 4.3.3 still works for this stochastic security-constrained OPF model.

4.5 Case Study

4.5.1 Test System Description

A 33-bus distribution system [43] is used as a microgrid in this chapter for case study. It is indicated by [77] that this system is suitable for microgrid tests. The predicted active and reactive loads are scaled up to 7.43 MW and 4.60 MVar, respectively. There are five microturbines installed in the system and their parameters are shown in Table 4.1. Besides, there are eight PV systems connected to buses 9, 11, 13, 21, 22, 25, 27 and 29 respectively, and the predicted power generation of each PV system is 243kW.

The price for the energy bought from the main grid is set as 61.7 $/MWh [111]. The microturbine generation cost parameters according to [112] are shown in Table 4.2. The load shed-ding cost is set as 200 $/MWh.

Table 4.1 Microturbine Parameters

Microturbine No.	Bus No.	Capacity (MVA)	Frequency Droop Coefficient (p.u.)	Voltage Droop Coefficient (p.u.)
1	1	2	-0.04	-0.04
2	6	1	-1	-1
3	13	1.5	-0.2	-0.1
4	25	1.2	-0.5	-0.3
5	33	1.4	-0.2	-0.2

Table 4.2 Generation Cost Parameters

Microturbine No.	1	2	3	4	5
Generation Cost ($/MWh)	169.5	186.5	176.3	180.5	177.1

Bus 1 is treated as the reference bus for both grid-connected OPF (master problem) and islanded OPF (slave problem). Moreover, V_{min} and V_{max} are 0.95 p.u. and 1.05 p.u., respectively. The branch current limit $I_{branch,b}^{max}$ is assumed equal for the whole system as 650A. In the islanded mode, the limits of the system frequency deviation and the reference bus voltage deviation are set as [-0.02, 0.02] p.u. and [-0.04, 0.04] p.u. In this chapter, the maximal allowed percentage of load shedding ls_{max} is set as 20%. The operation period is set as 30 minutes which is practical [113].

This simulation is conducted on a 64-bit PC with 4.10GHz CPU and 64 GB RAM utilizing YALMIP [86] toolbox in MATLAB platform. The proposed stochastic security-constrained OPF problem is solved by GUROBI solver [87].

4.5.2 Probabilistic Model of Uncertainties

Gaussian PDF is used for both PV power generation and loads. The means are set to the predicted values and the standard deviations are 0.05 for PV power generation and 0.04 for loads, respectively. The applied PDFs are presented in Fig. 4.4.

Using (4.55) and (4.56), the values of states and the corresponding occurrence probabilities states can be obtained. Moreover, since the standard deviation of PV power output is larger than that of loads, its state number is determined twice of the load demand one. Hence, the loads are divided into 4 states while that of PV power generation is divided into 8 states. P_m^u and ρ_m^u of loads and PV power generation are shown in Fig. 4.5.

These states are then combined to generate (4.57)-(4.59) and used in the stochastic OPF model (4.60)-(4.65).

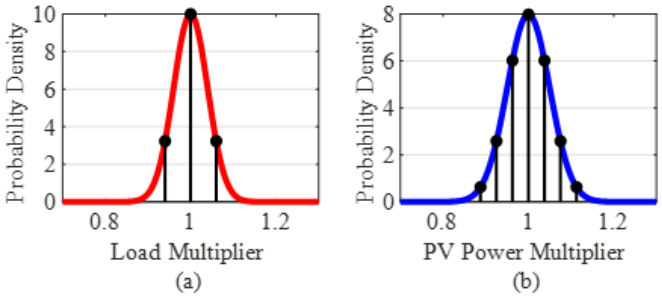

Figure 4.4. Probability Density: (a) Load; (b) PV Output.

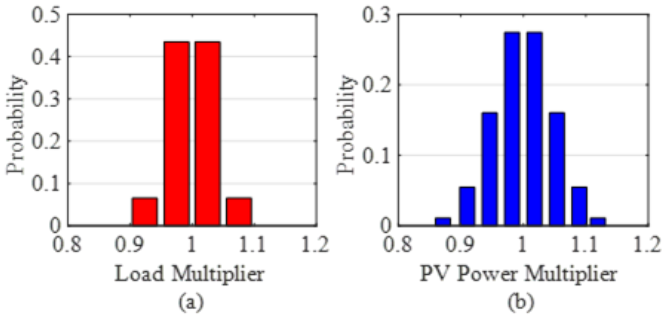

Figure 4.5. State Occurrence Probability: (a) Load; (b) PV Output.

4.5.3 Convergence Performance

Using the modified Benders decomposition method developed in Chapter 4.3.2, the proposed stochastic security constrained OPF problem is solved for the further operating condition update.

The upper bound is the objective value given by (4.28)-(4.33) while the sub-problem (4.38)-(4.41) is feasible. The lower bound is the result obtained by the optimization problem reformed by (4.35) to (4.37). The algorithm converges when the gap between the upper and lower bounds is reduced to an acceptable level. This convergence progress is the inner loop of the whole Benders decomposition based solution algorithm.

With the solutions provided by the modified Benders decomposition method, the operating conditions are updated by the Benders decomposition based solution algorithm as Fig. 4.3 shows. In detail, the values of the system frequency deviation, the objective and the reference bus voltage in the islanded mode for each iteration of the outer loop are demonstrated in Fig. 4.6-4.8, respectively.

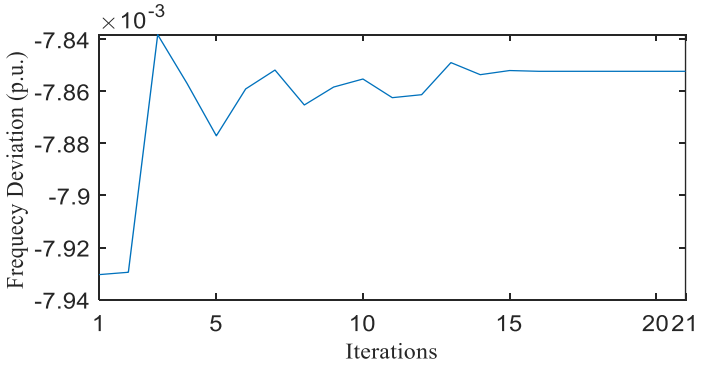

Figure 4.6. Convergence Progress of Frequency Deviation.

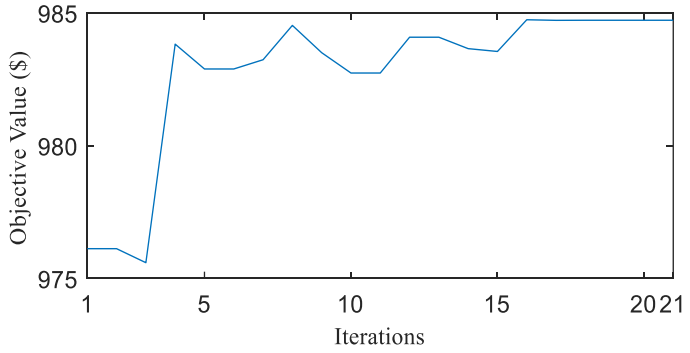

Figure 4.7. Convergence Progress of Objective Value.

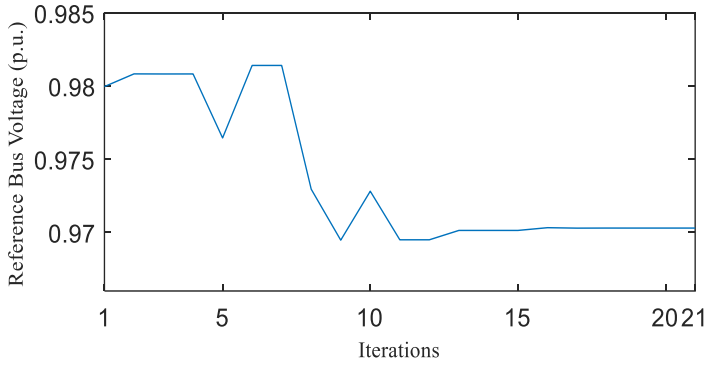

Figure 4.8. Convergence Progress of Reference Bus Voltage.

Firstly, it is that the initial values of Δf, V_r and V_k can be estimated in advance for reducing iteration times. These sets of initial values are obtained by running grid-connected and islanded OPF independently. Eq. (4.19) indicates that the system frequency deviation is actually caused by the total active power imbalance.

Then, by using an estimated frequency deviation given by (4.19), the system frequency deviation only drifts within a small range shown by Fig. 4.6, which implies that the sum of ΔP_{Gi}

can be estimated at the beginning of the algorithm. Similarly, in Fig. 4.7, the OPF objective value, which is determined by P_{Gi} and LS, also varies within a small range. It indicates that the total active power required for the system can also be estimated at the beginning of the algorithm.

However, the reference bus voltage V_r has heavier oscillations compared to other iterative values, which implies the sum of ΔQ_{Gi} is oscillating according to Eq (4.20). The reason is because the proposed method sets two system operating conditions to judge whether the innermost bus voltage loop is converged or not, as shown in Fig. 4.3. In detail, when the objective value is converged, the bus voltages may be still oscillating. Due to droop control, ΔQ_{Gi} is oscillating and so is the reference bus voltage V_r. Finally, the convergence of V_r occurs when the sum of ΔQ_{Gi} does not change much. On the other hand, in terms of the optimization model, the fundamental reason for this phenomenon is that it is hard to determine the reactive power outputs since they are not involved in the objective function.

Once V_r is becoming constant after the 13th iteration as shown in Fig. 4.8, the frequency deviation and the objective values immediately tend to converge within 3 iterations as shown in Fig. 4.6 and 4.7.

The proposed solution algorithm takes 21 iterations to reach convergence with the total solver time of 175.6 seconds. Since the proposed OPF method is designed for a 30-minute operation period, the solver time is fully compatible for practical online use.

4.5.4 Optimization Results

Applying the Benders decomposition based solution algorithm introduced in Chapter 4.3.3. The optimized objective (3.35) is 534.23$, which is efficiently minimized by the proposed OPF method. The microturbine setpoints considering islanded mode are optimized and presented in Fig. 4.9.

With considering the possible islanded operation mode, the microturbines No.1 and No.5 have high active power generation setpoints, while the No.2 and No.3 have high reactive power setpoints. Generating active power by microturbines in the grid-connected mode is used for avoiding the breakout due to the ramping limits while tie-line switching to the islanded mode. In addition, the reactive power is used for voltage regulation when the microgrid becoming islanded.

When the microgrid disconnects from the main grid, the frequency decreases with negative frequency deviations as shown by Fig. 4.6. Under this condition, the frequency droop control works and all the microturbines generate more active power than the setpoints.

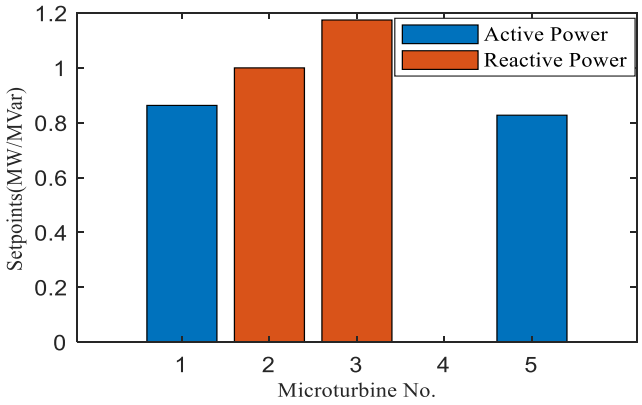

Figure 4.9. Optimized Microturbine Setpoints.

4.5.5 Robustness Check for Grid-Connected Model

To check the solution robustness for the grid-connected operation mode, 1000 scenarios are randomly by Monte Carlo sampling with the PDFs given in Chapter 4.5.2. These scenarios are used generated as uncertainty realizations to test the performance of the proposed stochastic OPF method with probabilistic modelling. For comparison, a conventional deterministic OPF method, which optimizes the microturbine setpoints for the grid-connected mode with only the predicted mean values of the uncertainties, is applied and tested by the same 1000 scenarios. It is noted that this conventional method does not consider the possible islanded mode during the optimization progress. The result indices, such as the average operating cost, the average and the maximal absolute bus voltage deviations, as well as the constraint satisfaction rate for all the 1000 scenarios, are obtained and given in Table 4.3.

Table 4.3 Robustness Check for Grid-Connected Mode

Method	*Conventional*	*Proposed*
Average Operating Cost ($)	348.62	588.89
Average Absolute Voltage Deviation (p.u.)	0.0309	0.0258
Maximal Absolute Voltage Deviation (p.u.)	0.0635	0.0542
Constraint Satisfaction Rate (%)	52.8%	98.2%

From the result comparison table, it is seen that even though the average operation cost is higher, the proposed stochastic OPF method outperforms the conventional one on the other three indices. It is worth noting that the maximal voltage deviation of the proposed method is slightly out of the allowed range, while that of the conventional method is far from the allowed 0.05 p.u. Moreover, the proposed method can achieve a remarkably high robustness degree against uncertainty realizations, with the higher constraint satisfaction rate than the conventional method.

Considering that it is imperative to keep the operation constraints and reduce the bus voltage deviations, a sacrifice on the operating cost is acceptable. Thus, the proposed stochastic OPF method is highly suggested.

4.5.6 Security Check for Islanded Mode

At last, assuming that there is a contingency in the main grid, the microgrid will automatically switch to the islanded operation mode. To check the security of the microgrid operation during this tie-line switching action, this applies the 1000 uncertainty realization scenarios generated in Chapter 4.5.5 to test the islanded microgrid operation performance with the microturbine setpoints obtained by the proposed stochastic security-constrained OPF method. For comparison, the conventional grid-connected OPF method which does not consider the possible islanded mode is applied as well.

The proposed stochastic security-constrained OPF method can satisfy all the operation constraints under all the 1000 scenarios, which validates full operation security under the condition of tie-line switching to the islanded mode. However, the conventional method can only achieve secure operation for 3.1% of the uncertainty realization scenarios.

Therefore, considering that the system operation security is the priority and requires a 100% guarantee, the proposed stochastic security-constrained OPF method is superior for practical use.

4.6 Conclusion

In this chapter, a new stochastic security-constrained OPF problem for microgrids is formulated with consideration of tie-line switching from the grid-connected to the islanded mode.

Then, this chapter develops a Benders decomposition based solution algorithm to solve this problem.

Via numerical simulations, firstly, the convergence of the proposed solution algorithm is demonstrated. Then, with comparison with the conventional method, the high solution robustness and fully operation security of the microgrid is validated. Thus, the proposed stochastic security-constrained OPF method can efficiently address the uncertainty and the security issues when considering microgrid tie-line switching from the grid-connected to the islanded mode.

Chapter 5 SENSITIVITY REGION BASED OPTIMIZATION FOR MAXIMIZING RENEWABLE GENERATION HOSTING CAPACITY OF AN ISLANDED MICROGRID

Renewable energy based distributed generators are key components in islanded microgrids. However, their power intermittency and uncertainty may impair power quality and cause system operating constraint violations. It is imperative to evaluate and maximize the hosting capacity of an islanded microgrid for renewable generation. Besides, conventional optimization methods focus on improving the solution robustness on constraints under uncertainties but ignoring that on the optimization objective. To address these unsolved issues, a sensitivity region (SR) based optimization method for maximizing renewable generation hosting capacity of an islanded microgrid is proposed. This chapter firstly proposes an optimization model considering microgrid frequency variation and microturbine droop control functionality. Secondly, SR and feasibility-SR are adopted to quantify solution robustness against uncertainties of renewable generation and load. It is expected to enlarge these two regions to cover all the possible uncertainty realizations, thus providing robust solutions. Last, this chapter develops an SR based optimization method with a new solution algorithm. Through comprehensive numerical simulations, the proposed SR based hosting capacity maximization method is verified with high solution robustness on both objective and operating constraints.

5.1 Introduction

Increasing countries have committed to changing their energy structure for reducing carbon emission and building a sustainable energy future [64]. To achieve targets of decarbonization, installations of renewable distributed generations (DGs) such as wind turbines (WTs) and photovoltaics (PVs) continue growing at a rapid speed. Such renewable DGs can contribute to

supplying cost-effective and clean energy in microgrids, especially islanded microgrids of rural areas or islands [114].

From the perspective of microgrid operation, increasing penetration of renewable generation cause various problem, such as network operating constraint variations, and power quality issues [65]. Hosting capacity of a network for renewable generation has become a timely focus in research. The hosting capacity can be defined as the maximum renewable generation can be injected into a network while keeping network operating constraints. The authors of [115] propose a hosting capacity evaluation method with active distribution network management schemes, which applies on-load tap changers and static var compensators to maximize the hosting capacity without technical limit violation. In [116], a hosting capacity assessment method considering load and renewable power uncertainties via distributionally robust optimization is proposed. Furthermore, the work of [117] aims to coordinate various devices including capacitors, voltage regulators, branch switches and DG inverters to maximize the hosting capacity via a mixed integer nonlinear model solved by a genetic algorithm (GA). The work [118] formulates an optimization model for maximizing renewable generation hosting capacity and minimizing total energy consumption in a distribution system considering thermal smart loads. In [119], the authors propose an economic dispatch model considering the power balance between supply and demand, to maximize PV hosting capacity of a distribution network. In [120], the authors consider maximizing hosting capacity as one of multiple objectives in a battery energy storage system (BESS) planning problem. The work of [121] further optimizes BESS allocation in an unbalanced three phase distribute network to maximize the hosting capacity, with an advanced robust optimization method. These existing works focus on distribution networks, and it is imperative to assess and maximize the hosting capacity of an islanded microgrid.

On the other hand, for microgrids, optimal allocation of DGs has been studied in literature to enhance economic and technical benefits. In [122], the authors optimize DG placement in a grid-connected microgrid to minimize multiple costs. The work of [123] considers dynamic line rating conditions, which depend on seasonal temperatures, in a DG planning model. The authors of [124] optimize both DG allocation and microgrid topology via a two-step solution procedure. It is indicated by the literature that the optimal DG planning can improve technical

and economic benefits for microgrids. However, it is worth noting that these optimization models of grid-connected microgrids do not suit for islanded microgrids where system frequency/voltage control is essential to be considered and addressed by microturbines. Recently, in [125], the authors aim to maximize PV hosting capacity for an off-grid industrial microgrid with BESS considering post-fault recovery. This method applies commercial simulation software with an iterative algorithm to validate the hosting capacity step by step, which is not a mathematical optimization model.

Due to increasing beneficial renewable DGs, it is the time to maximize the hosting capacity of a droop-controlled islanded microgrid with an accurate power flow model and network operating constraints, which has never been reported in the literature. The emerging power flow models of islanded microgrid considering droop control are proposed by [77] and [78], and an optimal power flow model is further developed by [94]. These models allow development of maximizing hosting capacity of an islanded microgrid which is this chapter's focus.

Uncertainties of non-dispatchable renewable generation (e.g., wind power) and load have significantly adverse impacts on microgrid operation, which are expected to be considered and addressed in optimization models. Two mainstream methods for addressing the uncertainty issues are introduced below.

In [126], the authors apply a stochastic programming (SP) method with a large amount of uncertain PV power generation scenarios following beta probability distribution. To alleviate the heavy computing burden of SP caused by the numerous scenarios, a fast backward scenario reduction method [55] or a probabilistic modeling method [100] can be used to reduce the number of scenarios. Such scenario-based SP methods are used in the DG planning problems [82] and [127], and in the hosting capacity maximization problem [66], with specific probability distribution functions for various uncertainties. For these SP models, it is difficult to select the efficient number of uncertainty scenarios. A small number of scenarios may lead to failure in guaranteeing network operating constraints, while a large number may lead to curse of dimensionality.

Apart from the SP, robust optimization (RO) is another method to address uncertainties. In [129] and [122], RO methods are applied for minimizing the costs of DG investment and

microgrid operation by modeling multiple uncertainties into uncertainty sets. Moreover, the authors in [130] introduce a resilient planning model considering natural disasters where uncertain disasters and sequential impacts are addressed by a RO method. The RO methods can solve the problems with high computing efficiency. However, the optimization solutions obtained under the worst case of typical uncertainty realization are over-conservative. To this end, a probability-weighted RO method [10] can be applied to reduce the solution conservativeness, only if long-term uncertainty probability is available or assumable.

The SP and RO methods can deal with uncertainties to keep network operating constraints. However, besides achieving solution robustness on the constraints, it is expected to keep the expected objective under uncertainty realizations, which presents solution robustness on the objective [62]. To this point, uncertainty impacts to the hosting capacity have not been addressed, leaving a significant research gap. To enhance the solution robustness on the objective, a sensitivity region (SR) method is developed in [61] and it aims to make the expected objective only vary within an acceptable range. Furthermore, this method is expanded with a feasibility sensitivity region (FSR) [131] to guarantee operating states within limits. This work also defines an index to directly assess the solution robustness. It is worth noting that these SRs can quantify the solution robustness on the objective and constraints under uncertainties. Thus, they are expected to be enlarged to cover all possible uncertainty realizations, so that a fully robust solution can be obtained. It is sensible and essential to develop a SR based optimization method for maximizing the renewable generation hosting capacity of an islanded microgrid.

To address the unsolved issues mentioned above, this chapter proposes a hosting capacity maximization model for an islanded microgrid, and develops a SR based optimization method to guarantee solution robustness on both objective and operating constraints. The main contributions of this chapter are summarized as follows.

To address the unsolved issues mentioned above, this chapter proposes a hosting capacity maximization model for an islanded microgrid, and develops a SR based optimization method to guarantee solution robustness on both objective and operating constraints. The main contributions of this chapter are summarized as follows.

1) An optimization model is proposed to maximize the renewable generation hosting capacity of an islanded microgrid considering system frequency variation and microturbine droop control functionality.

2) SR and FSR are adopted to quantify the solution robustness on objective and constraints, respectively, against uncertainties of renewable generation and load.

3) A SR based optimization method is developed to obtain a robustly maximal hosting capacity under the uncertainties. Accordingly, a new solution algorithm is proposed.

The remainder of this chapter is organized as follows. Chapter 5.2 presents mathematical formulation of maximizing renewable generation hosting capacity of an islanded microgrid (taking WT as an example of renewable DG in this chapter). Chapter 5.3 introduces the SR and FSR concepts for the uncertainty modelling, as well as two robustness indices. Chapter 5.4 presents a SR based optimization method and a new solution algorithm. Chapter 5.5 demonstrates numerical simulations of the proposed hosting capacity maximization method with comprehensive tests and analysis results. At last, Chapter 5.6 concludes the whole chapter.

5.2 Maximizing Hosting Capacity of An Islanded Microgrid

Considering WT as the renewable DG, this chapter aims to maximize the hosting capacity of an islanded microgrid for the uncertain wind power. Other types of renewable DG such as PVs can also be considered when necessary. It is noted that the system frequency and bus voltages fluctuate, and they are expected to be controlled within secure ranges. This chapter also takes the practice that dispatchable microturbines are enabled with droop control functionality for both frequency and voltage control in the islanded microgrid. To provide better power quality, it is necessary to minimize the system frequency deviation of the islanded microgrid. Thus, this chapter proposes a multi-objective optimization model which maximizes the hosting capacity and minimizes the system frequency deviation simultaneously. This chapter adapts a droop-controlled microgrid power flow model to obtain the microgrid operating conditions and verify them within the secure ranges.

5.2.1 Droop-Controlled Microgrid Power Flow

The direct load flow method [49] is efficient for radial microgrids, and dummy buses can be used to allow this method working for weakly meshed microgrids. Based on this method, a further droop-controlled power flow model is developed in [77], and it is adapted for estimation of islanded microgrid operating condition.

Distributed energy resources including microturbines should provide both frequency and voltage control services in power systems [1]. In islanded microgrids, frequency-active power (freq-watt) and voltage-reactive power (volt-var) droop control functions are generally enabled in microturbines [77]-[78]. In this chapter, microturbines are capable of providing both freq-watt and volt-var droop control. It is noted that other control functions such as voltage-active power (volt-watt) function can also be considered and used if necessary

Firstly, due to system frequency and bus voltage variations, the adjustments on active and reactive power outputs ΔP_j^{MT} and ΔQ_j^{MT} are directly calculated by (5.1) and (5.2), respectively. Then, they are added to the optimized power setpoints $P_j^{MT,0}$ and $Q_j^{MT,0}$ by (5.3) and (5.4). Here, P_j^{MT} and Q_j^{MT} present the total active and reactive power outputs of the microturbine at bus j, m_{pj} and m_{qj} are frequency and voltage droop coefficients of the microturbines. F is the system frequency and F_0 is the nominal value.

$$\Delta P_j^{MT} = \frac{\Delta F}{m_{pj}}, \forall j \tag{5.1}$$

$$\Delta Q_j^{MT} = \frac{\Delta V_j}{m_{qj}}, \forall j \tag{5.2}$$

$$P_j^{MT} = P_j^{MT,0} + \Delta P_j^{MT}, \forall j \tag{5.3}$$

$$Q_j^{MT} = Q_j^{MT,0} + \Delta Q_j^{MT}, \forall j \tag{5.4}$$

Secondly, the apparent power injection $P_j + jQ_j$ at bus j is calculated by (5.5) with the microturbine power $P_j^{MT} + jQ_j^{MT}$, wind power generation P_j^{WT} and load $P_j^{LD} + jQ_j^{LD}$, while

the current injection I_j^{node} from bus j is calculated by (5.6). V_j^* denotes the conjugate of the bus voltage V_j.

$$P_j + jQ_j = \left(P_j^{MT} + jQ_j^{MT}\right) + P_j^{WT} - \left(P_j^{LD} + jQ_j^{LD}\right), \forall j \tag{5.5}$$

$$I_j^{node} = \frac{P_j - jQ_j}{V_j^*}, \forall j \tag{5.6}$$

Thirdly, the bus voltages V_j expressed by a vector $\boldsymbol{V}$ are calculated through (5.7)-(5.9). Here, $\boldsymbol{I^{branch}}$ stands for the vector of branch current, $\Delta\boldsymbol{V}$ for the vector of the bus voltage deviation to the reference bus voltage. BIBC and BCBV are two the parameter matrices derived based on the microgrid topology and branch impedances, while the details are introduced in [49]. $\boldsymbol{V_r}$ denotes the vector of reference bus voltage V_r.

$$\boldsymbol{I^{branch}} = [\boldsymbol{BIBC}]\, \boldsymbol{I^{node}} \tag{5.7}$$

$$\Delta\boldsymbol{V} = [\boldsymbol{BCBV}]\, \boldsymbol{I^{branch}} \tag{5.8}$$

$$\boldsymbol{V} = \boldsymbol{V_r} - \Delta\boldsymbol{V} \tag{5.9}$$

Further, the system frequency drop ΔF is calculated in (5.10) by multiplying the system equivalent active power droop coefficient m_{peq} and the total active power imbalance at the reference bus. Similarly, the reference bus voltage drop ΔV_r is obtained in (5.11) by multiplying the system equivalent voltage droop coefficient m_{qeq} and the total reactive power imbalance. The subscript r indicates the reference bus. Functions $Re(z)$ and $Im(z)$ are used for obtaining the real and imaginary parts of a complex number z, respectively.

$$\Delta F = m_{peq}\left[P_r^{load} + Re\left(\sum V_r I_r^{branch*}\right) - P_r^{MT,0}\right] \tag{5.10}$$

$$\Delta V_r = m_{qeq}\left[Q_r^{load} + Im\left(\sum V_r I_r^{branch*}\right) - Q_r^{MT,0}\right] \tag{5.11}$$

These system equivalent droop coefficients can be computed as below.

$$m_{(.)eq} = (\sum m_{(.)j}^{-1})^{-1} \tag{5.12}$$

The bus connected to the main microturbine is expected to be chosen as the reference bus which is treated as the slack bus of the islanded microgrid system. It is worth noting that in an islanded microgrid the voltage of this slack bus is varying rather that assumed as a constant in a grid-connected microgrid. Hence, the reference bus voltage V_r is required to be updated as follows. V_0 is the nominal voltage, i.e., 1 p.u.

$$V_r = V_0 - \Delta V_r \tag{5.13}$$

The system frequency F can be updated by $F_0 - \Delta F$.

The above models are conducted iteratively to obtain the islanded microgrid operating conditions, including the system frequency and the bus voltages, until the changes of system frequency and reference bus voltage decreases into the pre-set thresholds. The detailed iteration process can be referred to [94].

5.2.2 Optimization Model

5.2.2.1 Objective Function

This chapter considers multiple objectives including maximizing the hosting capacity of an islanded microgrid and minimizing the system frequency deviation caused by uncertainties. The hosting capacity is defined as the maximum amount of wind power that can be injected at all candidate buses simultaneously. It can be an assessment result for further system operation or wind turbine planning purposes. The objective function is formulated as follows.

$$min\{-\sum_{j \in M} P_j^{WT}, |\Delta F|\} \tag{5.14}$$

Herein, P_j^{WT} means the rating power of WT installation at bus j. M is the set of candidate buses where WTs can be installed to inject power into the microgrid. "−" is used to convert the maximization objective of wind power generation into a minimization one. ΔF is the system frequency deviation which is obtained by (5.10). $|\Delta F|$ is the absolute system frequency deviation.

To guarantee effectiveness, this multi-objective function can be addressed by a weighted sum multi-objective programming method [132]. while ξ is a multiplier determined according to total load of the microgrid.

5.2.2.2 Operating Constraints

Being obtained by the droop-controlled power flow model, the microgrid operating conditions must meet all the following secure operating constraints.

Constraint (5.15) indicates that the apparent power output of microturbine with the droop control should be less than the rated power.

$$P_j^{MT\,2} + Q_j^{MT\,2} \leq \left(S_j^{MT}\right)^2, \forall j. \tag{5.15}$$

The network operating constraints are formulated as below for bus voltage in (5.16), for current injection in (5.17) and for branch current in (5.18). Herein, $V^{min/max}$, I_j^{cap} and $I_j^{b,cap}$ denote the corresponding operating limits.

$$V^{min} \leq V_j \leq V^{max}, \forall j \tag{5.16}$$

$$-I_j^{cap} \leq I_j^{node} \leq I_j^{cap}, \forall j \tag{5.17}$$

$$-I_j^{b,cap} \leq I_j^{branch} \leq I_j^{b,cap}, \forall j \tag{5.18}$$

Overall, the objective function (5.14) subject to the constraints (5.15)-(5.18) forms the proposed multi-objective optimization problem, maximizing the hosting capacity and minimizing the system frequency deviation, with the power flow model (5.1)-(5.13) for operating condition estimation. In this optimization problem, the control variables include microturbine power setpoints $P_j^{MT,0}$ and $Q_j^{MT,0}$. In this optimization problem, the control variables include microturbine power setpoints $P_j^{MT,0}$ and $Q_j^{MT,0}$.

It is worth noting that the proposed optimization model aims to assess and maximize the hosting capacity of an islanded microgrid under a specific operating condition. With the

maximized hosting capacity, this chapter aims to provide an insight into how much wind power can be injected in an islanded microgrid. To this point, the hosting capacity as a useful assessment result can further be used for both short-term operation and long-term planning problems.

With assumption that the power factor of each bus is constant, the reactive power load Q_j^{load} can be calculated with the active power load P_j^{load}. However, it is noted that P_j^{WT} and P_j^{load} are uncertainty variables which significantly impact the optimized objective and the operating constraints.

In the following two sections, SR concepts and a new SR based optimization method are proposed to obtain a robust solution for the proposed optimization problem under the uncertainties.

5.3 Sensitivity Region and Robust Index

To address the uncertainty impacts on the objective function and constraints simultaneously, SR concepts and two robustness indices are introduced and utilized.

The proposed hosting capacity maximization problem can be expressed in a general optimization form as (5.19)-(5.21).

$$min\ f(\boldsymbol{x}, \boldsymbol{p}) \tag{5.19}$$

s.t. $$G(\boldsymbol{x}, \boldsymbol{p}) \leq 0 \tag{5.20}$$

$$H(\boldsymbol{x}, \boldsymbol{p}) = 0 \tag{5.21}$$

Herein, f is the objective function. $\boldsymbol{x}$ and $\boldsymbol{p}$ are the vectors of control variable and uncertainty variable, respectively. *G* and *H* present the inequality constraints (5.15)-(5.18) and equality constraints (5.1)-(5.13), respectively. It is noted that *H* is specifically for the islanded microgrid power flow model. For the proposed hosting capacity maximization problem, the control variables include the output power setpoints of microturbines, and the uncertainty variables are the load and the wind power generation.

5.3.1 Principle of Sensitivity Region

Firstly, $\boldsymbol{x}_0$ is a solution of control variables, while $\boldsymbol{p}_0$ represents the expected values of uncertainty. $f(\boldsymbol{x}_0, \boldsymbol{p}_0)$ is regarded as an expected objective result. It is obvious that f changes with varying $\boldsymbol{p}$, and a maximum acceptable changing amount of f is denoted as Δf_0. When a variation of uncertainty $\Delta\boldsymbol{p}$ realizes, the change in the objective $\Delta f(\boldsymbol{x}_0, \boldsymbol{p}_0, \Delta\boldsymbol{p})$ can be calculated as the follows.

$$\Delta f(\boldsymbol{x}_0, \boldsymbol{p}_0, \Delta\boldsymbol{p}) = f(\boldsymbol{x}_0, \boldsymbol{p}_0 + \Delta\boldsymbol{p}) - f(\boldsymbol{x}_0, \boldsymbol{p}_0) \tag{5.22}$$

For testing the sensitivity of $\boldsymbol{x}_0$ to the objective, a set of $\Delta\boldsymbol{p}$ centering at $\boldsymbol{p}_0$ can be defined to ensure $\Delta f(\boldsymbol{x}_0, \boldsymbol{p}_0, \Delta\boldsymbol{p})$ less than or equal to Δf_0, as the follows.

$$S(\boldsymbol{x}_0, \boldsymbol{p}_0) = \{\Delta\boldsymbol{p} \in R^2 : [\Delta f(\boldsymbol{x}_0, \boldsymbol{p}_0, \Delta\boldsymbol{p})]^2 \leq [\Delta f_0]^2\} \tag{5.23}$$

Taking a 2-dimension space of $\Delta\boldsymbol{p}$ (there are two kinds of uncertainty variable) as an example, $S(\boldsymbol{x}_0, \boldsymbol{p}_0)$ can form a SR as Fig. 5.1 shows.

There are three different types of points describing the uncertainty realization cases. Point A is right at the edge of the SR, which means the variation of uncertainty $\boldsymbol{p}$ at Point A causes the change in the objective $\Delta f(\boldsymbol{x}_0, \boldsymbol{p}_0, \Delta\boldsymbol{p})$ equal to the acceptable amount Δf_0. Points B and C represent the variations of uncertainty cause the changes in the objective smaller and larger than the acceptable amount, respectively. Obviously, this SR represents the area of the points like Points A and B, meeting the constraint (5.30).

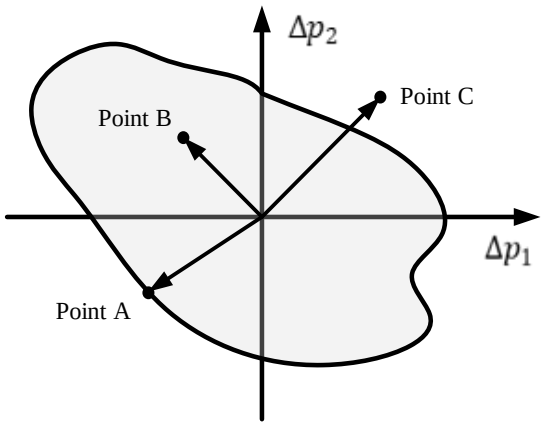

Figure 5.1. Sensitivity Region.

For all the uncertainty realization cases within the SR, the objective varies within the acceptable amount regarding the expected result. It is regarded that the SR can quantify the solution robustness on the objective. Hence, it is expected to enlarge the SR to cover all the possible uncertainty realization cases, thus enhancing the solution robustness on the objective.

5.3.2 Worst-Case Sensitivity Region

It is hard to measure the size of SR which generally has an asymmetric and irregular shape. However, a worst-case scenario of SR can be identified based on the most sensitive direction, such that the size of the worst-case SR (WCSR) demonstrated in Fig. 5.2. can be assessed.

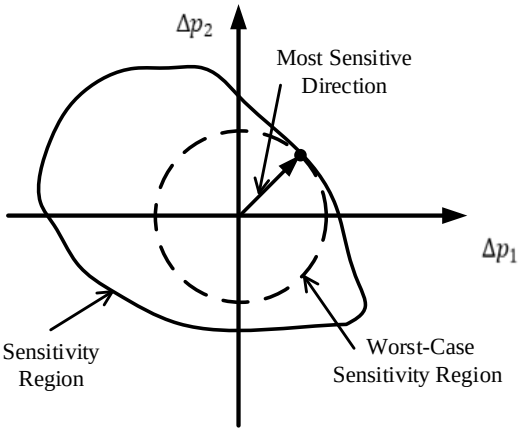

Figure 5.2. Worst-case Sensitivity Region.

As Fig. 5.2 shows, firstly, the most sensitive direction of the SR, which indicates the shortest distance from the edge to $\boldsymbol{p}_0$, is obtained. Then, with this distance as the radius, a circle centering at $\boldsymbol{p}_0$ is drawn as the WCSR. Thus, to calculate the radius of the WCSR, the following optimization model is formulated to be solved.

$$\min R_f(\Delta \boldsymbol{p}) = [\sum_{k}^{2} |\Delta p_k|^q]^{\frac{1}{q}} \tag{5.24}$$

s.t. $$\frac{|\Delta f|}{\Delta f_0} - 1 = 0 \tag{5.25}$$

$$\Delta f = f(\boldsymbol{x}_0, \boldsymbol{p}_0 + \Delta \boldsymbol{p}) - f(\boldsymbol{x}_0, \boldsymbol{p}_0) \tag{5.26}$$

This objective function (5.24) aims to find the minimal Euclidian distance from the boundary of SR to the origin, i.e., $\boldsymbol{p}_0$. Besides, q in (5.24) is the value to determine the distance norm for the solution robustness evaluation. It can be selected as 2 as suggested by [61]. Constraints (5.25) and (5.26) ensure that the point leading to the radius of the WCSR is located at the boundary of SR.

5.3.3 Feasibility Sensitivity Region and Worst Case

The above SR concept can be extended to form a FSR for assessing the solution robustness on the constraints.

Firstly, for a solution $\boldsymbol{x}_0$ and the nominal values of uncertainty $\boldsymbol{p}_0$, (5.20) can be written as the follows.

$$g_n(\boldsymbol{x_0}, \boldsymbol{p_0}) \leq 0, \forall n \tag{5.27}$$

Herein, index n denote the nth constraint in (5.20).

Secondly, with a variation of uncertainty $\Delta\boldsymbol{p}$, the following constraint should be held to keep the solution robustness.

$$g_n(\boldsymbol{x_0}, \boldsymbol{p_0} + \Delta\boldsymbol{p}) \leq 0, \forall n \tag{5.28}$$

Then, all the points of Δp which fulfill (5.28) can form an area which is defined as an FSR. This FSR can quantify the solution robustness on the constraints.

Similarly, a worst-case FSR (WCFSR) can be identified based on the most sensitive direction and the nearest point on the boundary. An example of FSR and its WCFSR are illustrated in Fig. 5.3.

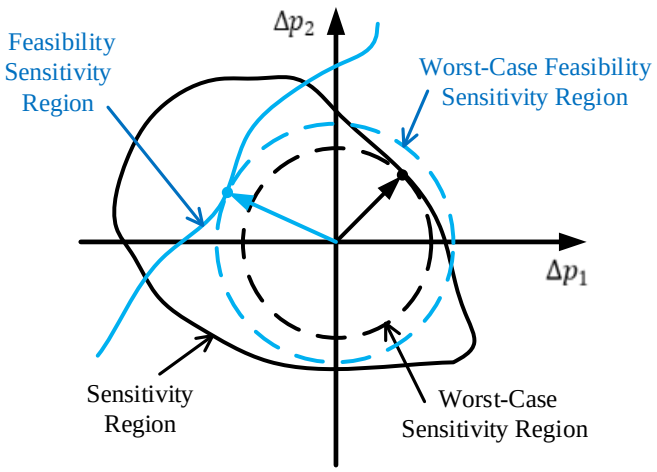

Figure 5.3. Worst-case Feasibility Sensitivity Region.

In this example, the WCFSR is larger than the WCSR. It is noted that the WCFSR can be smaller than or equal to the WCSR, depending on the coverage of the FSR and the SR.

An optimization model is formulated to obtain the radius of FWCSR as the follows.

$$\min R_g(\Delta \boldsymbol{p}) = [\sum_{k}^{2} |\Delta p_k|^q]^{\frac{1}{q}} \tag{5.29}$$

s.t. $$\max_{g}\{g_n(\boldsymbol{x}_0, \boldsymbol{p}_0 + \Delta \boldsymbol{p})\} = 0 \tag{5.30}$$

$$H(\boldsymbol{x}_0, \boldsymbol{p}_0 + \Delta \boldsymbol{p}) = 0 \tag{5.31}$$

This objective function (5.29) aims to find the minimal Euclidian distance from the boundary of FSR to the origin, i.e., $\boldsymbol{p}_0$. Constraint (5.30) ensures all the inequalities under the cases with $\Delta \boldsymbol{p}$. Constraint (5.31) calculates the islanded microgrid power flow.

5.3.4 Robustness Index

It is expected to enlarge the WCSR and WCFSR to cover all the possible realization cases of uncertain wind power generation and load. Two robustness indices are introduced to assess whether the WCSR and WCFSR are large enough.

As mentioned, $\Delta \boldsymbol{p}$ space is two-dimensional of uncertain WT output power and load. The expected values of uncertainty are further defined as $\Delta p_{1,0}$ and $\Delta p_{2,0}$ for the wind power and

load, respectively. The uncertainty varying ranges can also be predicted as $[\Delta p_k^{min}, \Delta p_k^{max}]$, symmetric centering at the expected values. The uncertainty variables of wind power Δp_1 and load Δp_2 are predicted to realize within the corresponding ranges. A tolerance region can be formed with normalized ranges $[\Delta p_k^{min*}, \Delta p_k^{max*}]$ as a square covering all the possible realization cases, as shown in Fig.5.4.

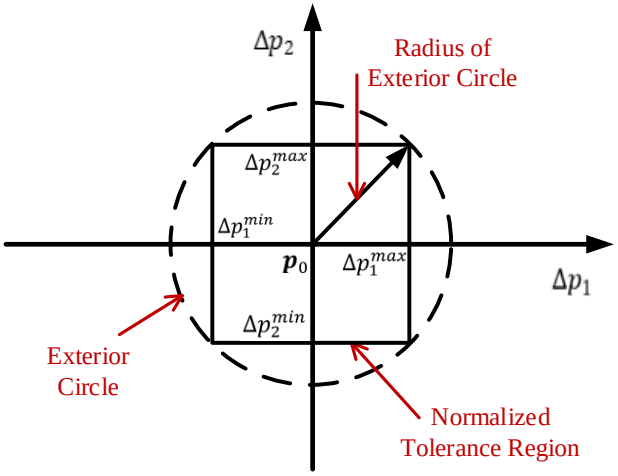

Figure 5.4. Normalized Tolerance Region.

To ensure a robust solution on both objective and constraints, the allowed WCSR and WCFSR should be larger than or equal to the exterior circle of the tolerance region. The radius of this exterior circle is defined as R_E. Then, two robustness indices for the objective and the constraints respectively can be defined as follows.

$$\eta_f = \frac{R_f}{R_E} \tag{5.32}$$

$$\eta_g = \frac{R_g}{R_E} \tag{5.33}$$

Herein, R_f and R_g are the radii of WCSR and WCFSR, respectively, which are obtained by (5.24) and (5.29).

These two indices η_f and η_g are expected greater than or equal to the corresponding pre-defined robustness targets η_f^T and η_g^T. By setting the robustness targets as 1, it means the WCSR and WCFSR can cover the tolerance region, thus achieving a robust solution on both objective and constraints. In addition, by setting the robustness targets as different values, the optimization

priority and the solution robustness can be adjusted according to operator expectations. Sensitivity analysis on the robustness targets is given in Chapter 5.5.6.

5.4 Sensitivity Region Based Optimization Method

With the SR concepts and the robustness indices given in Chapter 5.3, a SR based optimization method is developed for maximizing the renewable generation hosting capacity of an islanded microgrid. An optimization model is formulated first, followed by a new solution algorithm which contains the islanded microgrid power flow and the assessment of the robustness indices.

5.4.1 Sensitivity Region Based Optimization Model

This chapter proposes to minimize the objective (5.14), while satisfying the constraints and keeping the two robustness indices η_f and η_g greater than or equal to the robustness targets η_f^T and η_g^T, respectively. A SR based optimization model is formulated and introduced as follows.

$$min\ f(\boldsymbol{x}, \boldsymbol{p}_0) \tag{5.34}$$

s.t. $$G(\boldsymbol{x}, \boldsymbol{p}_0) \leq 0 \tag{5.35}$$

$$H(\boldsymbol{x}, \boldsymbol{p}_0) = 0 \tag{5.36}$$

$$\eta_f \geq \eta_f^T \tag{5.37}$$

$$\eta_g \geq \eta_g^T \tag{5.38}$$

Objective function (5.34) is formulated by (5.14) with $\boldsymbol{x}$ including the control variables, i.e., $P_j^{MT,0}$ and $Q_j^{MT,0}$, and $\boldsymbol{p}_0$ for the mean values of the uncertain load and wind power generation. Inequality constraint (5.35) is formed by (5.15)-(5.18) and the islanded microgrid power flow model (5.1)-(5.13) is expressed as (5.35). Constraints (5.37) and (5.38) indicated the requirements for the robustness indices on the objective and constraints.

It is noted that the proposed SR based optimization method uses the uncertainty varying ranges (introduced in Chapter 5.3) to cover all the uncertainty realizations rather than specified profiles of uncertainty.

5.4.2 Solution Algorithm

It is impossible to directly solve the above optimization problem, due to the subproblems (5.24)-(5.26) and (5.29)-(5.31) for calculating the radii of WCSR and WCFSR, as well as the iterative process of the islanded microgrid power flow. Thus, using the GA framework [133], this chapter develops a new solution algorithm.

This solution algorithm is iterative with the following key steps including generating solutions, conducting the islanded microgrid power flow, checking the constraints and the robustness indices.

Step 1: A series of GA parameters are set, including population size, maximum generations, crossover fraction and mutation rate.

Step 2: The first generation is initialized according to the variable bounds.

Step 3: The individuals providing feasible solutions $\boldsymbol{x}_0$ which can be obtained by (5.34) are applied with checking the constraints (5.35)-(5.36). In detail, the islanded microgrid power flow (5.1)-(5.13) is conducted to get the system frequency, bus voltages and line currents. These state variables are checked if they meet the constraints (5.15)-(5.18).

Step 4: If an individual has any constraint violations, a penalty is added to the individual's objective. For this individual, all out-of-bound absolute values of (5.15)-(5.18) are obtained, and the largest value is set as E_{max}. Then, the penalty for this individual is calculated as $Pen_1 = A_1 \times E_{max} + B_1$. Here, B_1 is a constant number to differentiate the individuals with constraint violations from the others. Go to *Step 5* for the feasible individuals.

Step 5: The radius of WCFSR R_g is obtained by (5.29)-(5.31), the robustness index η_g is evaluated and checked if $\eta_g \geq \eta_g^T$. The radius of WCSR R_f is obtained by (5.24)-(5.26), the robustness index η_f is evaluated and checked if $\eta_f \geq \eta_f^T$.

Step 6: If an individual does not meet the required feasibility design (i.e., $\eta_g \geq \eta_g^T$) or objective design (i.e., $\eta_f \geq \eta_f^T$), a penalty is added to the individual's objective. Under this condition, the penalty is calculated as $Pen_2 = A_2 \times \max\{(\eta_g^T - \eta_g), (\eta_f^T - \eta_f)\} + B_2$. Herein, B_2 is a constant number to differentiate the individuals with unsatisfying designs from the others. Go to *Step 7* for the individuals which meet the required feasibility and robustness designs.

Step 7: The termination criterion, i.e., the minimal fitness value does not change, is checked. If the termination criterion is not fulfilled, offspring is generated based on all the individual objectives and go to *Step 3*; otherwise, the algorithm is terminated with an optimized solution.

The whole solution algorithm is demonstrated in Fig. 5.5.

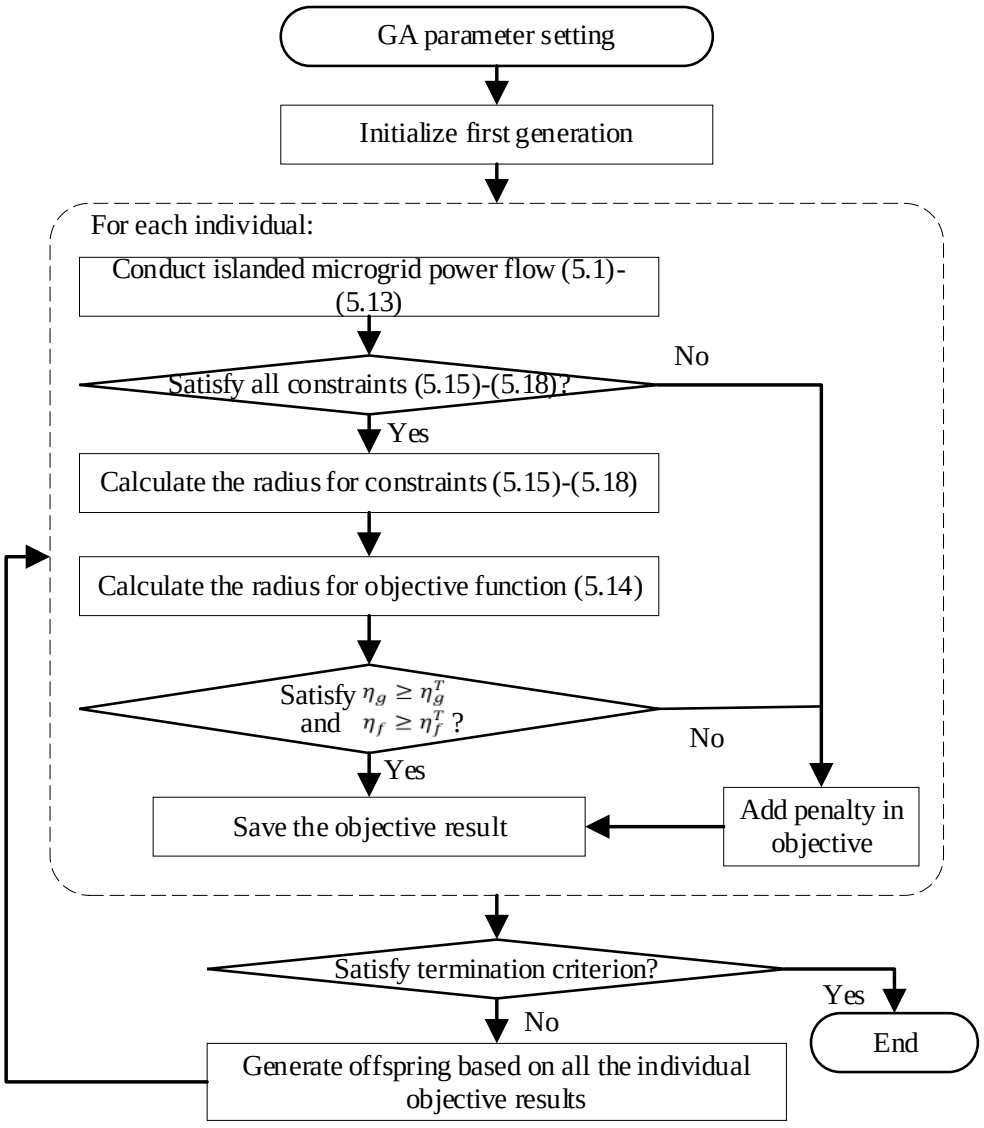

Figure 5.5. Solution Algorithm for Sensitivity Region Based Optimization.

5.5 Case Study

5.5.1 Test System Description

In this chapter, a 33-bus distribution system [43] is modified as an islanded microgrid, by setting Bus 1 as the reference bus without connected to the up-stream network.

33-bus system is a widely used standard system for microgrids [77]-[78]. Besides, according to [49], the determining factor for effectiveness of BFS is whether the BIBC and BCBV of a system can be obtained. In another word, it depends on the system's topology rather than system's scale. If the system is radial or weakly meshed, its BIBC and BCBV are available. The method for obtaining two matrixes of a weakly meshed system is proposed in [49]. In [51], the BFS method is used to calculate power loss of a weakly meshed distribution network, which verifies the method of [49].

Another problem caused by system scale is the computing time. Since the algorithms proposed in Chapters 2-4 are solved by commercial solver (Gurobi) and their solver time are much lower than 15 minutes. (The solver time of most time-consuming algorithm, introduced in Chapter 4 is 175.6 seconds) A larger system will not cause unacceptable solver time. For the algorithm proposed in Chapter 5, since the hosting capacity maximization is not time pressed, the proposed algorithm can also be expanded for large-scale systems. Besides, the GA program running time can be significantly reduced by parallel computing

The network topology is demonstrated in Fig. 5.6. This system has been widely used for microgrid operation and control tests [77][78][94]. The allowed voltage range is [0.9, 1.1] p.u. In addition, the line current limit is 650 A.

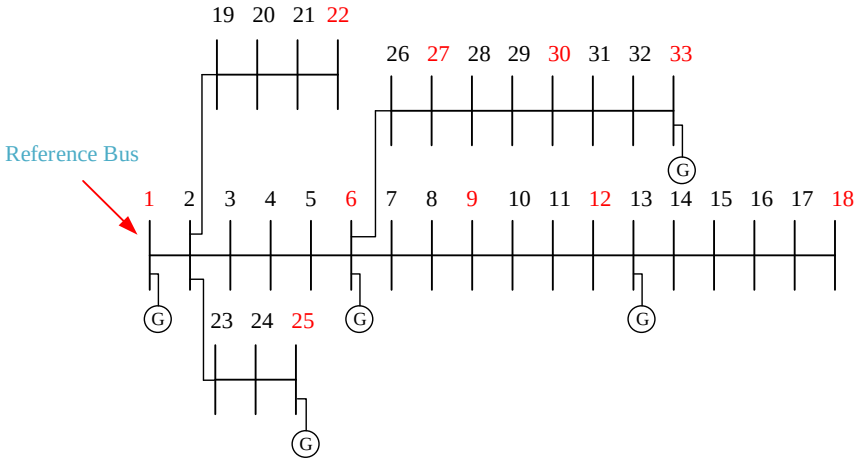

Figure 5.6. Test Network Topology.

Five microturbines are installed in the system with the mark "G" and their parameters are given in Table 5.1. Using eq. (5.12), the system equivalent frequency/voltage droop coefficients is -0.0345 p.u. Since Bus 1 is the reference bus, the microturbine at this bus is regarded as the main generator for the islanded microgrid power flow calculation.

Table 5.1 Microturbines Parameters

Microturbine No.	**Bus No.**	**Capacity (MVA)**	**Frequency Droop Coefficient (p.u.)**	**Voltage Droop Coefficient (p.u.)**
1	1	1.4	-0.1	-0.1
2	6	1.4	-0.25	-0.25
3	13	1.4	-0.15	-0.15
4	25	1.4	-0.3	-0.3
5	33	1.4	-0.2	-0.2

The candidate buses of WT installation are Buses 1, 6, 9, 12, 18, 22, 25, 27, 30, 33, marked with red color.

The candidate buses of wind power injection are Buses 1, 6, 9, 12, 18, 22, 25, 27, 30, 33, marked with red color in Fig. 5.6. Note that selection of candidate buses depends on renewable source location and adequacy [134], system operating limits on locations, and even sensitivity to system operating performance [135]. The proposed hosting capacity maximization method is generic to any given set of candidate buses. To validate the applicability of the proposed method,

in Section 5.5.8, three additional cases of candidate buses are given for the hosting capacity maximization.

For the proposed solution algorithm, A_1 and B_1 are set as 5000 and 1000, while A_2 and B_2 are set as 2000 and 5. For the GA, the individual number is set as 200 and the crossover rate is 0.8. The termination criterion that the average relative change in the minimum fitness values over 50 continuous generations is less than or equal to 1×10^{-4} is set.

The numerical simulation is conducted on a 64-bit PC with 4.10GHz CPU and 64 GB RAM utilizing the GA toolbox on MATLAB platform.

5.5.2 Uncertainty Parameters

The predicted peak loads of active and reactive power are 4.64 MW and 2.88 MVar, respectively. The predicted load variation ranges are from 60% to 100% of the peak values.

On the other hand, it is assumed that the WTs can generate power from 0% to 100 % of the rating power.

Δp_1 and Δp_2 are defined as the variations of load and wind power, respectively, such that $\Delta \boldsymbol{p}$ is on a two-dimensional space. The robustness targets η_f^T and η_g^T are set as 1 to achieve a full robust solution. It is noted that the variation ranges of loads and wind power must be normalized to form a square tolerance region as shown in Fig. 5.4.

Since the WT rating power P_j^{WT} in (5.14) does not have any variations under the uncertainties, the objective robustness is only considered and to be guaranteed on the minimization of system frequency deviation. Thus, for constraint (5.25), the maximum acceptable changing amount Δf_0 is set as 6 % of the expected system frequency under the mean condition.

5.5.3 Verification of Algorithm Convergence

Using the proposed solution algorithm, the SR based optimization problem (5.34)-(5.38) is solved by 131 generations of GA. The convergence processes of the minimum fitness value among all the individuals and the minimum robustness index are presented in Fig. 5.7 and Fig. 5.8, respectively. It is noted that the fitness value is the sum of objective (5.14) and the penalty if any for each individual. For the first two generations, all the individuals lead to constraint

violations so that the fitness values are very large. Thus, the minimum fitness values of the first two generations are not presented in these two figures. In other words, from the third generation, there is at least one individual which does not have any penalty, i.e., one feasible solution can be obtained.

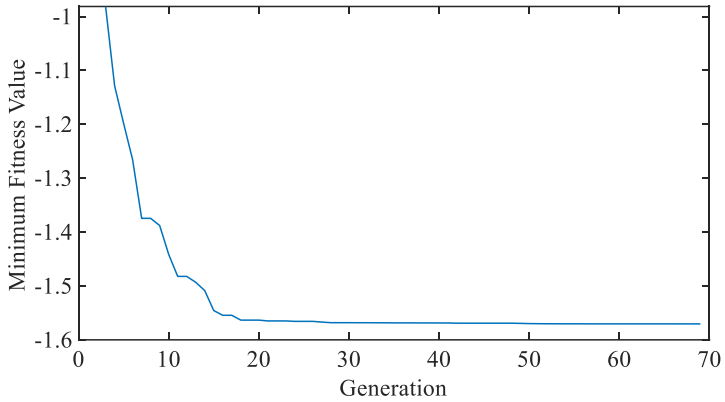

Figure 5.7. Convergence Process of Best Fitness Value.

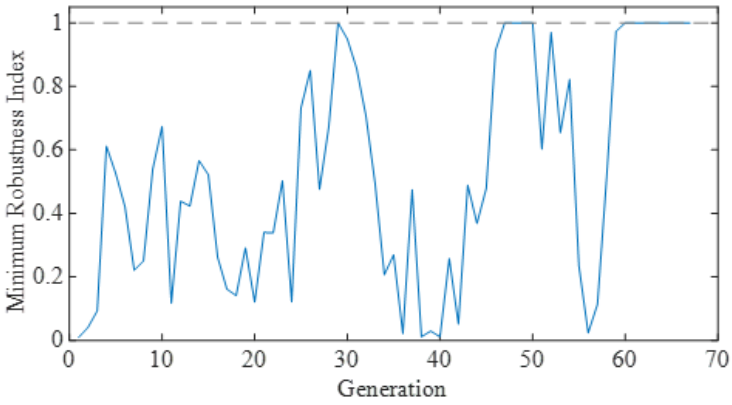

Figure 5.8. Convergence Process of Minimum Robustness Index.

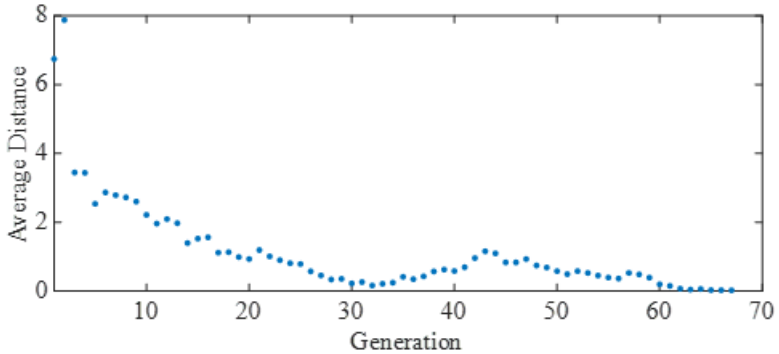

Figure 5.9. Average distance of individuals.

As Fig. 5.7 shows, since the third generation, there is no constraint violation under the mean condition. After the third generation the proposed solution algorithm optimize the microturbine power setpoints to maximize the hosting capacity and minimize the system frequency deviation. There is no oscillation in the convergence process of the optimization. Considering the mechanism of GA, most advantaged individuals are treated as elites and passed to the next generation. Relatively suboptimal individuals are selected as parents to produce children with crossover. Hence, once some individuals occur in a centered feasible region, their advantages guarantee that they have much more offspring. As a result, the proposed algorithm leads a sharp drop from -0.9814 to -1.4823 during the generations from 3 to 9. Hereafter, the downtrend continues with only small changes. It can be seen in Fig. 5.7 that the minimum fitness value is gradually reduced and the relative change over 50 continuous generations is reduced to the termination criterion at the 69th generation, indicating the convergence.

Fig. 5.8 intuitively illustrates the searching process to enlarge the robustness indices, where the robust index presented is the smaller one of η_g and η_f. It can be seen that the convergence oscillates heavily until the 60th generation. The reason is that the proposed solution algorithm uses the fitness value to check the performance and constraint violations of individuals first, and then considers the penalty caused by the unsatisfied robustness indices. Thus, the individuals with small fitness values have the robustness indices in the large range. After the 60th generation, the algorithm intensively enlarges the robustness indices. At the 69th generation, these robustness indices are eventually greater than or equal to the robustness targets (set as 1), fulfilling the constraints of the required designs, i.e., (5.37) and (5.38). This also verifies the convergence.

In addition, Fig. 5.9 shows the average distance of all the individuals, which indicates the algorithm convergence process as well. It is noted that the average distance increases after the 30th generation, since the algorithm alternatively enlarges η_f and η_g, making the penalty Pen_2 increasing and fluctuating.

From the above convergence result, it can be concluded that the proposed solution algorithm can effectively solve the SR based optimization problem (5.34)-(5.38) with the robustness indices larger than or equal to the targets.

5.5.4 Optimization Results

With the proposed SR based optimization method, the maximized hosting capacity of this islanded microgrid is 1.573 MW. The allowed maximal wind power generation of each candidate bus is shown in Fig. 5.10.

For comparison, a conventional stochastic programming method is applied. It is assumed that wind power generation and loads follow continuous uniform distribution. 1000 scenarios are generated by Monte Carlo sampling and then reduced to 50 presentative scenarios via a backward reduction technique [55]. The allowed maximal wind power generation obtained by this conventional method is also shown in Fig. 5.10.

To guarantee full solution robustness on both the objective of minimizing the system frequency deviation and the network operating constraints, the proposed method significantly reduces the allowed wind power generation at buses 6 and 27. Besides, the proposed method makes the allowed wind power generation more evenly distributed across the network.

Moreover, the optimized microturbine power output setpoints are also demonstrated for comparison in Fig. 5.11.

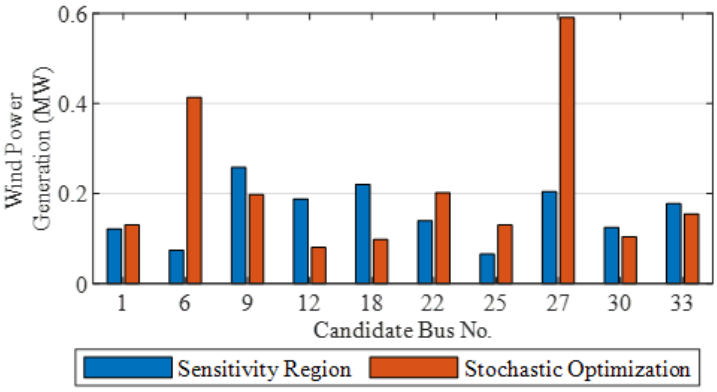

Figure 5.10. Allowed Maximal Wind Power Generation.

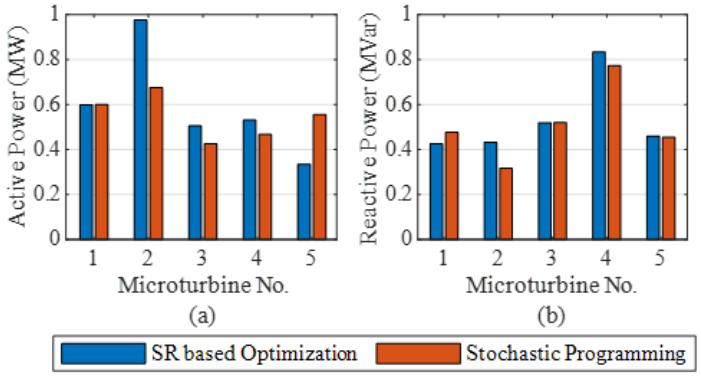

Figure 5.11. Optimized Microturbine Setpoints: a) Active Power; b) Reactive Power.

From this figure, the total active and reactive power outputs determined by the proposed method are higher than those of the stochastic one, despite the local differences.

It can be concluded that since the proposed SR based optimization method aims to ensure the solution robustness, the islanded microgrid relies more on the droop-controlled microturbines with the compromised hosting capacity.

5.5.5 Verification of Solution Robustness

To verify the advantage of the proposed SR based optimization method on solution robustness, a robustness test is conducted with simulation of uncertainty realization.

By using Monte Carlo sampling, 5000 scenarios are generated as the cases of uncertainty realizations. Then, two sets of optimized microgrid operation are tested under these uncertainty realization cases. The test results including the average, minimum and maximum values of the system frequency as well as the operating constraint satisfaction rate (the case number of no constraint violation to all the cases) are presented in Table 5.2.

Table 5.2 Solution Robustness Test

Method	SR based Optimization	Stochastic Programming
Average Frequency (Hz)	1.0005	1.002
Minimum Frequency (Hz)	0.9419	0.9344
Maximum Frequency (Hz)	1.0581	1.0685
Constraint Satisfaction Rate (%)	100	98.54

Firstly, for the objective of minimizing the system frequency deviation, the microgrid operation optimized by the proposed method can make the frequency closer to 1 p.u. with a smaller variation range. This indicates the high efficiency of the proposed method in keeping the system frequency deviation less changing under the uncertainties. In comparison, the conventional SP method cannot provide solution robustness on the objective.

Secondly, the proposed SR based optimization method can ensure no violation to any operating constraint under the uncertainties, thus achieving the full solution robustness. Although the SP method with sufficient presentative scenarios can also improve the solution robustness on the operating constraints, it cannot provide the full solution robustness.

In short summary, the proposed SR based optimization method can maximize the hosting capacity of an islanded microgrid where the optimized operation is robust on both objective and operating constraints against the uncertainties.

5.5.6 Sensitivity Analysis on Robustness Indices

As mentioned in Chapter 5.3.4, the proposed SR based optimization method can adjust the optimization priority and the solution robustness degree by changing the robustness targets η_f^T and η_g^T. With the smaller robustness targets, the optimization results will be more radical but with the lower constraint satisfaction rate. Oppositely, the larger robustness targets will lead to more conservative optimization results.

In this sub-section, different values are set to the robustness targets and then the hosting capacity is maximized accordingly. With the 5000 Monte Carlo sampled scenarios, the performance of the optimized microgrid operation under the uncertainty realizations are simulated and compared. The maximized hosting capacities and the simulation results under the uncertainty realizations are given in Table 5.3.

Table 5.3 Simulation Results with Different Robustness Targets

η_f^T and η_g^T	0.8	0.9	1	1.1
Hosting Capacity (MW)	2.43	1.97	1.57	1.20
Average Frequency (Hz)	1.0006	1.0005	1.0005	1.0004
Minimum Frequency (Hz)	0.9275	0.9350	0.9419	0.9483

Maximum Frequency (Hz)	1.0725	1.0650	1.0581	1.0517
Constraint Satisfaction Rate (%)	96.42	99.22	100	100

Firstly, as the robustness targets increase, the hosting capacity is reduced, indicating the solution conservativeness is increased as a drawback. On the other hand, as the robustness targets decrease from 1, the hosting capacity is further enhanced. With the robustness targets of 0.9, the hosting capacity of the proposed SR based optimization method is similar to that of the conventional SP method.

Secondly, via the Monte Carlo simulations, the system frequency variation range is tightened by a large value of η_f^T. As this robustness target on the objective increases, the WCFSR is enlarged. This means the proposed optimization method can prepare a robust solution against a larger region of uncertainty realization, to keep the objective varying within the allowed range. In other words, the solution has the higher capability of keeping the objective less varying. For the solution with a larger η_f^T, because the uncertainty realizations must be within the power rating of WT and within the predicted range of loads, i.e., the region of uncertainty realization is kept constant, the system frequency variation is reduced to a smaller range.

Thirdly, the constraint satisfaction rate is 100%, indicating full solution robustness on the constraints, when the robustness target η_g^T is set greater than or equal to 1. This is because the WCSR is large enough to cover all the uncertainty realizations. On the other hand, once this robustness target is smaller than 1, uncovered uncertainty realizations will cause constraint violations, leading to the constraint satisfaction rate less than 1. Compared to the conventional SP method, even taking 0.9 as the robustness targets, the constraint satisfaction rate of the proposed method is higher. The constraint satisfaction rate suffers an accelerated drop as the robustness target η_g^T decreases from 1.

Based on the above analysis, it is noted that using large robustness targets η_f^T and η_g^T can efficiently enhance solution robustness, while leading to conservative solutions. To guarantee full solution robustness on both the objective and the operating constraints, the robustness targets η_f^T and η_g^T are expected to be set as 1. However, if a few constraint violations and compromised

system frequency variations are accepted, 0.9 can also be considered for practical use, which leads to a further improved hosting capacity result.

It is an advantage that the optimization priority and the solution robustness can be adjusted to the operator expectations by selecting different robustness targets.

5.5.7 Sensitivity Analysis on GA Settings

Given different GA settings, the proposed SR based optimization method is applied to maximize the hosting capacity of this islanded microgrid. The settings as well as the optimization results are shown in Table IV. Setting 1 is the initial one used in Chapters 5.5.3 to 5.5.6. Compared to the initial setting, the crossover rate is increased and decreased in Settings 2 and 3, respectively, while the population is increased and decreased in Settings 4 and 5.

Table 5.4 Optimization Results with Different GA Settings

Setting No.	1	2	3	4	5
Crossover Rate	0.8	0.9	0.7	0.8	0.8
Population	200	200	200	300	100
Hosting Capacity (MW)	1.573	1.570	1.569	1.570	1.570

The hosting capacity results with the five different settings are almost same, which verifies the proposed method can find the optimum. The affects from the GA settings can be ignored.

It is noted that a GA is utilised in the developed solution algorithm, since it is compatible with the SR based optimization method and the power flow model of droop-controlled islanded microgrid. It can provide local optima, and an advanced heuristic algorithm can be considered to improve optimality.

5.5.8 Different Cases of Candidate Buses

To validate applicability of the proposed method as well as evaluate impacts of wind power injection candidate buses on hosting capacity maximization results, three additional study cases of different candidate bus selections are applied. All the cases are shown in Table 5.5, and Case 1 is the initial one used in Chapters 5.5.3 to 5.5.7. Cases 1 and 2 have 10 candidate buses, while

Cases 3 and 4 have 7 candidate buses. Some of candidate buses are common among the different study cases.

Table 5.5 Study Cases of Different Candidate Buses

Study Cases	Candidate Buses	Number of Candidate Buses
Case 1	1, 6, 9, 12, 18, 22, 25, 27, 30, 33	10
Case 2	1, 6, 10, 13, 17, 21, 25, 27, 31, 33	10
Case 3	6, 12, 18, 22, 25, 30, 33	7
Case 4	1, 9, 12, 22, 25, 27, 30	7

The simulation results including the hosting capacity and the optimized power setpoints of microturbines under the different study cases are given in Table 5.6.

Table 5.6 Optimization Results under Different Study Cases

Study Cases	Hosting Capacity (MW)	$P_1^{MT,0}$ (MW)	$P_6^{MT,0}$ (MW)	$P_{13}^{MT,0}$ (MW)	$P_{25}^{MT,0}$ (MW)	$P_{33}^{MT,0}$ (MW)
Case 1	1.573	0.599	0.976	0.506	0.531	0.336
Case 2	1.564	0.627	0.422	0.593	0.519	0.794
Case 3	1.569	0.599	0.704	0.619	0.498	0.525
Case 4	1.570	0.595	0.672	0.470	0.770	0.441

The hosting capacity results under these cases have only slight differences, while the optimized power setpoints are quite different. The main reason is that in this islanded microgrid, the hosting capacity can be maximized by optimizing the operation of the five microturbines which have sufficient capacities. Besides, according to [135], the microturbines are at the most sensitive buses, which can efficiently reduce the impacts of different candidate bus selections on the hosting capacity result. Thus, the microturbine capacities and locations play a key role in improving the hosting capacity of the islanded microgrid.

This simulation also validates the proposed SR based optimization method is generic for different study cases, indicating the high applicability.

5.6 Conclusion

In this chapter, firstly, a hosting capacity maximization model for an islanded microgrid is proposed, where system frequency variation and microturbine droop control functionality are fully considered. Then, SR and FSR are introduced to quantify solution robustness against uncertainties of renewable generation and load. Last, this chapter develops a SR based optimization method with a new solution algorithm. A comprehensive case study is conducted to verify the efficiency of the proposed model, method and algorithm.

In case study, the convergence of the proposed solution algorithm, the performance of the optimized solution, and the solution robustness are verified in sequence. The numerical simulation results denote high efficiency of the proposed model, method and algorithm. Besides, sensitivity analysis is conducted for the robustness targets. Overall, the advantages including the effective SRs for performance assessment under the uncertainties, the robust microgrid operation solution for the maximal hosting capacity, and the adjustment ability between the solution robustness and conservativeness can be brought.

Therefore, this chapter achieves an efficient SR based optimization method for maximizing the renewable generation hosting capacity of an islanded microgrid.

In future works, advanced heuristic algorithms like ant colony optimization and particle swarm optimization algorithms can be used for the proposed SR based optimization method.

Chapter 6 CONCLUSIONS AND FUTURE WORKS

With the emerging technology development, renewable distributed generation (DG) is not only environmentally friendly but also economically competitive. However, they are not efficiently integrated into power systems due to their non-controllable characteristics. Microgrid is an appropriate platform for renewable DG. Since a microgrid cannot exchange power with the main grid in an islanded mode, the operating issues in an islanded microgrid which are caused by uncertainties of renewable distribution generation and load are more likely to occur with higher impacts.

This thesis focuses on the optimal operation and renewable hosting capacity maximization for high-renewable islanded microgrids. A series of models and methods are proposed and presented, while efficient optimization tools and solution algorithms are developed and validated. This thesis is concluded with the following achievements.

1. Minimal operating cost of an islanded microgrid with microturbine droop control.
2. Minimal operating cost with full consideration of uncertainties of load and renewable power generation, thus guaranteeing operating constraint satisfaction.
3. Stable and secure operation of a microgrid under the condition of tie-line switching from the grid-connected to islanded mode, while minimizing operating cost.
4. Efficient solution algorithm to address the coupled constraints when considering tie-line switching in the optimization model, with high computing efficiency.
5. Maximal renewable hosting capacity of an islanded microgrid while minimizing system frequency deviation.
6. Effective sensitivity region (SR) model with indices to quantify solution robustness on both objective and constraints under uncertainties.
7. Efficient solution algorithm to maximize the hosting capacity while keeping high solution robustness indices.

Based on the above research outcomes and considering the limitations, further works can be done as follows.

1. All models and methods proposed in this thesis are designed for a single-phase microgrid. In the future, they can be extended for three-phase unbalanced systems.
2. Since energy storage systems (ESSs), such as batteries and electric vehicles, further improve flexibility of microgrid operation, they will be considered in the future works of the islanded microgrid operation and planning.
3. More power system performance indicators can be treated as optimization objectives, such as voltage stability, bus voltage deviation, capital cost and gas emission.
4. Some smart sampling schemes like Latin Hypercube Sampling Quasi-Monte Carlo method will be applied to reduce the scenarios.
5. Renewable DG control, such as inverter control will be considered.

BIBLIOGRAPHY

[1] "IEEE Standard for Interconnection and Interoperability of Distributed Energy Resources with Associated Electric Power Systems Interfaces," in *IEEE Std 1547-2018 (Revision of IEEE Std 1547-2003)*, vol., no., pp.1-138, 6 April 2018.

[2] G. Pepermans, J. Driesen, D. Haeseldonckx, R. Belmans, W. D'haeseleer, "Distributed generation: definition, benefits and issues," *Energy Policy*, Volume 33, Issue 6, Pages 787-798, 2005.

[3] E.S.N. Raju P, Trapti Jain, "Chapter 2 - Distributed energy resources and control," Editor(s): Rajeev Kumar Chauhan, Kalpana Chauhan, Distributed Energy Resources in Microgrids, Academic Press, Pages 33-56, 2009.

[4] Ismail, M.S. Moghavvemi, M. Mahlia, T.M.I., "Current utilization of microturbines as a part of a hybrid system in distributed generation technology," *Renewable and Sustainable Energy Reviews*, Elsevier, vol. 21(C), pages 142-152, 2013.

[5] Bansal, R., "Handbook of Distributed Generation Electric Power Technologies, Economics and Environmental Impacts: Cham, " Springer International Publishing, 2017.

[6] M. M. Rahman, M. Hasanuzzaman, N.A.Rahim, "Effects of various parameters on PV-module power and efficiency," *Energy Conversion and Management* 103 (2015): 348-358.

[7] E. A. Martínez Ceseña, T. Capuder and P. Mancarella, "Flexible Distributed Multienergy Generation System Expansion Planning Under Uncertainty," in *IEEE Transactions on Smart Grid*, vol. 7, no. 1, pp. 348-357, Jan. 2016.

[8] JINKO Solar, Available at: https://www.jinkosolar.com/.

[9] F. Fertig et al., "Q CELLS > 24% Silicon Solar Cells With Mass-Production Processes," in *IEEE Journal of Photovoltaics*, vol. 12, no. 1, pp. 22-25, Jan. 2022.

[10] C. Zhang, Y. Xu and Z. Y. Dong, "Probability-Weighted Robust Optimization for Distributed Generation Planning in Microgrids," in *IEEE Transactions on Power Systems*, vol. 33, no. 6, pp. 7042-7051, Nov. 2018.

[11] GE Renewable Energy, Available at: https://www.ge.com/renewableenergy/home.

[12] R. H. Lasseter and P. Paigi, "Microgrid: a conceptual solution," *2004 IEEE 35th Annual Power Electronics Specialists Conference* (IEEE Cat. No.04CH37551), pp. 4285-4290 Vol.6, 2004.

[13] B. Lasseter, "Microgrids [distributed power generation]," *2001 IEEE Power Engineering Society Winter Meeting. Conference Proceedings* (Cat. No.01CH37194), Columbus, OH, USA, 2001.

[14] W. Bower, D. Ton, R. Guttromson, S. Glover, "The advanced microgrid. Integration and interoperability," U.S. Department of Energy, Available at: https://www.osti.gov/servlets/purl/1204100.

[15] CIGRÉ. Working Group C6.22 Microgrids Evolution Roadmap, *Microgrids 1: Engineering, Economics, & Experience*.

[16] "IEEE Guide for Smart Grid Interoperability of Energy Technology and Information Technology Operation with the Electric Power System (EPS), End-Use Applications, and Loads," in *IEEE Std* 2030-2011, vol., no., pp.1-126, 10 Sept. 2011.

[17] "IEEE Application Guide for IEEE Std 1547(TM), IEEE Standard for Interconnecting Distributed Resources with Electric Power Systems," in *IEEE Std 1547.2-2008* , vol., no., pp.1-217, 15 April 2009.

[18] A. Ravichandran, P. Malysz, S. Sirouspour and A. Emadi, "The critical role of microgrids in transition to a smarter grid: A technical review," 2013 *IEEE Transportation Electrification Conference and Expo* (ITEC), pp. 1-7, 2013.

[19] H. Farhangi, "The path of the smart grid," in *IEEE Power and Energy Magazine*, vol. 8, no. 1, pp. 18-28, January-February 2010.

[20] Y. Riffonneau, S. Bacha, F. Barruel and S. Ploix, "Optimal Power Flow Management for Grid Connected PV Systems With Batteries," in *IEEE Transactions on Sustainable Energy*, vol. 2, no. 3, pp. 309-320, July 2011.

[21] S. Ahn, S. Nam, J. Choi and S. Moon, "Power Scheduling of Distributed Generators for Economic and Stable Operation of a Microgrid," in *IEEE Transactions on Smart Grid*, vol. 4, no. 1, pp. 398-405, March 2013.

[22] P. Malysz, S. Sirouspour and A. Emadi, "An Optimal Energy Storage Control Strategy for Grid-connected Microgrids," in *IEEE Transactions on Smart Grid*, vol. 5, no. 4, pp. 1785-1796, July 2014.

[23] J. Liu, H. Chen, W. Zhang, B. Yurkovich and G. Rizzoni, "Energy Management Problems Under Uncertainties for Grid-Connected Microgrids: A Chance Constrained Programming Approach," in *IEEE Transactions on Smart Grid*, vol. 8, no. 6, pp. 2585-2596, Nov. 2017.

[24] C. Ju, P. Wang, L. Goel and Y. Xu, "A Two-Layer Energy Management System for Microgrids With Hybrid Energy Storage Considering Degradation Costs," in *IEEE Transactions on Smart Grid*, vol. 9, no. 6, pp. 6047-6057, Nov. 2018.

[25] T. Paul, S. Ghosh, S. Kamalasadan and P. Mandal, "A quadratic programming based optimal power and battery dispatch for grid connected microgrid," *2016 IEEE Industry Applications Society Annual Meeting*, 2016, pp. 1-8.

[26] T. G. Paul, S. J. Hossain, S. Ghosh, P. Mandal and S. Kamalasadan, "A Quadratic Programming Based Optimal Power and Battery Dispatch for Grid-Connected Microgrid," in *IEEE Transactions on Industry Applications*, vol. 54, no. 2, pp. 1793-1805, March-April 2018.

[27] M. Rafiee Sandgani and S. Sirouspour, "Energy Management in a Network of Grid-Connected Microgrids/Nanogrids Using Compromise Programming," in *IEEE Transactions on Smart Grid*, vol. 9, no. 3, pp. 2180-2191, May 2018.

[28] Y. Zheng, S. Li and R. Tan, "Distributed Model Predictive Control for On-Connected Microgrid Power Management," in *IEEE Transactions on Control Systems Technology*, vol. 26, no. 3, pp. 1028-1039, May 2018.

[29] J. Choi, Y. Shin, M. Choi, W. Park and I. Lee, "Robust Control of a Microgrid Energy Storage System Using Various Approaches," in *IEEE Transactions on Smart Grid*, vol. 10, no. 3, pp. 2702-2712, May 2019.

[30] U. Manandhar *et al*., "Energy Management and Control for Grid Connected Hybrid Energy Storage System Under Different Operating Modes," in *IEEE Transactions on Smart Grid*, vol. 10, no. 2, pp. 1626-1636, March 2019.

[31] Q. Jiang, M. Xue and G. Geng, "Energy Management of Microgrid in Grid-Connected and Stand-Alone Modes," in *IEEE Transactions on Power Systems*, vol. 28, no. 3, pp. 3380-3389, Aug. 2013.

[32] R. Palma-Behnke *et al*., "A Microgrid Energy Management System Based on the Rolling Horizon Strategy," in *IEEE Transactions on Smart Grid*, vol. 4, no. 2, pp. 996-1006, June 2013.

[33] J. Li, Y. Liu and L. Wu, "Optimal Operation for Community-Based Multi-Party Microgrid in Grid-Connected and Islanded Modes," in *IEEE Transactions on Smart Grid*, vol. 9, no. 2, pp. 756-765, March 2018.

[34] C. Chen, J. Wang, F. Qiu and D. Zhao, "Resilient Distribution System by Microgrids Formation After Natural Disasters," in *IEEE Transactions on Smart Grid*, vol. 7, no. 2, pp. 958-966, March 2016.

[35] B. Zhao, X. Dong and J. Bornemann, "Service Restoration for a Renewable-Powered Microgrid in Unscheduled Island Mode," in *IEEE Transactions on Smart Grid*, vol. 6, no. 3, pp. 1128-1136, May 2015.

[36] Guo, L., Liu, W., Jiao, B., Hong, B. and Wang, C. (2014), Multi-objective stochastic optimal planning method for stand-alone microgrid system. IET Gener. Transm. Distrib., 8: 1263-1273. https://doi.org/10.1049/iet-gtd.2013.0541

[37] X. Cao, J. Wang and B. Zeng, "Networked Microgrids Planning Through Chance Constrained Stochastic Conic Programming," in *IEEE Transactions on Smart Grid*, vol. 10, no. 6, pp. 6619-6628, Nov. 2019.

[38] Y. Guo and C. Zhao, "Islanding-Aware Robust Energy Management for Microgrids," in *IEEE Transactions on Smart Grid*, vol. 9, no. 2, pp. 1301-1309, March 2018.

[39] J. Lee, S. Lee and K. Lee, "Multistage Stochastic Optimization for Microgrid Operation Under Islanding Uncertainty," in *IEEE Transactions on Smart Grid*, vol. 12, no. 1, pp. 56-66, Jan. 2021.

[40] S. Y. Lee, Y. G. Jin and Y. T. Yoon, "Determining the Optimal Reserve Capacity in a Microgrid With Islanded Operation," in *IEEE Transactions on Power Systems*, vol. 31, no. 2, pp. 1369-1376, March 2016.

[41] A. Khodaei, "Microgrid Optimal Scheduling With Multi-Period Islanding Constraints," in *IEEE Transactions on Power Systems*, vol. 29, no. 3, pp. 1383-1392, May 2014.

[42] Z. Shi, H. Liang, S. Huang and V. Dinavahi, "Distributionally Robust Chance-Constrained Energy Management for Islanded Microgrids," in *IEEE Transactions on Smart Grid*, vol. 10, no. 2, pp. 2234-2244, March 2019.

[43] M. E. Baran and F. F. Wu, "Network reconfiguration in distribution systems for loss reduction and load balancing," in *IEEE Transactions on Power Delivery*, vol. 4, no. 2, pp. 1401-1407, April 1989.

[44] H. Yeh, D. F. Gayme and S. H. Low, "Adaptive VAR Control for Distribution Circuits With Photovoltaic Generators," in *IEEE Transactions on Power Systems*, vol. 27, no. 3, pp. 1656-1663, Aug. 2012.

[45] W. Wei, J. Wang and L. Wu, "Distribution Optimal Power Flow With Real-Time Price Elasticity," in *IEEE Transactions on Power Systems*, vol. 33, no. 1, pp. 1097-1098, Jan. 2018.

[46] W. Lin and E. Bitar, "Decentralized Stochastic Control of Distributed Energy Resources," in *IEEE Transactions on Power Systems*, vol. 33, no. 1, pp. 888-900, Jan. 2018.

[47] S. Ma, B. Chen and Z. Wang, "Resilience Enhancement Strategy for Distribution Systems Under Extreme Weather Events," in *IEEE Transactions on Smart Grid*, vol. 9, no. 2, pp. 1442-1451, March 2018.

[48] Y. Xu, Z. Y. Dong, R. Zhang and D. J. Hill, "Multi-Timescale Coordinated Voltage/Var Control of High Renewable-Penetrated Distribution Systems," in *IEEE Transactions on Power Systems*, vol. 32, no. 6, pp. 4398-4408, Nov. 2017.

[49] Jen-Hao Teng, "A direct approach for distribution system load flow solutions," in *IEEE Transactions on Power Delivery*, vol. 18, no. 3, pp. 882-887, July 2003.

[50] L. S. M. Guedes, A. C. Lisboa, D. A. G. Vieira and R. R. Saldanha, "A Multiobjective Heuristic for Reconfiguration of the Electrical Radial Network," in *IEEE Transactions on Power Delivery*, vol. 28, no. 1, pp. 311-319, Jan. 2013.

[51] S. Sharma and A. R. Abhyankar, "Loss Allocation for Weakly Meshed Distribution System Using Analytical Formulation of Shapley Value," in *IEEE Transactions on Power Systems*, vol. 32, no. 2, pp. 1369-1377, March 2017.

[52] T. Tewari, A. Mohapatra and S. Anand, "Coordinated Control of OLTC and Energy Storage for Voltage Regulation in Distribution Network With High PV Penetration," in *IEEE Transactions on Sustainable Energy*, vol. 12, no. 1, pp. 262-272, Jan. 2021.

[53] N. Karthikeyan, J. R. Pillai, B. Bak-Jensen and J. W. Simpson-Porco, "Predictive Control of Flexible Resources for Demand Response in Active Distribution Networks," in *IEEE Transactions on Power Systems*, vol. 34, no. 4, pp. 2957-2969, July 2019.

[54] P. Fortenbacher, A. Ulbig and G. Andersson, "Optimal Placement and Sizing of Distributed Battery Storage in Low Voltage Grids Using Receding Horizon Control Strategies," in *IEEE Transactions on Power Systems*, vol. 33, no. 3, pp. 2383-2394, May 2018.

[55] L. Wu, M. Shahidehpour and T. Li, "Stochastic Security-Constrained Unit Commitment," in *IEEE Transactions on Power Systems*, vol. 22, no. 2, pp. 800-811, May 2007.

[56] P. A. Ruiz, C. R. Philbrick, E. Zak, K. W. Cheung and P. W. Sauer, "Uncertainty Management in the Unit Commitment Problem," in *IEEE Transactions on Power Systems*, vol. 24, no. 2, pp. 642-651, May 2009.

[57] E. Hajipour, M. Bozorg and M. Fotuhi-Firuzabad, "Stochastic Capacity Expansion Planning of Remote Microgrids With Wind Farms and Energy Storage," in *IEEE Transactions on Sustainable Energy*, vol. 6, no. 2, pp. 491-498, April 2015.

[58] A. R. Malekpour and A. Pahwa, "Stochastic Networked Microgrid Energy Management With Correlated Wind Generators," in *IEEE Transactions on Power Systems*, vol. 32, no. 5, pp. 3681-3693, Sept. 2017.

[59] P. Li, D. Xu, Z. Zhou, W. -J. Lee and B. Zhao, "Stochastic Optimal Operation of Microgrid Based on Chaotic Binary Particle Swarm Optimization," in *IEEE Transactions on Smart Grid*, vol. 7, no. 1, pp. 66-73, Jan. 2016.

[60] H. Nafisi, S. M. M. Agah, H. Askarian Abyaneh and M. Abedi, "Two-Stage Optimization Method for Energy Loss Minimization in Microgrid Based on Smart Power Management Scheme of PHEVs," in *IEEE Transactions on Smart Grid*, vol. 7, no. 3, pp. 1268-1276, May 2016.

[61] S. Gunawan, and S. Azarm."Non-Gradient Based Parameter Sensitivity Estimation for Single Objective Robust Design Optimization," ASME J. Mech. Des. May 2004.

[62] Y. Chi, Y. Xu and R. Zhang, "Many-Objective Robust Optimization for Dynamic VAR Planning to Enhance Voltage Stability of a Wind-Energy Power System," in *IEEE Transactions on Power Delivery*, vol. 36, no. 1, pp. 30-42, Feb. 2021.

[63] J.A. Peças Lopes, N. Hatziargyriou, J. Mutale, P. Djapic, N. Jenkins, "Integrating distributed generation into electric power systems: A review of drivers, challenges and opportunities," *Electric Power Systems Research*, Volume 77, Issue 9, 2007, Pages 1189-1203,

[64] "A Clean Planet for all: A European strategic long-term vision for a prosperous, modern, competitive and climate neutral economy" [Online] Available: https://eur-lex.europa.eu/

[65] Sherif M. Ismael, Shady H.E. Abdel Aleem, Almoataz Y. Abdelaziz, Ahmed F. Zobaa, "State-of-the-art of hosting capacity in modern power systems with distributed generation," *Renewable Energy*, Volume 130, 2019, Pages 1002-1020.

[66] S. F. Santos, D. Z. Fitiwi, M. Shafie-Khah, A. W. Bizuayehu, C. M. P. Cabrita and J. P. S. Catalão, "New Multistage and Stochastic Mathematical Model for Maximizing RES Hosting Capacity—Part I: Problem Formulation," in *IEEE Transactions on Sustainable Energy*, vol. 8, no. 1, pp. 304-319, Jan. 2017.

[67] H. AlSaadi, R. Zivanovic and S. F. AlSarawi, "Probabilistic Hosting Capacity for Active Distribution Networks," in *IEEE Transactions on Industrial Informatics*, vol. 13, no. 5, pp. 2519-2532, Oct. 2017.

[68] F. Capitanescu, L. F. Ochoa, H. Margossian and N. D. Hatziargyriou, "Assessing the Potential of Network Reconfiguration to Improve Distributed Generation Hosting Capacity in Active Distribution Systems," in *IEEE Transactions on Power Systems*, vol. 30, no. 1, pp. 346-356, Jan. 2015.

[69] S. Wang, Y. Dong, L. Wu and B. Yan, "Interval Overvoltage Risk Based PV Hosting Capacity Evaluation Considering PV and Load Uncertainties," in *IEEE Transactions on Smart Grid*, vol. 11, no. 3, pp. 2709-2721, May 2020.

[70] A. Arshad and M. Lehtonen, "A Stochastic Assessment of PV Hosting Capacity Enhancement in Distribution Network Utilizing Voltage Support Techniques," in *IEEE Access*, vol. 7, pp. 46461-46471, 2019.

[71] T. Gush, C. -H. Kim, S. Admasie, J. -S. Kim and J. -S. Song, "Optimal Smart Inverter Control for PV and BESS to Improve PV Hosting Capacity of Distribution Networks Using Slime Mould Algorithm," in *IEEE Access*, vol. 9, pp. 52164-52176, 2021.

[72] D. E. Olivares et al., "Trends in Microgrid Control," in *IEEE Trans. Smart Grid*, vol. 5, no. 4, pp. 1905-1919, July 2014.

[73] D. E. Olivares, J. D. Lara, C. A. Cañizares and M. Kazerani, "Stochastic-Predictive Energy Management System for Isolated Microgrids," in *IEEE Trans. Smart Grid*, vol. 6, no. 6, pp. 2681-2693, Nov. 2015.

[74] D. E. Olivares, C. A. Cañizares and M. Kazerani, "A Centralized Energy Management System for Isolated Microgrids," in *IEEE Trans. Smart Grid*, vol. 5, no. 4, pp. 1864-1875, July 2014.

[75] P. P. Vergara, J. C. López, M. J. Rider and L. C. P. da Silva, "Optimal Operation of Unbalanced Three-Phase Islanded Droop-Based Microgrids," in *IEEE Trans. Smart Grid*, vol. 10, no. 1, pp. 928-940, Jan. 2019.

[76] P. P. Vergara *et al*., "A Generalized Model for the Optimal Operation of Microgrids in Grid-Connected and Islanded Droop-Based Mode," in *IEEE Transactions on Smart Grid*, vol. 10, no. 5, pp. 5032-5045, Sept. 2019.

[77] G. Díaz, J. Gómez-Aleixandre and J. Coto, "Direct Backward/Forward Sweep Algorithm for Solving Load Power Flows in AC Droop-Regulated Microgrids," in *IEEE Trans. Smart Grid*, vol. 7, no. 5, pp. 2208-2217, Sept. 2016.

[78] F. Hameed, M. Al Hosani and H. H. Zeineldin, "A Modified Backward/Forward Sweep Load Flow Method for Islanded Radial Microgrids," in *IEEE Trans. Smart Grid*, vol. 10, no. 1, pp. 910-918, Jan. 2019.

[79] H. Farzin, M. Fotuhi-Firuzabad and M. Moeini-Aghtaie, "Stochastic Energy Management of Microgrids During Unscheduled Islanding Period," in *IEEE Trans. Industrial Informatics*, vol. 13, no. 3, pp. 1079-1087, June 2017.

[80] C. Zhang, Y. Xu, Z. Y. Dong and K. P. Wong, "Robust Coordination of Distributed Generation and Price-Based Demand Response in Microgrids," in *IEEE Trans. Smart Grid*, vol. 9, no. 5, pp. 4236-4247, Sept. 2018.

[81] J. Wang, M. Shahidehpour and Z. Li, "Security-Constrained Unit Commitment With Volatile Wind Power Generation," in *IEEE Trans. Power Systems*, vol. 23, no. 3, pp. 1319-1327, Aug. 2008.

[82] W. Su, J. Wang and J. Roh, "Stochastic Energy Scheduling in Microgrids With Intermittent Renewable Energy Resources," in *IEEE Trans. Smart Grid*, vol. 5, no. 4, pp. 1876-1883, July 2014.

[83] L. Subramanian and H. B. Gooi, "Stochastic Backward/Forward Sweep Power Flow Analysis for Islanded Microgrids," *2018 IEEE Innovative Smart Grid Technologies - Asia* (ISGT Asia), Singapore, 2018

[84] N. M. M. Razali and A. H. Hashim, "Backward reduction application for minimizing wind power scenarios in stochastic programming," *2010 4th International Power Engineering and Optimization*.

[85] N. Growe-Kuska, H. Heitsch and W. Romisch, "Scenario reduction and scenario tree construction for power management problems," *2003 IEEE Bologna Power Tech Conference Proceedings*, Bologna, Italy, 2003, pp. 7 pp. Vol.3-.

[86] J. Lofberg, "YALMIP : a toolbox for modeling and optimization in MATLAB," *2004 IEEE International Conference on Robotics and Automation* (IEEE Cat. No.04CH37508), New Orleans, LA, 2004, pp. 284-289.

[87] GUROBI. Available: http://www.gurobi.com/

[88] W. Wei, J. Li, B. Chen, et al, "Embodied greenhouse gas emissions from building China's large-scale power transmission infrastructure, " Nature Sustainability, 2021.

[89] Australia Energy Market Operator "Black system South Australia 28 September 2016 final report", Available:https://www.aemo.com.au/.

[90] A. Gholami, F. Aminifar and M. Shahidehpour, "Front Lines Against the Darkness: Enhancing the Resilience of the Electricity Grid Through Microgrid Facilities," *IEEE Electrification Magazine*, vol. 4, no. 1, pp. 18-24, March 2016.

[91] M. Panteli, D. N. Trakas, P. Mancarella and N. D. Hatziargyriou, "Boosting the Power Grid Resilience to Extreme Weather Events Using Defensive Islanding," *IEEE Trans Smart Grid*, vol. 7, no. 6, pp. 2913-2922, Nov. 2016.

[92] F. Teymouri, T. Amraee, H. Saberi and F. Capitanescu, "Toward Controlled Islanding for Enhancing Power Grid Resilience Considering Frequency Stability Constraints," *IEEE Trans Smart Grid*, vol. 10, no. 2, pp. 1735-1746, March 2019.

[93] X. Liu, M. Shahidehpour, Z. Li, X. Liu, Y. Cao and Z. Bie, "Microgrids for Enhancing the Power Grid Resilience in Extreme Conditions," *IEEE Trans Smart Grid*, vol. 8, no. 2, pp. 589-597, March 2017.

[94] D. Liu, C. Zhang, G. Chen, Y.Xu and Z. Y. Dong, "Stochastic security-constrained optimal power flow for a microgrid considering tie-line switching," *Int. J. Elec. Power and Energy Syst.*, vol. 134, Jan. 2022.

[95] J. D. Lara, D. E. Olivares and C. A. Cañizares, "Robust Energy Management of Isolated Microgrids," IEEE Systems Journal, vol. 13, no. 1, pp. 680-691, March 2019.

[96] W. Shi, X. Xie, C. Chu and R. Gadh, "Distributed Optimal Energy Management in Microgrids," *IEEE Trans Smart Grid*, vol. 6, no. 3, pp. 1137-1146, May 2015.

[97] E. Dall'Anese, H. Zhu and G. B. Giannakis, "Distributed Optimal Power Flow for Smart Microgrids," *IEEE Trans Smart Grid*, vol. 4, no. 3, pp. 1464-1475, Sept. 2013.

[98] R. Jamalzadeh and M. Hong, "Microgrid Optimal Power Flow Using the Generalized Benders Decomposition Approach," *IEEE Trans Sustainable Energy*, vol. 10, no. 4, pp. 2050-2064, Oct. 2019.

[99] P. Kall and S. W. Wallace, Stochastic Programming. New York: Wiley, 1994.

[100] C. Zhang and Y. Xu, "Hierarchically-Coordinated Voltage/VAR Control of Distribution Networks Using PV Inverters," *IEEE Trans Smart Grid*, vol. 11, no. 4, pp. 2942-2953, July 2020

[101] J. Dupaˇcová, N. Gröwe-Kuska, and W. Römisch, "Scenario reduction in stochastic programming: An approach using probability metrics," *Math. Program.*, vol. A 95, pp. 493–511, 2003.

[102] D. Liu, C. Zhang and Z. Dong, "Stochastic Optimal Power Flow for Islanded Microgrids Considering Droop Control," *2019 IEEE Innovative Smart Grid Technologies - Asia* (ISGT Asia), Chengdu, China, 2019.

[103] C. Battistelli, Y. P. Agalgaonkar and B. C. Pal, "Probabilistic Dispatch of Remote Hybrid Microgrids Including Battery Storage and Load Management," in *IEEE Transactions on Smart Grid*, vol. 8, no. 3, pp. 1305-1317, May 2017.

[104] Y. Levron, J. M. Guerrero and Y. Beck, "Optimal Power Flow in Microgrids with Energy Storage," in *IEEE Transactions on Power Systems*, vol. 28, no. 3, pp. 3226-3234, Aug. 2013.

[105] M. Z. Kamh and R. Iravani, "Unbalanced Model and Power-Flow Analysis of Microgrids and Active Distribution Systems," in *IEEE Transactions on Power Delivery*, vol. 25, no. 4, pp. 2851-2858, Oct. 2010.

[106] H. Nikkhajoei and R. Iravani, "Steady-State Model and Power Flow Analysis of Electronically-Coupled Distributed Resource Units," in *IEEE Transactions on Power Delivery*, vol. 22, no. 1, pp. 721-728, Jan. 2007.

[107] M. M. A. Abdelaziz, H. E. Farag, E. F. El-Saadany and Y. A. I. Mohamed, "A Novel and Generalized Three-Phase Power Flow Algorithm for Islanded Microgrids Using a Newton Trust Region Method," in *IEEE Transactions on Power Systems*, vol. 28, no. 1, pp. 190-201, Feb. 2013.

[108] F. Mumtaz, M. H. Syed, M. A. Hosani and H. H. Zeineldin, "A Novel Approach to Solve Power Flow for Islanded Microgrids Using Modified Newton Raphson with Droop Control

of DG," in *IEEE Transactions on Sustainable Energy*, vol. 7, no. 2, pp. 493-503, April 2016.

[109] Y. Xu, Z. Y. Dong, R. Zhang, K. P. Wong and M. Lai, "Solving Preventive-Corrective SCOPF by a Hybrid Computational Strategy," in *IEEE Transactions on Power Systems*, vol. 29, no. 3, pp. 1345-1355, May 2014.

[110] Conejo, Antonio J. Decomposition Techniques in Mathematical Programming: Engineering and Science Applications. Berlin: Springer, 2006.

[111] Ausgrid. Available: www.ausgrid.com.au/Industry/Regulation/Network-prices

[112] U.S. Department of Energy " Combined Heat and Power Technology Fact Sheet Series," DOE/EE-1329 • July 2016.

[113] AEMO. Available: aemo.com.au/energy-systems/electricity/national-electricity-market-nem

[114] CIGRE-C6, [Online] Available: http://c6.cigre.org/

[115] S. Wang, S. Chen, L. Ge and L. Wu, "Distributed Generation Hosting Capacity Evaluation for Distribution Systems Considering the Robust Optimal Operation of OLTC and SVC," *IEEE Transactions on Sustainable Energy*, vol. 7, no. 3, pp. 1111-1123, July 2016.

[116] X. Chen, W. Wu, B. Zhang and C. Lin, "Data-Driven DG Capacity Assessment Method for Active Distribution Networks," *IEEE Transactions on Power Systems*, vol. 32, no. 5, pp. 3946-3957, Sept. 2017.

[117] F. Ding and B. Mather, "On Distributed PV Hosting Capacity Estimation, Sensitivity Study, and Improvement," *IEEE Transactions on Sustainable Energy*, vol. 8, no. 3, pp. 1010-1020, July 2017.

[118] D. A. Quijano and A. Padilha-Feltrin, "Assessment of Distributed Generation Hosting Capacity of Microgrids with Thermal Smart Loads," *2020 IEEE PES Innovative Smart Grid Technologies Europe (ISGT-Europe)*, The Hague, Oct. 2020, pp. 764-768

[119] J. Lee, Jean-Philippe Bérard, G. Razeghi, S. Samuelsen, "Maximiz-ing PV Hosting Capacity of Distribution Feeder Microgrid," Ap-plied Energy, vol. 261, 114400, pp. 1-17, March 2020.

[120] N. Jayasekara, M. A. S. Masoum and P. J. Wolfs, "Optimal Operation of Distributed Energy Storage Systems to Improve Distribution Network Load and Generation Hosting Capability," *IEEE Transactions on Sustainable Energy*, vol. 7, no. 1, pp. 250-261, Jan. 2016.

[121] B. Wang, C. Zhang, Z. Y. Dong and X. Li, "Improving Hosting Capacity of Unbalanced Distribution Networks via Robust Allocation of Battery Energy Storage Systems," *IEEE Transactions on Power Systems*, vol. 36, no. 3, pp. 2174-2185, May 2021.

[122] Z. Wang, B. Chen, J. Wang, J. Kim and M. M. Begovic, "Robust Optimization Based Optimal DG Placement in Microgrids," *IEEE Transactions on Smart Grid*, vol. 5, no. 5, pp. 2173-2182, Sept. 2014.

[123] K. Morozovska, M. Heleno, A. V. Meza and P. Hilber, "Including Dynamic Line Rating Into the Optimal Planning of Distributed Energy Resources," *IEEE Transactions on Smart Grid*, vol. 12, no. 6, pp. 5052-5059, Nov. 2021.

[124] S. Mohamed, M. F. Shaaban, M. Ismail, E. Serpedin and K. A. Qaraqe, "An Efficient Planning Algorithm for Hybrid Remote Microgrids," *IEEE Transactions on Sustainable Energy*, vol. 10, no. 1, pp. 257-267, Jan. 2019.

[125] S. Arif, A. E. Robbi, S. U. Ahmed and M. S. Hossain Lipu, " Enhancement of Solar PV Hosting Capacity in a Remote Industrial Microgrid: A Methodical Techno-Economic Approach," Sustainability, vol. 14, 8921, 2022.

[126] M. Bazrafshan and N. Gatsis, "Decentralized Stochastic Optimal Power Flow in Radial Networks With Distributed Generation," *IEEE Transactions on Smart Grid*, vol. 8, no. 2, pp. 787-801, March 2017.

[127] Z. Wang, B. Chen, J. Wang and M. M. Begovic, "Stochastic DG Placement for Conservation Voltage Reduction Based on Multiple Replications Procedure," *IEEE Transactions on Power Delivery*, vol. 30, no. 3, pp. 1039-1047, June 2015.

[128] S. F. Santos, D. Z. Fitiwi, M. Shafie-Khah, A. W. Bizuayehu, C. M. P. Cabrita and J. P. S. Catalão, "New Multistage and Stochastic Mathematical Model for Maximizing RES Hosting Capacity—Part I: Problem Formulation," *IEEE Transactions on Sustainable Energy*, vol. 8, no. 1, pp. 304-319, Jan. 2017.

[129] A. Khodaei, S. Bahramirad and M. Shahidehpour, "Microgrid Planning Under Uncertainty," *IEEE Transactions on Power Systems*, vol. 30, no. 5, pp. 2417-2425, Sept. 2015.

[130] W. Yuan, J. Wang, F. Qiu, C. Chen, C. Kang and B. Zeng, "Robust Optimization-Based Resilient Distribution Network Planning Against Natural Disasters," *IEEE Transactions on Smart Grid*, vol. 7, no. 6, pp. 2817-2826, Nov. 2016.

[131] M. Li, S. Azarm and V. Aute. “A multi-objective genetic algorithm for robust design optimization.” GECCO 05 (2005).

[132] C. Zhang, Y. Xu, Z. Y. Dong and R. Zhang, "Multi-Objective Adaptive Robust Voltage/VAR Control for High-PV Penetrated Distribution Networks," *IEEE Transactions on Smart Grid*, vol. 11, no. 6, pp. 5288-5300, Nov. 2020.

[133] M. Mitchell, “An introduction to genetic algorithms”. The MIT Press. 1996.

[134] L. C. Rodman and R. K. Meentemeyer, "A Geographic Analysis of Wind Turbine Placement in Northern California," Energy Policy, vol. 34, no. 15, pp. 2137-2149, Oct. 2006.

[135] C. Zhang, Y. Xu, Z. Y. Dong and J. Ma, "A composite sensitivity factor based method for networked distributed generation planning," 2016 Power Systems Computation Conference, Genoa, June 2016, pp. 1-7.